A STUDY OF ADDITIVE MANUFACTURING CONSUMPTION, EMISSION, AND OVERALL IMPACT WITH A FOCUS ON FUSED DEPOSITION MODELING

by

Timothy Simon

Dissertation

Submitted to the Faculty of Purdue University

In Partial Fulfillment of the Requirements for the degree of

Doctor of Philosophy

Division of Environmental and Ecological Engineering

West Lafayette, Indiana

August 2021

THE PURDUE UNIVERSITY GRADUATE SCHOOL
STATEMENT OF COMMITTEE APPROVAL

Dr. Fu Zhao, Chair

School of Mechanical Engineering and Environmental & Ecological Engineering

Dr. John W. Sutherland

School of Environmental & Ecological Engineering

Dr. John A. Howarter

School of Material Science Engineering and Environmental & Ecological Engineering

Dr. Rebecca E. Ciez

School of Mechanical Engineering and Environmental & Ecological Engineering

Approved by:

Dr. John W. Sutherland

I dedicate this work to my Dad, who always inspired curiosity and understanding in the fields of science and engineering from a young age. "You were born blessed and therefore it is your responsibility to give back to the Earth and help those less fortunate." Dr. Robert R Simon

ACKNOWLEDGMENTS

First and foremost, I want to acknowledge my advisor Dr. Fu Zhao who for the past 5 years has been a tremendous coach, mentor, and counselor through all of my work. Dr. Zhao taught me how to be a better researcher and stronger writer. Whenever I had questions or issues with my work he was always patient and passed on the necessary skills to not only identify complex problems but also solve them. Finally, he allowed me to expand my skills by working on an assortment of projects so as to reach outside of my comfort zone. I want to acknowledge my committee members Dr. John W. Sutherland, Dr. John A. Howarter, and Dr. Rebecca E. Ciez. Dr. Sutherland and Dr. Howarter took a special interest in my work offering instrumental advice that strengthened the final outcome of the project. Working with Dr. Sutherland on conference writing and lecturing helped improve my skills in presenting. Dr. Howarter's expertise in polymer research proved extremely beneficial when using him as a consultant.

While at Purdue I had the pleasure of working with several other knowledgeable researchers on this project and others. Wo Jae Lee, Yiran Yang, and Jing Zhao helped with some of the AM studies performed. I have also worked with Edwin Kpodzro, Eduardo Fenollal, Rachel Gehr, and Tai-Yuan Hang who became great colleagues and friends. Finally, I had the pleasure of working with and learning from several Professors outside of my committee including Professors Luciano Castillo, James Braun, and David Warsinger to name a few.

I couldn't have gotten through any of this without the support of my family and friends. Blessed with parents that support and encourage me, my Father and Mother Dr. Robert Simon and Marilynn Simon have always been encouraging of my education and supportive through all of mine and my brothers endeavors. My brothers Adam and Jeremy have also always been a huge support. Whether it was proofreading a paper or listening to a practice presentation my entire family was always there and I am extremely grateful for that. My girlfriend Annie Lohrstorfer was also a huge support in the final years of my graduate program; I'd like to acknowledge her for the significance and importance she holds in my life. Finally, my roommates Tom Ransegnola, Garrett Matthews, Coleton Joiner, and Caleb Heitkamp, the members of our band "The Siberian Mangos," my workout buddies Mason Pellegrini and David Rowe, and several others were a source of relief and enjoyment throughout my time here.

This work was supported by the National Science Foundation under Grant No. 1605472. Any opinions, findings, and conclusions or recommendations expressed in this material are those of the authors and do not necessarily reflect the views of the National Science Foundation. Additional funding was provided by Purdue School of Mechanical Engineering in several TA positions I was granted while here.

TABLE OF CONTENTS

LIST OF TABLES

LIST OF FIGURES

SYMBOLS

E_{total}	Total energy consumption (Wh)
$E_{projector}$	Projector Total Energy Consumption (Wh)
E_{motor}	Energy of Motor (Wh)
$E_{computer}$	Total Energy Consumption of the Computer (Wh)
E_{board}	Total Energy Consumption of the Computer (Wh)
E_{curing}	Projector Curing Stage Energy Consumption (Wh)
$E_{idle,p}$	Projector Idle Stage Energy Consumption (Wh)
$P_{computer}$	Computer Rated Power (W)
P_{board}	Control Board Rated Power (W)
P_{curing}	Curing Power (W)
P_{idle}	Projector idle stage power (W)
P_{motor}	Power Requirement of Motor (W)
N_{bottom}	Total Number of Bottom Layers $(\#)$
N	Total Number of Layers $(\#)$
d	Layer thickness (mm)
$T_{printing}$	Printing Time (sec)
T_{LS}	Layer Lift and Sequence Time (sec)
$T_{curing,b}$	Curing Time for Each Bottom Layers (sec)
T_{curing}	Curing Time for Each Layer (sec)
T_{idle}	Total Idle Time (sec)
T_{post}	Post-processing Time (sec)
T_{pre}	Pre-processing Time (sec)
$ER(t)_{volatilization}$	VOC Emission due to the Volatilization Process (g/sec)
S_{part}	Surface Area of Printed Part (cm^2)

V_{part}	Volume of Printed Part (m^3)
m_{input}	Mass of Input Raw Materials, liquid (g)
m_{part}	Mass of Finished Part, solid (g)
$m_{waste,g}$	Mass of Gaseous VOC Emission (g)
$m_{waste,l}$	Liquid Waste Percentage (g)
m_{waste}	Total Material Waste (g)
v_z	Air Flow Speed (cm/sec)
α	Liquid Resin Coating thickness (cm)
ρ_a	Air Density (kg/m^3)
ρ_{part}	Solid Part Density (kg/m^3)
ρ_{resin}	Resin Density (kg/m^3)
ρ_v	Vapor Pressure of Liquid (atm)
Δz	Length of Air-liquid Interface in the Direction of Flow (cm)
D	Air Diffusivity (cm/sec)
K	Mass Transfer Coefficient (cm/sec)
M	Molecular Weight of Resin $(g/g \cdot mole)$
P	Ambient Air Pressure (atm)
Q	Mass Transfer Rate $(g \cdot mole/cm^2 \cdot sec)$
R	Universal Gas Constant $(cm^3 \cdot kPa/g \cdot mole \cdot K)$
S	Surface Area (cm^2)
Sc	The Schmidt Number (cm)
T	Absolute Temperature (K)
μ	Air Viscosity $(g/cm \cdot sec)$
t_{print}	FDM Print time (s)
xy_{dist}	Distance traveled between xy coordinate machine moves (m)
f	Extruder Moving Speed $(^m/_s)$
SA_{part}	Surface Area of Part
$Layer\ Height$	Extrusion layer thickness (m)

$Number\ of\ Shells$	Total number of solid boundary layers on printed part (#)
V_{part}	Total Part Volume (m^3)
m_{part}	Total part mass (g)
$Percent\ infill$	Percentage of part that is filled with material (%)
ρ	Material Density $(^{g}/_{m^3})$

ABBREVIATIONS

ABS	Acrylonitrile Butadiene
AM	Additive manufacturing
EBM	Electron beam melting
ELPI	Electrical low pressure impactor
FDM	Fused deposition modeling
GCMS	Gas chromatography mass spectrometry
LCI	Life cycle inventory
LCMA	Liquid chromatography mass spectrometry
MIP	Mask image projection
OPS	Optical particle sizer
PLA	Polylactic Acid
SLA	Stereolithography
SMPS	Scanning mobility particle sizer
SPME	Solid phase microextraction
SVC	Semi-volatile compounds
TEM	Transmission electron microscopy
UFP	Ultrafine Particle
UPLCI	Unit process life cycle inventory
UV	Ultraviolet
VOC	Volatile organic compound

ABSTRACT

Additive manufacturing (AM) can be an advantageous substitute to various traditional manufacturing techniques. Due to the ability to rapidly create products, AM has been traditionally used to prototype more efficiently. As the industry has progressed, however, use cases have gone beyond prototyping into production of complex parts with unique geometries. Amongst the most popular of AM processes is fused deposition modeling (FDM). FDM fabricates products through an extrusion technique where plastic filament is heated to the glass transition temperature and extruded layer by layer onto a build platform to construct the desired part. The purpose of this research is to elaborate on the potential of this technology, while considering environmental impact as it becomes more widespread throughout industry, research, and academia.

Although AM consumes resources more conservatively than traditional methodologies, it is not free from having environmental impacts. Several studies have shown that additive manufacturing can affect human and environmental health by emitting particles of a dynamic size range into the surrounding environment during a print. To begin this study, chapters investigate emission profiles and characterization of emissions from FDM 3D printers with the intention of developing a better understanding of the impact from such devices. Background work is done to confirm the occurrence of particle emission from FDM using acrylonitrile butadiene styrene (ABS) plastic filament. An aluminum bodied 3D printer is enclosed in a chamber and placed in a Class 1 cleanroom where measurements are conducted using high temporal resolution electrical low-pressure impactor (ELPI), scanning mobility particle sizer (SMPS), and optical particle sizer (OPS), which combined measure particles of a size range 6-500nm. Tests were done using the NIST standard test part and a honeycomb infill cube. Results from this study show that particle emissions are closely related to filament residence time in the extruder while less related to extruding speed. An initial spike of particle concentration is observed immediately after printing, which is likely a result of the long time required to heat the extruder and bed to the desired temperature. Upon conclusion of this study, it is theorized that particles may be formed through vapor condensation and coagulation after being released into the surrounding environment.

With confirmation of FDM ultrafine particle emission at notable concentrations, an effort was consequently placed on diagnosing the primary cause of emission and energy consumption based on developed hypotheses. Experimental data suggests that particle emission is mainly the

result of condensing and agglomerating semi-volatile organic compounds. The initial emission spike occurs when there is dripping of semi-liquid filament from the heated nozzle and/or residue left in the nozzle between prints; this supports the previously stated hypothesis regarding residence time. However, the study shows that while printing speed and material flow influence particle emission rate, the effects from these factors are relatively insignificant. Power profile analysis indicates that print bed heating and component temperature maintaining are the leading contributors to energy consumption for FDM printers, making time the primary variable driving energy input.

To better understand the severity of FDM emissions, further investigation is necessary to diligence the makeup of the process output flows. By collecting exhaust discharge from a Makerbot Replicator 2x printing ABS filament and diffusing it through a type 1 water solution, we are able to investigate the chemical makeup of these compounds. Additional exploration is done by performing a filament wash to investigate emissions that may already be present before extrusion. Using solid phase micro-extraction, contaminants are studied using gas chromatography mass spectrometry (GCMS) thermal desorption. Characterization of the collected emission offers more comprehensive knowledge of the environmental and human health impacts of this AM process.

Classification of the environmental performance of various manufacturing technologies can be achieved by analyzing their input and output material, as well as energy flows. The unit process life cycle inventory (UPLCI) is a proficient approach to developing reusable models capable of calculating these flows. The UPLCI models can be connected to estimate the total material and energy consumption of, and emissions from, product manufacturing based on a process plan. The final chapter focuses on using the knowledge gained from this work in developing UPLCI model methodology for FDM, and applying it further to the second most widely used AM process: stereolithography (SLA). The model created for the FDM study considers material input/output flows from ABS plastic filament. Energy input/output flows come from the running printer, step motors, heated build plate, and heated extruder. SLA also fabricates parts layer by layer, but by the use of a photosensitive liquid resin which solidifies when cured under the exposure of ultraviolet light. Model material input/output flows are sourced from the photosensitive liquid resin, while energy input/output flows are generated from (i) the projector used as the ultraviolet light source and (ii) the step motors. As shown in this work, energy flow is mostly time dependent;

material flows, on the other hand, rely more on the nature of the fabrication process. While a focus on FDM is asserted throughout this study, the developed UPLCI models show how conclusions drawn from this work can be applied to different forms of AM processes in future work.

1. INTRODUCTION

Additive manufacturing (AM) is the industrial production name given to 3D printing which is a computer controlled process that creates three dimensional objects by depositing material, usually in layers [1]. AM has the ability to rapidly produce parts of variable complexities while substantially shortening the product supply chain. This could offer many environmental and financial benefits. As a result, AM has compelled growing interest among a variety of different industries including aerospace, automotive, machine tool production, healthcare and medicine, dentistry and dental technology, architecture and construction, retail/apparel, and food [2]. Some of these materials include but are not limited to plastics, resins, rubbers, ceramics, glass, concretes, and metals [3]. With the wide variety of materials accommodated by AM the use of this manufacturing technique is subject to grow. It has been suggested that AM could reduce environmental impact with consideration to material utilization and life cycle performance [4]. This has been shown in studies of comparative life cycle assessment relating AM processes like fused deposition modeling and inkjet/polyjet printing to popular traditional manufacturing techniques like CNC milling [5].

1.1 Life Cycle Considerations in Additive Manufacturing

One interesting approach to evaluating the adoption of AM is using a sustainable value roadmapping framework for AM. Despeisse et al. did this with a goal to build a tool to advise product developers in how AM can be integrated to accomplish several potential benefits including internalizing all processes from design to manufacturing, enhancing innovation capabilities, reducing costs, decreasing distribution, decreasing time to market / lead times, and reducing overall waste [6]. They introduced the six areas, shown in Figure 1.1 where AM can enhance sustainability from the life cycle perspective as follows:

- Design of products and process for efficiency: material waste reduction and improved product performance
- Manufacturing system configuration: improved flexibility and responsiveness for on-demand production, elimination of inventory, and reduced storage cost.

- New business models: increased collaborations between manufacturer and consumer through the customization and personalization of the product
- Efficiency in use: improved energy efficiency in use phase through the adoption of lightweight products
- Product life extension / repair: more durable products through simpler assemblies
- Closed loop systems: enhanced recyclability through simpler supply chain and less material diversity

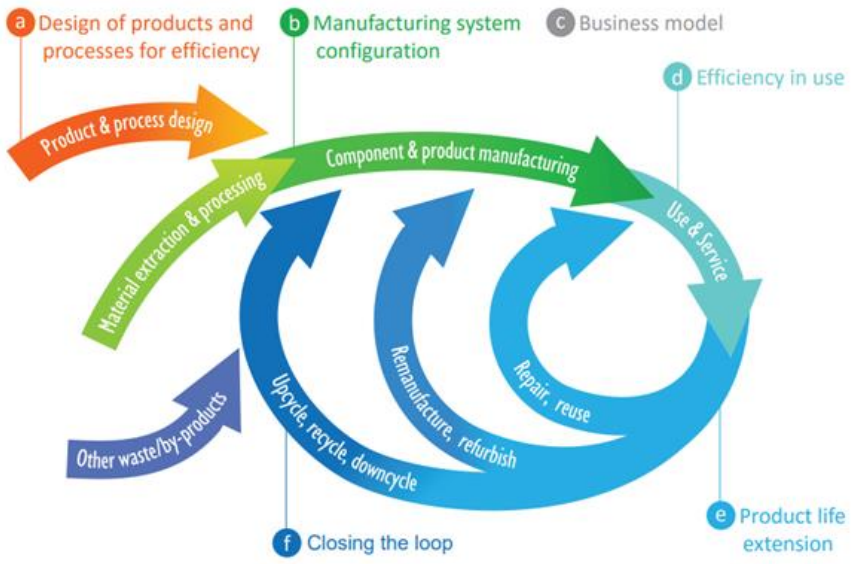

Figure 1.1 Six areas for sustainable benefits using AM [6]

In the study by Despeisse et al. [6], a clear argument was made for how considering AM in product development can offer economic benefits while simultaneously producing less environmentally taxing products. Additional research is being done on how different industries can capitalize on these benefits. With the design freedom to produce complex parts with unique geometries, the automotive and aerospace industries have a lot to gain by implementing AM [7]. When investigating benefits for commercial vehicles, some AM processes may not always show significant environmental improvements considering manufacturing energy and material savings, however, environmental gains can be made by decreasing weight and optimizing performance in specific essential vehicle components [8]. The AM process can be used to reduce weight in aircraft components as well, offering substantial energy savings by improving fuel economy and reducing

on material requirements [9]; it is claimed here that fuel consumption can be reduced by as much as 6.4%. With emphasis on redesign of components for AM, material and energy saving can be made both during manufacturing and use phases of aircraft and automotive components.

With each AM process having unique performance capabilities it is important to consider differing environmental implications. For example, the majority of energy consumed in the selective laser melting (SLM) process results from the powder production and energy consumption during a print [10]. It has been shown that process energy consumption for electron beam melting (EBM) printers is only weakly related to geometry and design features [11]. For both fused deposition modeling (FDM) and stereolithography (SLA) printers, the time to print has been shown to be the primary factor in specific energy consumption [12], [13]. These studies suggest that complex geometry does not significantly impact energy consumption when using AM but rather part volume is more significant. This is a promising consideration given it reduces environmental implications of producing parts with complex geometric features using AM over CM, resulting in reduced design limitations and improved performance scenarios during a product use phase.

The life cycle of a product includes initial manufacturing in the earliest stage of an assessment. To implement proper sustainable life cycle design, it is essential to integrate downstream life cycle data for more sustainable product performance during all LCA phases [14]. Several comparative studies have been conducted to illustrate how different AM processes compare to CM techniques, and while results in manufacturing implications vary, the common drawn conclusion is that considerations need to go beyond the manufacturing stage to deliberate on the entire product life cycle [15], [16]. The common life cycle stages of additively manufactured and machined parts are presented in Figure 1.2; some AM processes require a machining process as post-processing to achieve the desired product quality (called hybrid process). As seen in Figure 1.2, the two parts go through different paths from the raw material processing stage. Therefore, the entire life cycle stages should be taken into account when justifying the environmental superiority of AM over CM.

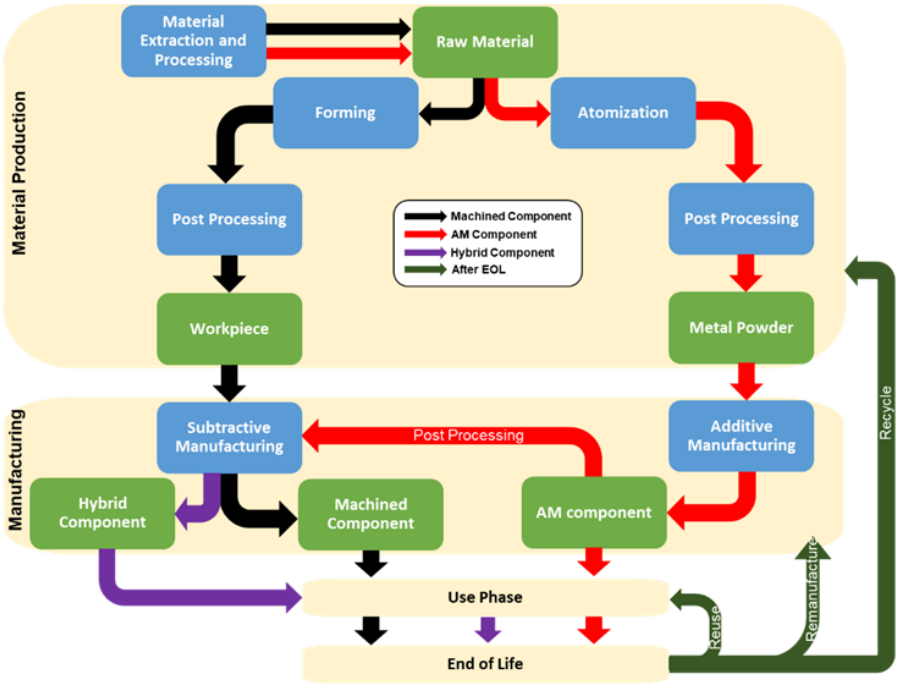

Figure 1.2 Life cycle of additive and machined parts

A study done on binder jetting and milling showed that the atomization produced metal powders and steel stock are insignificant when considering embodied energy of a product, which suggests that change in geometry is a better approach to material and energy savings [17]. Consequently, studies further recommend implementing AM from a design approach. It is stressed that in order for AM to reach its full potential, products need to be redesigned for AM and not simply reproduced using AM enforcing both designer and manufacturer to think as one unit [18]. This suggests a bottom-up design approach implementing geometric modeling software to reduce mass while enhancing functional features of a product [18]. By applying the concept of design for sustainable additive manufacturing (DFSAM) flux models can be used to help engineers design parts optimized for AM with an environmental point of view [19]. With advances in predictive empirical and analytical material / energy flow models for several AM processes [5], [12], [20], [21], designers can use developing tools to predict product sustainability during the design process. The implementation of AM can therefore improve product life cycle by reducing manufacturing related impacts but perhaps more predominantly by enhancing product environmental performance during use.

Product end of life (or perhaps more appropriately, product end-of-use) is increasingly being considered in current product development. There are many avenues a product or part can take at its end of life, the most common being ending in a landfill, being recycled, or reused/remanufactured. AM can impact several end of life scenarios depending on the process and the part. Bioplastics are one option to improve on product sustainability and end of life but can be damaging to overall energy demand considering pre-processing of material [22]. Compared to injection molding and milling, FDM printers exhibit low energy demand and specific costs for batch sizes below 72 parts when using PLA bioplastic [22]. These conclusions are driven by the low power demand in production and high material efficiency of FDM. Additional studies have shown the potential for AM processes, most notably FDM, to use recycled material in filament and powder form to close the loop in a products life cycle [23]–[26], however, it is shown that the change in material properties must be considered. Another promising approach being studied considers direct material reuse by employing AM to further build on pre-existing parts and consequently ending with an entirely new product [27]. By reflecting on this concept in the initial design of a part or product, opportunities to design for redesign can be implemented to consider end of life in the early stages of product development. This concept is expanded in studies that consider repair and remanufacturing of sometime non-repairable components such as wind turbine blades [28]. In this study of repairing wind turbine blades it is shown that with relatively small defects (low volume ie. ~10%), laser direct deposition is favorable over remanufacturing of a turbine blades showing at least 45% reduction in carbon footprint and 36% reduction in total energy use. The primary drawback to AM when considering end of life concerns high cycle fatigue of AM products, where there is a presented need to link sustainable aspects with better surface roughness and fatigue life [29]. Nevertheless, some of these issues can be countered by optimizing printer process parameters for better material properties [30].

With developing methods to better advance sustainable design for AM there is potential to increase product life cycle sustainability. Additionally, by reducing product lead time, transportation, and the need for remote factories AM has potential to shorten product supply chains and eliminate steps in product development. Consequently, environmental impact of products produced using AM can be improved from cradle to gate. Combined techniques shown in referenced literature offer potential to reduce steps in the manufacturing of products by the use of several mechanisms. It’s been shown how remanufacturing of products decreases the demand for

raw material and saves on energy as well. The comparison of wind turbine blades is displayed in Figure 1.3 exemplifying this scenario [28].

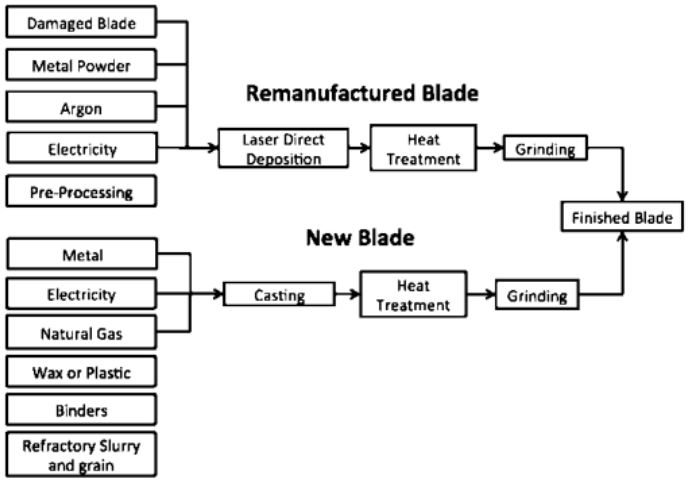

Figure 1.3 Wind turbine blade remanufacturing using LDD vs new blade production [28].

In the early stages of AM, prototyping was made the primary focus which eliminated the need for part transportation or outsourcing component manufacturing. The same is true for producing final components using AM. Additionally, with the added value of being able to produce unibody components, overall assembly is reduced. All considered, if suggested mechanisms are adopted into manufacturing and design, AM offers significant opportunities for improved life cycle performance of a variety of products. By advancing our understanding of AM life cycle inventory in adopted processes, designers can further the use of this technology to improve product performance in a more dynamic and comprehensive way.

1.2 Introduction to Study

Fused deposition modeling (FDM) 3D printing is one of the most widespread AM technologies in use [31]. FDM printers work by extruding molten filament layer by layer onto a print bed to produce a desired part, this process is shown in Figure 1.4. Due to the material variety, low cost, machine simplicity, and time to print it is the desired choice of AM in many industries. To better understand the environmental footprint of this technology it is crucial to investigate life cycle inventory (LCI) i.e. input and output material and energy flows. Several studies have been

conducted investigating particle and gaseous emissions from FDM during the print process [13], [32]–[36]. It has been shown that ultrafine particle emission (UFP) and both volatile and semi-volatile gaseous emissions is ubiquitous at various concentrations during all stages of the printing process in said studies. To properly assess LCI and apply more accurate input/output flows to overall life cycle assessments of products produced by FDM, a better understanding of the primary cause of said emissions and energy flows must be further investigated.

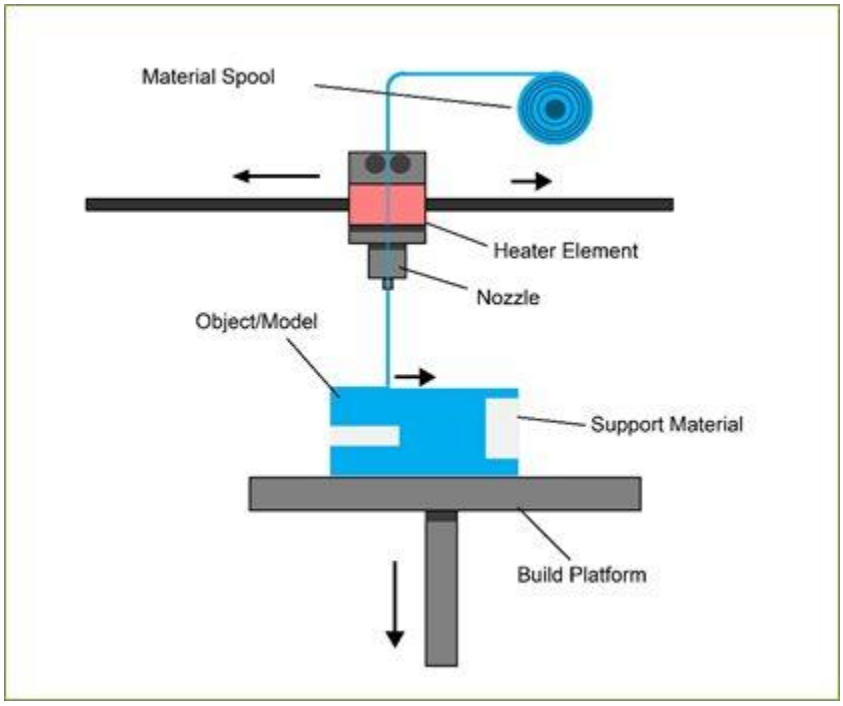

Figure 1.4 Fused deposition modeling printing process [37]

Studying any product or process requires development of an understanding of both how and why observed behaviors occur. While it has been recognized that UFP and VOC emissions are a byproduct of the FDM process, the correlation between emission and what is happening during the printing process has not been thoroughly investigated. Investigations of how printing process parameters effect specific energy consumption yield results showing parallels between the two [38], however that is likely due to the resulting change in overall print time. Here geometries are also investigated but there is still a missing connection between particle emission, energy consumption, nozzle movement, and extrusion rates. Without the knowledge of how printer

procedures impact emission and energy consumption an accurate LCI model cannot be fully achieved.

With confirmed particulate and gaseous emissions at notable concentrations it becomes increasingly important to identify the chemical and molecular makeup of said byproducts. The effects of UFP exposure to the lungs is somewhat understood. Studies have shown particle-laden macrophages and chronic inflammation is a possible and perhaps probable outcome resulting from UFP exposure at high concentrations [39]. As particles decrease in size the reactivity tends to increase because of the increased surface area to volume ratio [40]. For this reason, characterization of emission off FDM printers is essential to fully understand environmental and human health impacts. Obtaining this information could better mold a more accurate life cycle assessment of FDM technology.

Procurement of known LCI impactors is a step towards developing useful tools in LCA assessment of AM processes. Useful unit process models can offer aid in determining accurate predictions of input/output flows based on set printer parameters and part geometry. Some attempts have been made in modeling energy flow for FDM and how it relates to process parameters through the use of computer-based mathematical modeling [41]. Nevertheless, few have attempted models that rely on a combination of printer specifications and physical/chemical properties. By developing a calculable correlation between a printed part and the printer itself, quantifying LCI flows is achieved with a better understanding of how to optimize process parameter and part specs for a lower overall life cycle impact.

The purpose of this study is to essentially tie all of this together to create a better process for FDM life cycle analysis. With known particle and gaseous emissions there was an effort to identify primary causes and correlations of emission during the printing process. From this research, suggested solutions can be drawn to decrease overall LCI impact. Considering the high concentrations of shown emissions it was important to characterize the composition of FDM output flows to better understand the effects it may have on environmental and human health. Finally, to draw a line that connects this all together a unit process life cycle inventory model is developed to represent input/output flows resulting from FDM production. To show how these models can be similarly applied to other AM process this model is transformed to work with another one of the most popular AM processes; stereolithography (SLA) or mask image projection. The information from these models can be further applied to LCA studies to increase cradle to grave impact

assessment accuracy on both an environmental and human health level. A simplified approach to this research is shown in Figure 1.5 to better understand how each chapter is connected. The work performed succeeded in accomplishing the goals outlined in Figure 1.5 to target the objective to investigate LCI of FDM 3D printers with the purpose of applying more accurate and better understood LCA predictions.

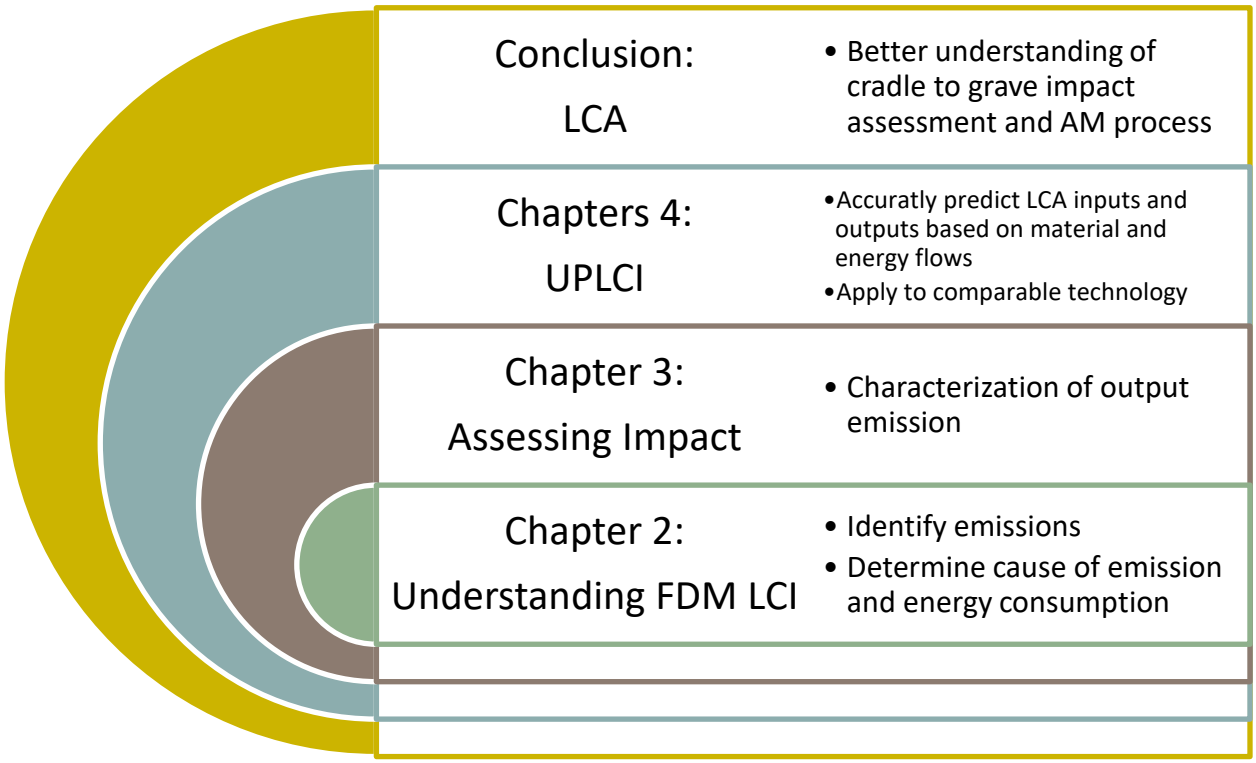

Figure 1.5 Overview of research approach for what is needed to end at desired outcome.

2. AN EXPERIMENTAL STUDY ON THE ENERGY CONSUMPTION AND EMISSION PROFILE OF THE FUSED DEPOSITION MODELING PROCESS

Throughout the past decade the popularity of additive manufacture (AM) has grown substantially. Although AM has been deemed as an environmentally friendly alternative to traditional processes, there have already been several studies done showing that AM processes can affect human health and the environment by emitting particles of a dynamic size range into its surrounding during a print. The objective of this study is to look deeper into the issue of particle emissions and to investigate energy consumption from one of the most popular AM processes i.e. fused deposition modeling (FDM). Particle emissions from a Makeblock and Monoprice Ultimate 3D printer enclosed in a chamber and placed in a Class 1 cleanroom are measured using a high temporal resolution electrical low pressure impactor (ELPI) which takes close-to-real-time measurements of particles in the range of 6-200nm. A honeycomb cube with side length 1.25" and the NIST standard testing part are printed using acrylonitrile butadiene styrene (ABS) filament. Results show that particle emissions are closely related to the filament residence time in the extruder while less related to extruding speed. The initial spike of particle concentration right after printing starts is likely due to the long time needed to heat the extruder and the bed to the desired temperature. It is suggested that part geometry/features and build path could significantly affect particle emissions. TEM images suggest that particles may be formed through vapor condensation and coagulation of small particles. Results are further investigated to explore how operating procedure and printing parameters affect the energy consumption and particulate emissions. Experimental data suggests that particle emission is mainly the result of condensing and agglomerating of semi-volatile organic compounds. The initial emission spike occurs when there is dripping of semi-liquid filament from the heated nozzle and/or there is residue left in the nozzle between print cycles. Printing speed and material flow have effects on particle emission rate but the effect is small. Power profile analysis indicates that print bed heating and temperature maintaining is the leading contributor to total energy consumption.

2.1 Introduction

Throughout several years manufacturing has continued to change and evolve as designs and products become more complex and advanced. Improvements in product geometry and material composition add to functionality and performance of products but can become extremely challenging to accomplish using traditional manufacturing techniques. To address this challenge, additive Manufacturing (AM), or 3D printing, has been suggested as a promising alternative. In the past, AM has mainly been used for the purpose of rapid prototyping of various designed parts and equipment while recent development has opened the door for other applications. There are many advantages of AM in a production setting, including the capability of making parts with various geometric complexities, advancements in material compositions, shortened supply chains, increased supply chain proficiency, lower environmental impacts, higher material utilization efficiency, and much more.

There are many different types of additive manufacturing techniques including fuse deposition modeling (FDM), Binder Jet Printing, Sheet Lamination, and Selective Laser Sintering (SLS). Each form of additive processing utilizes different forms of technology to adhere material layer by layer, causing each to have individual advantages and disadvantages. For example, it was concluded that for FDM to be more cost efficient than injection modeling the total production would have to be less than 7,500 parts [42]. In general, it is believed that additive manufacturing is preferred over traditional manufacturing techniques when considering material efficiency, geometric complexity, and prototyping lead time. It should also be noted that additive manufacturing is only in its early stages of development and much improved performance is expected.

Improved environmental performance has also been claimed as one of the advantages of AM processes. A common method to evaluate environmental performance of a process is life cycle assessment (LCA). LCA considers not only the direct process emissions and energy consumption, but also the resources, energy, and emissions associated with the production of feed materials. Some studies have already been conducted on LCA of AM processing and how it compares to traditional manufacturing in different industries [43] [44]. For example, by rapidly integrating AM into the production of specified aircraft components, complete life cycle primary energy consumption can be reduced by a range of 70-173 million GJ per year by 2050 [43].

Nevertheless, AM is not free from environmental impacts as it consumes materials and energy while generating emissions during operation. Experimental studies to determine total energy consumption of AM processes have been conducted for laser sintering [45], stereolithography [46], selective laser melting (SLM), electron beam melting (EBM) [47], and FDM [48]. For FDM, energy consumption and carbon footprint increase as the shape of the part becomes more complex [48]. Some efforts have been made to develop energy model and optimize process parameter to minimize energy consumption for stereolithography process [46] and FDM [49]. There have also been efforts to develop models to estimate feedstock, fluid, and energy consumption [19].

In addition to material and energy consumption, several studies have reported particle emissions as well as volatile organic compound (VOC) emissions from various AM processes. It should be noted that in referenced LCA studies, direct process emissions were not considered. Similar to other manufacturing processes, additive manufacturing involves heating and use of solvents in some cases, so air emissions are expected. Recent studies have shown that ultrafine particles (particles less than 100nm in diameter) are being generated during the FDM process at significant magnitudes. The number of particles generated and particle size range can be attributed to several factors but most important is the type of printer and the feedstock materials that is used. In addition to particle emissions, volatile organic compounds (VOC) have been reported as byproducts of this manufacturing technique. A study done assessing particle characterization and VOC emissions from binder jetting reported that due to the dry powder inside the printer chamber and the binder fluid, this type of AM processing emits measurable amounts of fine particulate matters and VOCs. Particle sizes were reported to vary between 205 and 407 nm for higher emission counts. Additionally, VOC concentrations were reported to be above the upper limit recommended by the Environmental Institute of European Commission [50]. This study, like many others, used both scanning mobility particle sizer (SMPS) and optical particle sizer (OPS) instruments to measure particle emissions in 1 min increments [50].

Among the various types of AM processing Fused Deposition modeling (FDM) is one of the most popular forms of 3D printing. This process works by heating thin plastic filament to a temperature high enough to soften the plastic so that it can be extruded onto a surface layer by layer. There are different types of material that go into 3D printing depending on the type of printer and the overall goals of what to achieve out of the products. The two most popular materials

currently used in FDM are polylactic acid (PLA) and acrylonitrile butadiene styrene (ABS) plastic. One of the important properties of the material that is used in additive manufacturing is its thermal properties. These thermal properties attribute to changes in the nozzle temperature during extrusion and the printing bed temperature of the printer. For example, PLA does not require layering over a heated bed while ABS does, however, ABS tends to show superior material properties when compared to PLA.

FDM printers have been shown to have particle emissions at significant magnitudes while printing both ABS (acrylonitrile butadiene styrene) and PLA (polylactic acid) filament. ABS filament has been shown to have a much higher particle emission count than PLA. Particle counts 33-38 times higher when printing ABS compared to PLA have been observed [51]. Additionally, particle sizes were found to be less than 100nm in diameter for 96% of emitted particles using ABS filament and 98% of PLA particles. Reported emission rates were 10^6 to 10^{11} #/min [51], [52]. A study analyzing 3D printer emission of UFP's and VOC's for several different filament types also reported the highest emitting filament to be ABS with a median ranging from $2x10^{10}$ to $9x10^{10}$ #/min. The lowest emissions reported from this study was from PLA filament having a median UFP emission rate of ~10^8 #/min. This study suggests that printer emission is primarily affected by filament type with minor attribution from nozzle and bed temperatures. The study used a TSI model 3007 condensation particle counter (CPC) logging at 1 min intervals. VOC emissions were also on the lower side for PLA ranging from 8-14 µg/min. ABS VOC emissions were much higher ranging from 25-65 µg/min [53]. Volatile organic compounds are therefore shown to have emission rates in correspondence with ultrafine particle emission during printing [53]. Additionally, it has been indicated that when testing several different types of filament ABS is among the highest emitter for VOCs, not just UFPs. VOC emissions when printing with ABS has been shown to range anywhere from ~10 to ~110 µg/min. [53]. It is also interesting to note that there was an initial spike of particles emitted from the printer before steady state emission rates were reached, but no explanation was given [53], [52].

Much less work has been done to reveal the mechanisms of air emissions during AM. Nevertheless, there is evidence that particle generation within the vicinity of the extrusion nozzle is due to the high concentrations of semi-volatile compounds (SVCs) which are emitted from the high temperature extruded filament. The SVCs may include semi-volatile organic compounds among other species associated with the filament, in this case ABS. It has been suggested that the

concentration of SVCs decreases as condensation of the compounds onto pre-existing particles occurs. Once printing begins the vapor concentrations increase until a substantial rate of new particle formation occurs due to nucleation of emitted semi-volatile vapors. After the formation of particles suspended in air, substantial growth has been detected to sizes greater than 7nm in diameter. Additional evidence has been presented showing that as nozzle temperature increases particle formation rate increases [32]. Several studies have suggested the growth and overall particle size distribution is attributed to coagulation of particles as they condense in the surrounding environment [52] [32] [33].

Previous research has also suggested that particle emission in FDM printers was likely due to residence time of filament siting in the extrusion nozzle. The possible cause of this is due to the chemical breakdown of polymer chains in the plastic as the filament begins to heat up [33]. This would explain the results shown in several publications indicating that ABS filament has much higher emission rates when compared to PLA considering that ABS is extruded at a much higher temperature than PLA onto a heated printing bed. Measurements conducted in controlled environments such as a cleanroom facility have yielded more conclusive results than those in less regulated areas. In the majority of the studies equipment used to measure particle emission rates and size distribution has included electrical low-pressure impactor (ELPI), scanning mobility particle sizer (SMPS), and optical particle sizer (OPS) in 1 second or 1 minute increments of a large size range. Several papers had shown results of a spike in particle emissions right after printing starts [53] [32] [33]. It has been hypothesized that by reducing the amount of time filament sits inside the extruding nozzle of a 3D printer, the particle emissions may potentially be reduced [53].

FDM printers have gained popularity among small size enterprise and home users due to low cost. While there is a good understanding of the fact that FDM printers do in fact have an issue with particle and VOC emissions there is no deep understanding on how changing operating procedure and printing parameters may affect this issue. In addition, the primary cause of particle emissions has only been hypothesized. Generation of these emissions can affect the health of both humans and the environment thus demonstrating the need for further investigation of the process. Additionally, to better understand why these particles are being emitted at their given rates measurements need to be taken in a more closed off environment to eliminate most of the background noise. In this study, focus is put on revealing the correlations between particle

emissions and process conditions during FDM such that the formation of particulates can be better understood. Electrical energy consumption during FDM printing is also measured and analyzed. It is expected that findings from this study could shed light on how to design and operate FDM printers for reduced air emissions and energy consumption. A better understanding on how particle emissions affected by printing conditions could guide the design and operation of 3D printers for reduced environmental impacts.

2.2 Methodology

2.2.1 Methods for Initial Emission Measurements

The 3D printer used in the 1st part of the study was a Makerbot Replicator 2X, one of the popular 3D printers used by personal users and small businesses. This Makerbot model came equipped with a heated printing bed making it capable of printing ABS. A TSI NanoScan scanning mobility particle sizer (SMPS) was used to measure particle emissions. This piece of equipment works by charging particles in the airstream and enlarging them in a liquid (usually isopropyl alcohol) to better count the number of particles being emitted. The particle size range detected by SMPS is 10-420nm.

Testing was done in a 12x8 foot office space and air circulation in the room was shut down during testing to avoid particles entering the room through the air inlet. Each test began with a 10 minute printer warm up and a 30 minute background measurement in the room to establish a baseline reading. During testing the door remained closed with only one person running tests in the room.

Once background measurements were established a cube with 1.25 inch sides was queued to print with a nozzle temperature of 230°C and heated bed temperature of 110°C as recommended by the manufacturer. Standard settings were used to print the cube including 20% infill and a 0.2mm layer height. Additionally, prints were made with a 0.5mm raft to create a level base for the part.

It should be noted that the experimental setting used in the preliminary study could not avoid interference from the surroundings. More importantly, very limited temporal resolution can be achieved due to the sampling frequency of SMPS. Since the printer is sitting in a large room and the diffusion of particles cannot be controlled, it is almost impossible to estimate the total amount

of particles emitted over the entire printing process. To gain better understanding on how variables such as features/geometry, building path, and printing parameters affect particle emissions a better experimental setup is needed.

For the 2nd part of the study, a Makeblock mElephant 3D printer made up of an aluminum frame was put into an enclosed chamber. A heated bed was added to the printer in order to print both PLA and ABS. For the chamber a filter box with 18" sides and 14" diameter inlets and outlets was used. This chamber was made of stainless steel so that particles would not react with the walls after being emitted. The outlet of the chamber was directed into a fume hood. A hole was drilled a foot away from the outlet of the chamber to allow for a non-static conducting tube to be inserted and attached to the sampling equipment. A small fan was added to the outlet side of the duct in order to force air flow through the chamber. The fan was a 90mm x 90mm x 25mm PC cooling fan that ran at 3V and 0.12A to produce airflow close to 7CFM. The system was put inside a Class 1 cleanroom to essentially eliminate background interference from measurements.

Rather than using an SMPS for this set of testing an electrical low-pressure impactor (ELPI) was used. The ELPI measures airborne particle size distribution in an air stream in almost real-time. The advantage of using and ELPI rather than SMPS is that it runs one second scans rather than scanning every minute thereby increasing the time-resolution and giving a better picture of how process conditions affect particles emission. Another added benefit of the ELPI is the ability for it to detect particles down to 6nm, increasing the range of detection and providing additional information on potential particle agglomeration. Figure 2.1 shows the setup of the equipment in the cleanroom.

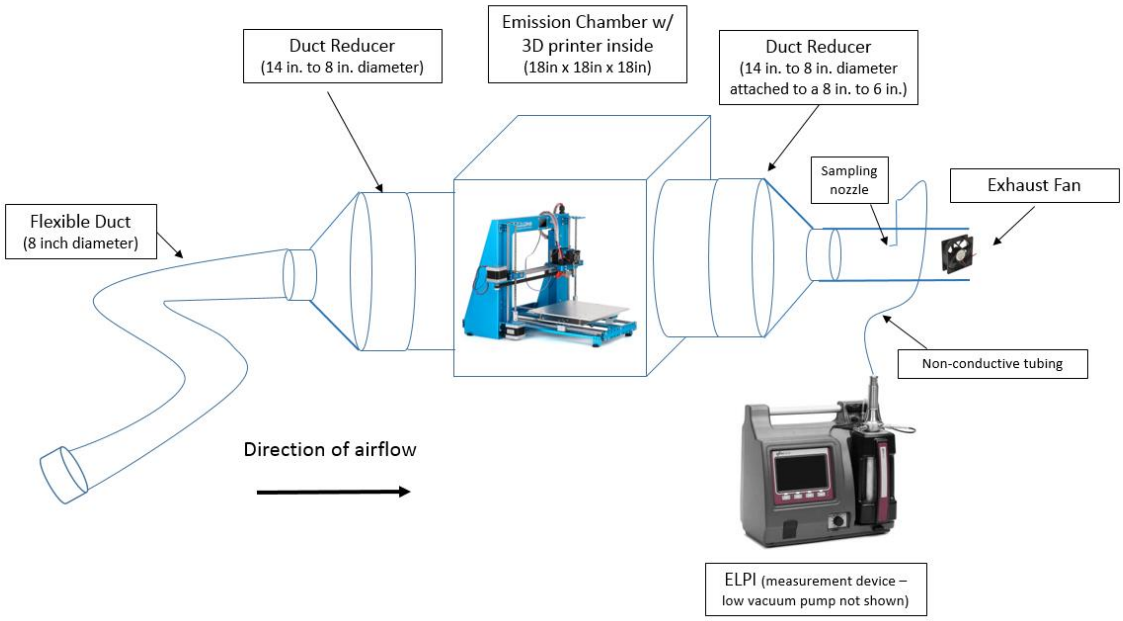

Figure 2.1 Schematic of the testing chamber system

While testing with the ELPI it was important to perform a leakage check to ensure the impactor was assembled correctly after it was opened to replace the foil substrate. Once the leakage check was passed the ELPI was allowed to run background measurements in the cleanroom for 30 minutes to stabilize in the ambient conditions. After the 30 minutes passed a zero check was done to establish a baseline. The zero check required the air pump on the ELPI to be turned on so that the air flow entering the device would be diverted and filtered before entering the impactor. With the ELPI zeroed the charger could be turned on and chamber background measurements could be taken before the printer turned on. After the background was complete the printer was turned on to start the printing process and then another 20 minute cool down measurement had to be taken when printing finished.

For the 2nd part of the study there were two different parts that were printed. In addition to the cube that was used in the 1st part of the study, a standardized part for additive manufacturing released by National Institute of Standards and Technology (NIST) was also printed. An image of the NIST part with all of its features is shown in Figure 2.2. The NIST standard part was designed with geometric complexities to test performance of different printers.

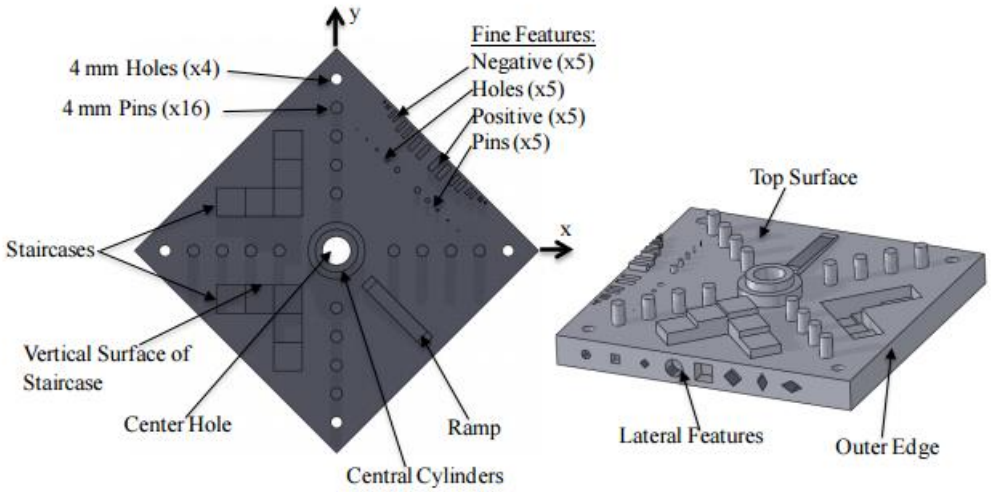

Figure 2.2 NIST standardized 3D printing test part

2.2.2 Methods for Testing Impact of Changing Printer Parameters

The FDM printer used in this study is a Monoprice Ultimate 3D Printer. This Monoprice model comes equipped with a heated printing bed making it capable of printing ABS, which is the filament material used. The printer has a 348 mm x 264 mm x 430 mm aluminium frame which avoids static charge building up and particle collection. A TSI NanoScan scanning mobility particle sizer (SMPS) and a TSI Optical Particle Sizer (OPS) are used to measure particle emissions. The particle size ranges detected by SMPS and OPS are 10-420nm and 420nm-10μm, respectively.

Figure 2.3 shows a schematic diagram of the experimental setup. All experiments were done in a fume hood located in a FS209E class 1 or ISO 14644-1 class 3 cleanroom to essentially eliminate background interference while taking particle emission measurements. The printer was sealed from all sides with one air inlet and one outlet. The diameter of the exhaust pipe was 56.19mm and the length was 165.1mm with a 73mm square opening at the end for an exhaust fan. The fan operates at 12V, 0.12A, and has a flow rate of 24.4 CFM. At two points in the exhaust pipe the collectors (non-conductive static free polycarbonate tubing) for the SMPS and OPS were attached for particulate measuring. The sampling point for the SMPS is closer to the printer as finer particles are the main focus. Mixing of the air within the printer was achieved by the fan attached to the printing nozzle. The sheets used to seal off the rest of the printer are made of static dissipative polycarbonate Plexiglas or printed pieces covered with air duct aluminium tape to minimize charge building and particles sticking to the walls.

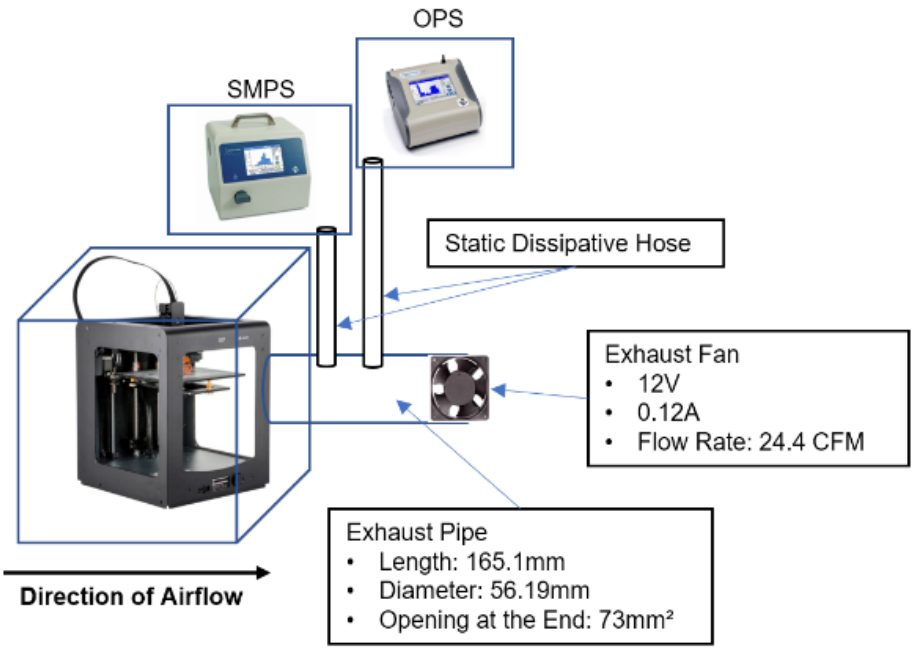

Figure 2.3 Schematic of testing setup inside cleanroom fume hood

Each set of the measurements begin with a 10-minute background measurement, before the printer warms up, to establish a baseline reading. During testing the fume hood was only open approximately 4-6 inches to allow for adjustments on the printer but ensure that the effluent air from the fan was not escaping the fume hood.

A series of experiments are conducted to test three major hypotheses including:

- Residence time of filament sitting inside heated extrusion nozzle contributes to the overall concentration of suspended semi-volatile compounds, thereby increasing new particle formation rate.
- The larger surface area of semi-liquid filament in contact with air, the higher the particle emission rate.
- Heating up the print bed platform and maintaining its temperature dominates electricity consumption.

To test the first hypothesis a 1.25 inch cube with 100% infill is printed and printing is periodically stopped for prolonged periods of time to investigate the effect of residence time of filament sitting in the heated nozzle on particle emissions. Once background measurements and printer warm-up are completed the printer proceeds to print for 10 minutes before the printing is paused for 1 minute and then allowed to print for another 10 minutes. This process is repeated with

pause times of 3,5,7,10, and 15 minutes between the 10-minute print windows. The printing is then allowed to continue for another 10 minutes after the 15-minute pause before the print is terminated and cooldown commences. Measurements are taken during the cooldown period as well.

Additional testing of the first hypothesis is done by adjustments of the printer speed and material flow during printing to measure the effects of these parameters on particle emissions. By adjusting printer speed and material flow from their default settings the duration of filament sitting in the heated portion of the nozzle before being extruded is altered. Default parameters for the printer are shown in Table 2.1. An increase in print speed will increase the entire process of printing by changing all printer parameters related to travel and extrusion simultaneously from the default settings. Higher speeds will decrease the filament residence time in the nozzle. Material flow offsets will only change the rate of material extrusion from the nozzle thus also changed layer thickness of the print. Increased material flow settings will also decrease filament residence time. After background measurements and printer warm-up the printer is allowed to print for 20 minutes on default settings of (100% speed and 100% material flow). Speed is then changed to 150% for 10 minutes, decreasing to 100%, 75%, 50%, and 25% for 10 minutes each for a negatively sloped linear pattern. After such measurements speed increased back to 100%, where it remained for the rest of the test. The same process is followed in regards to variations in material flow. 15 minutes of data is collected at default settings to finish testing. Printing is then stopped and cooldown commences. Data is taken during the cool down phase as well.

Table 2.1 Printer Default Parameters

Nozzle Diameter	0.4 mm
Outer Shell Speed	15mm/s
100% Infill Speed	50mm/s
Speed without extrusion	80mm/s
Material Flow Rate	2.5mm^3/s

In an effort to test the second hypothesis efforts are focused on the printer warmup period where dripping of semi-liquid filament is most likely to occur. The same 10 minute background measurement is taken again to establish a baseline. However, before the background measurements

are taken the filament is retracted upward into the nozzle about 20-30mm. This places the filament out of the heating zone of the nozzle and prevents any filament from dripping out of the nozzle in a semi-liquid/semi-solid state while the print bed is heated from ambient temperature to 110℃. The printer warmup period (heating of the extruding head and then the printing bed) occur after background measurements and then a print of a cube with 20% infill is started. After about 15minutes of printing all measurements are taken and printing is terminated.

To test the effects of filament residual within the nozzle during printer warmup period extra measurements are taken with the nozzle thoroughly cleaned first with a 0.11mm guitar string and then by heating the nozzle to 260℃ and allowing it to sit for 24 hours at that temperature to assure that all residual plastics were burned out of the extruding head. This is all done after removing the filament completely and then returning the filament into the nozzle 20-30mm above its normal position to prevent dripping during warm-up.

Final testing is done regarding the 2nd hypothesis to determine how distance between a 230℃ extrusion head and printing bed affects particle emission while dripping of semi-liquid filament is occurring. To do this the bed is manually lowered to three different levels from the extrusion nozzle. First a 10 minute background measurement is taken to establish a baseline, then the extrusion nozzle is heated from ambient temperature (22℃) to 230℃. Once the desired temperature is reached filament is manually extruded out of the nozzle for 1 minute at the first bed distance of ~15cm. Once measurements are finished the heated nozzle was shut off and the bed is raised to the next distance of ~8cm. The same procedure is followed at distances of 15cm, 8cm, and 1mm. The nozzle is allowed to cool below 100℃ between bed level changes.

To test the 3rd hypothesis, power profile is recorded during printing with different speed and material flow setting. The part to be printed is again the 1.25-inch cube. A WiTenergy Smart Socket electrical energy meter (Model Number: E100S) is used to log energy usage data every 1 minute. The input/output voltage and max loading of the energy meter are 120 VAC, 60 Hz and 15A/1800 W, respectively. Each test begins with a 10 minutes background measurement and has 10 minutes of cooling after printing.

2.3 Results and Discussion

2.3.1 Initial Emission Measurements

Figure 2.4 shows particulate concentration measured using SMPS for several repeated experiments over a one-week period (part 1 of the study). As mentioned before, during the 1st 30 minutes the printer is on but heating of extruder/bed printing is not started. Particle concentration was measured to establish the baseline. At Minute 31, the heating element is turned on and at about Minute 40 the extruder and the bed reach desired temperature and printing started. It can be seen that in each run there was a spike in concentration of particles when printing starts, followed by a sharp decrease after 5 minutes. Once that low point was reached particle concentration slowly increased over the course of printing until printing was finished and another spike was observed during the nozzle and bed cool down period. Each test followed the same general trend with the greatest difference being in the initial spike in concentration during the start of printing.

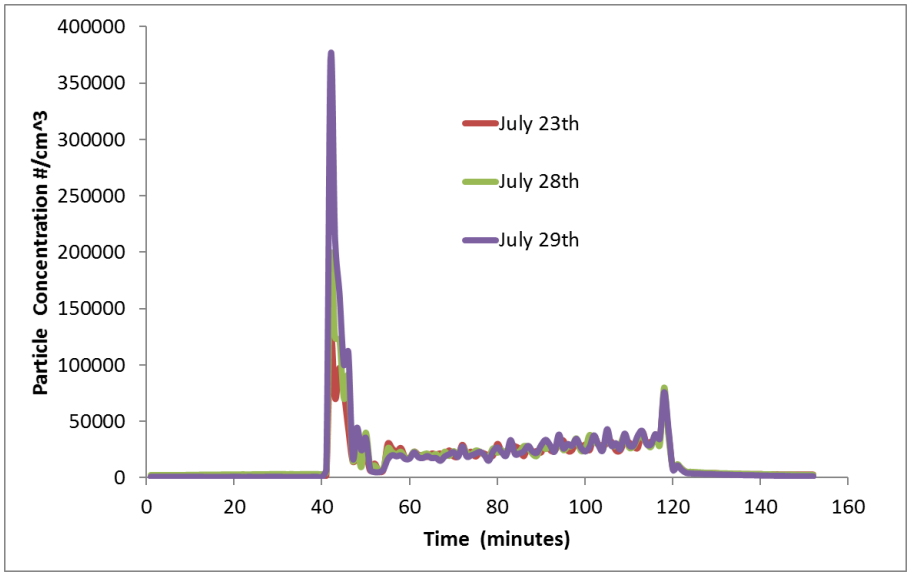

Figure 2.4 SMPS particle concentration measurements over a one week period

These tests confirmed that the 3D printer emits elevated concentrations of ultrafine particles (UFP's) in the office environment. The initial burst of particles right after printing starts was an interesting occurrence. During the heating phase the nozzle and bed temperatures increased from ambient temperature to a temperature of 230°C and 110°C, respectively. During the printing phase

the temperatures remained constant. Movement of the nozzle during printing is another major difference between these two phases. The extruder remains still during the heating and follows the design of the part during printing. Figure 2.5 shows the difference between the heating and printing phases.

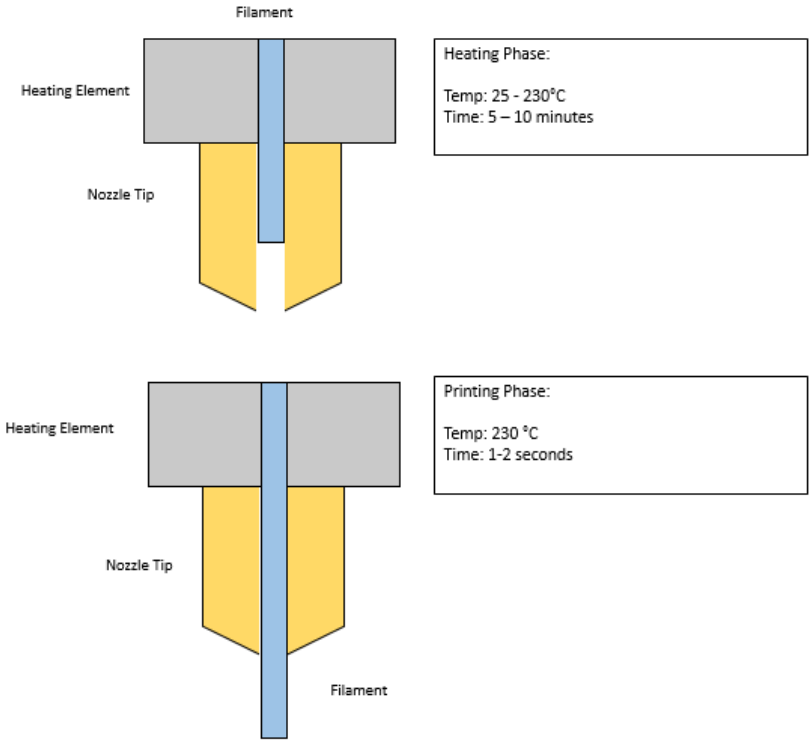

Figure 2.5 Difference between the heating and printing phase of testing

It became clear during analysis of results that the filament has a much longer residence time during the pre-printing heating phase. This residence time could lead to overheating of the filament and cause polymer decomposition and consequently the initial burst of particle emission. The glass transition temperature of ABS plastic is 110°C; at this temperature the plastic begins to soften and the bonds between subunits in the polymer loosen. Exceeding this temperature will further weaken bonds and potentially release segments or even monomers into the environment as UFP emissions.

The sharp decrease on particle concentration 5 minutes after printing starts may have been a result of coagulation of smaller particles (solid or liquid) forming larger particles. This

hypothesis was supported by TEM images of particles captured during the printing process which are shown in Figure 2.6.

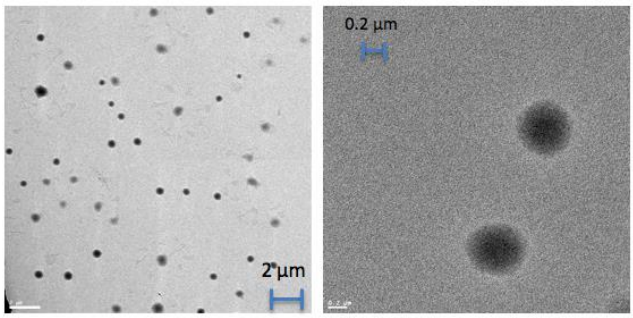

Figure 2.6 TEM images of particles captured during the printing process

As shown in the magnified TEM image the particles are dark at their core and spherical in shape enclosed by light colored rings. Without knowing the chemical composition of the particles, the dark core and lighter ring suggests that the particles started as a vapor/liquid droplet and solidified as they cooled. After the decrease in concentration, emission steadily increases and then peaked once again after the print was complete. The fluctuation in concentration could be due to printing path and speed while printing different features of the part.

By using the ELPI in the testing chamber described, measurements were close enough to detect real time shifts in particle concentration during the printing process. As expected from Part 1 of the study the same initial burst of particles was again observed. The concentration during the burst of particles was close to $1.0x10^7$ #/cm^3. The particle concentration remained elevated for the following 10 minutes until the raft had finished printing. Emission remained close to baseline until the top layer of the base of the part was started. The average concentration during this time was about $7.0x10^5$#/cm^3. Once the top layer of the base was started the concentration took a slight dip and increased only when the pin features were being printed where it reached a concentration of $4.0x10^5$#/cm^3.

By using the high temporal resolution of the ELPI we were able to take a deeper look into the behavior of particle emissions throughout the printing process as related to part features, shown in Figure 2.7. The initial burst of particles consisted mainly of particles in the size range of 10-50 nm. By taking a close up view of the initial burst it was observed that around 20 minutes the burst

starts and then the size of particles increases slightly from 30 to 50nm. Looking closer into the printing period it was observed that between the bottom side of the part and the base layer there were fluctuating particle concentration spikes at different points in time.

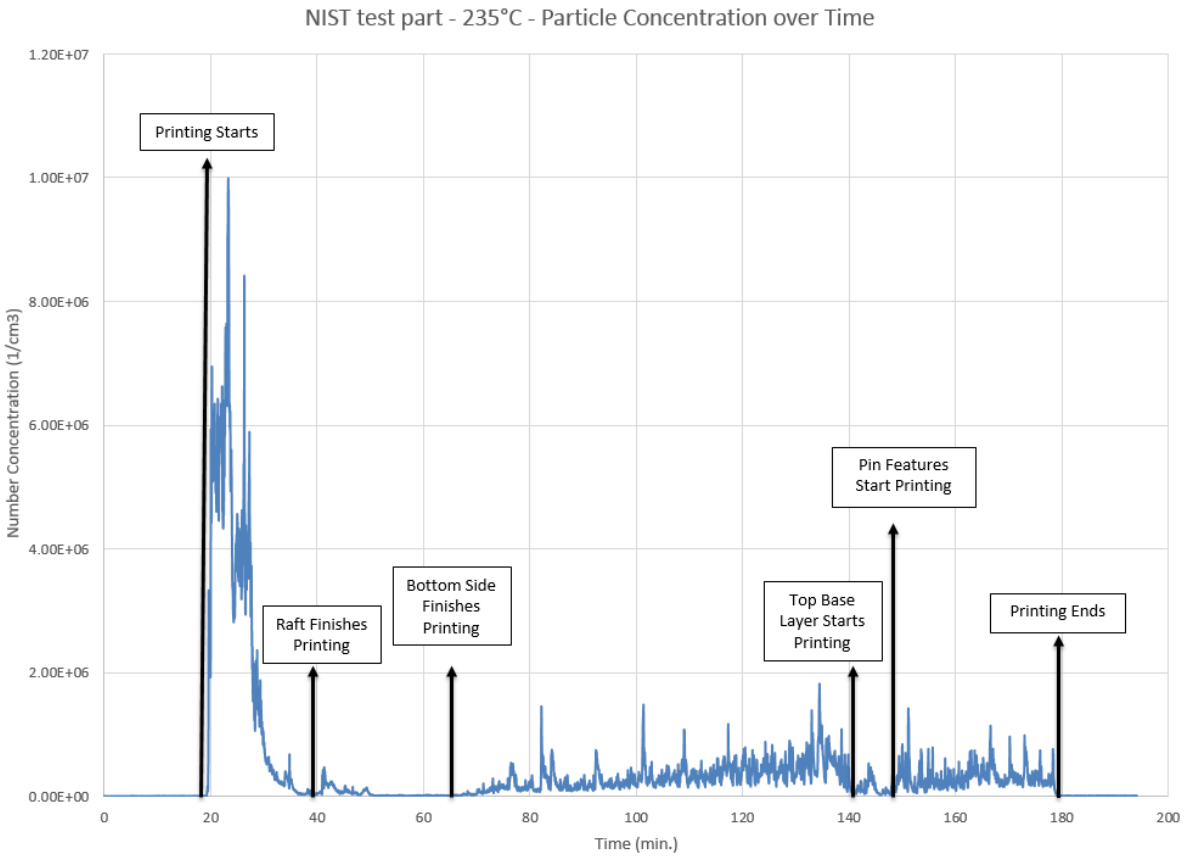

Figure 2.7 Particle concentration of NIST test part with respect to time

When the cube was printed using the ELPI and testing chamber, trends in results were very similar to what was seen in Part 1 of the study with bursts peaking at a concentration of $5.0x10^6$#/cm^3. The concentrations during cube printing is shown in Figure 2.8. The initial burst of particles observed was significantly smaller than that observed while printing the NIST part. Similar trends were seen after the initial burst with emissions running close to baseline and steadily increasing during printing of the infill layers. Particle concentration ranged from 7.0-$9.0x10^5$#/cm^3 during this period. A final spike was measured moments after printing ended with similar characteristics as the initial spike of particles.

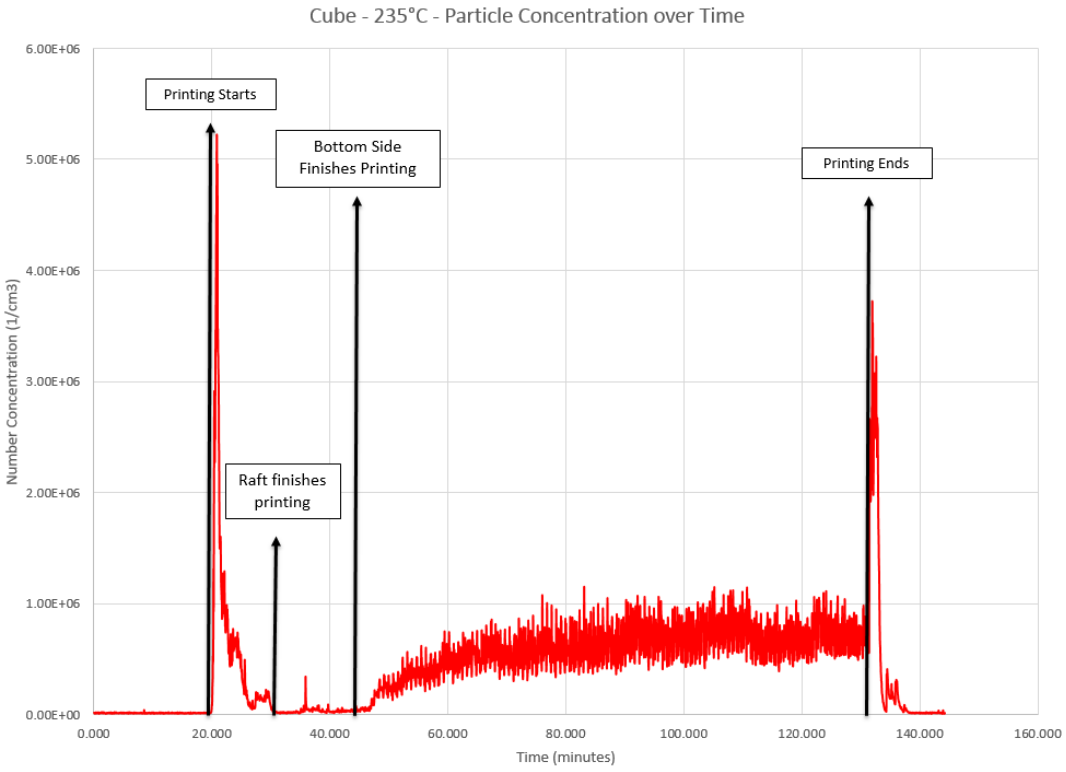

Figure 2.8 Particle concentration of test cube using ELPI with respect to time

Size distribution for the cube printing ranged from 6-200 nm. In the case of the cube printing the initial burst lasted only 1 minute before starting to decrease. Oddly enough there were no clear signs of particle growth or coagulation. Most particles were emitted between 20.5 and 21 with an average size of around 20nm. Looking deeper into the printing of the infill layers which made up 90% of the part a pattern was observed in density of particle emission concentration levels out shortly after the bottom layer of the part finishes printing.

Looking over changes in particle emission over time, the results seemed to suggest that particle generation was closely related to the type of layer that was being printed. Beginning with the base of the raft, this layer printed at the slowest speed extruding at a rate of 10mm/s to form thicker lines and a good base for the part to be printed on. The layer was made up of 1224.6 mm of filament and took 375.1 seconds to print. The average particle concentration was 2.20×10^{6}#/cm^{3}. The bottom side of the NIST part printed at an increased rate of 40mm/s at the outer edges and 90mm/s inside the edges. 865.43 mm of filament was used during the print of this layer and it took 285.0 seconds to print. During this time the average particle concentration was 5.45×10^{5}#/cm^{3}.

The middle layer, including infill, printed at a rate of 40-90mm/s made up of 140.45mm of filament and printing for 54.8 seconds. During this phase the concentration steadily increased until the top layer of the base was printed. The concentration was $7.32x10^5$#/cm^3. Results are shown in Table 2.2.

Table 2.2 Printing statistics of different layers extruded

Layer	Time to Complete (sec)	Filament Length (mm)	Extrusion per second (mm/s)	Average Concentration (#/cm^3)
Raft	375.1	1224.6	3.26	2.20×10^6
Bottom Side	285.0	865.43	3.04	5.45×10^5
Middle w/ Infill	54.8	140.35	2.56	7.32×10^5

Based on Table 2.2 there is no correlation between particle emission and amount of material being extruded. This implies that another factor must be contributing to particle emission. By observing the initial burst of particles most likely caused by heating of the filament in the nozzle, it seems logical to hypothesize that there is a correlation between filament residence time and concentration of emitted particles. The factors affecting residence time during the print are distance traveled by the extruder and extruding rate. That is when the extruder is traveling from point to point along the build path without extruding filament. Looking at the residence time data between the different layers it was observed that although the middle layer extruded less filament while traveling the same distance there was a higher residence time resulting in a higher average concentration of particles being emitted.

Examining residence time for the NIST test part was much more difficult than the cube due to all the complex features. There were four layers in the cube to be assessed, the first being the raft, then the top and bottom sides of the cube, and lastly two infill layers sandwiched between the top and bottom layers. Build path for each of these four layers can be observed in Figure 2.9. The extruding speeds between layers for the cube were the same as those reported for the NIST part.

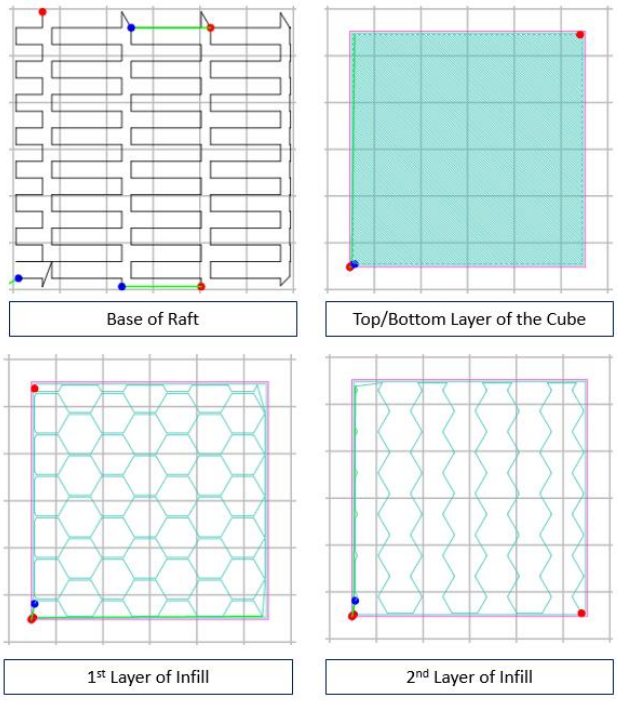

Figure 2.9 Build path of different layers of the test cube

By comparing the four layers it was observed that the raft print was part of the sharp decrease in particle concentration right after the burst at the end of the heating phase. Similar to the NIST part the cube raft was extruded at a slow rate of 10mm/s with short travel times. The top and bottom layers had an even shorter travel time comparted to time extruding. This suggests that the residence time was low for these layers. The low residence time for these layers corresponded to low particle concentrations. On the contrary the residence time of the infill layers was higher with low amounts of material being extruded. This is most likely the cause of the steady increase in particle concentration during the printing of the middle layers.

Although both parts were printed with a raft, the particle concentration and size distribution of the raft printing period had very different profiles. With respect to the base layer of the two parts they were both very similar with the only difference being that the base layer of the test part was much larger than the cube and contained a set of holes at each corner and in the middle. Even though the NIST part used more filament and was much larger, the particle concentration was much higher during most of the printing period of the cube than the printing of the NIST test part.

2.3.2 Effect of Printing Parameters and Filament Residence Time

While OPS measurements were taken, in correspondence with the SMPS, results from the OPS data are not included because the number of particles being emitted in the collection range of the OPS is not statistically different from background.

Figure 2.10 shows the particle emission rate from the residence time experiment where printing is paused for different time periods. An initial spike is observed as in previous studies. However, rather than at the start of printing the observed spike occurs when the extruding nozzle and printer bed are being heated close to target temperatures of 230℃ and 110℃, respectively. Excluding the initial spike Figure 2.11 shows a zoomed in plot for particle emissions after each pause. It can be seen that pauses in the printing process are in fact causing spikes in particle emission, however, duration of pausing does not have as much of an effect on the magnitude of the spikes as originally expected.

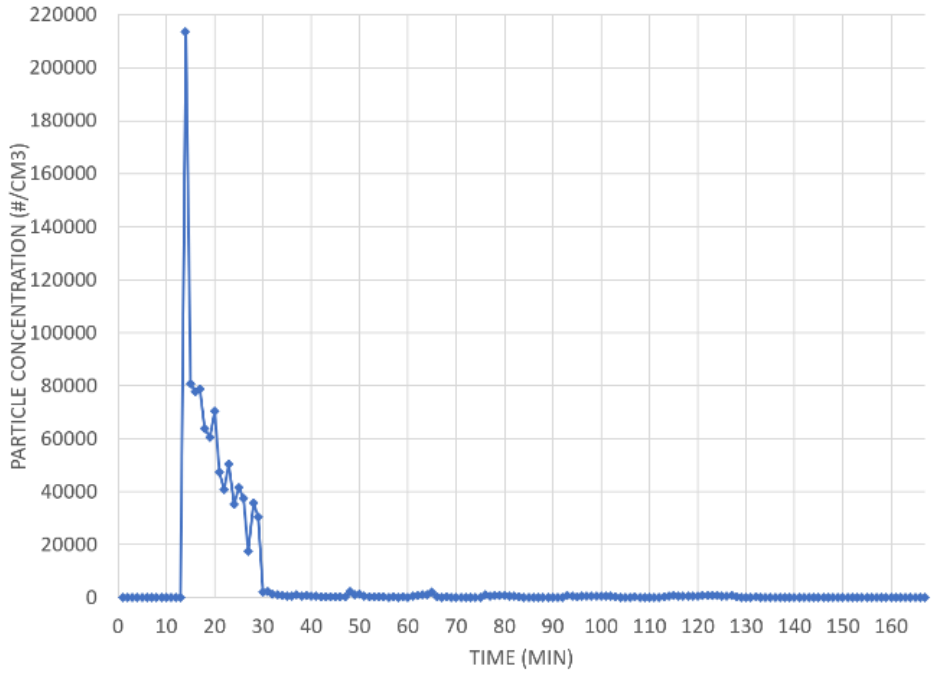

Figure 2.10 Printing test with different pausing period

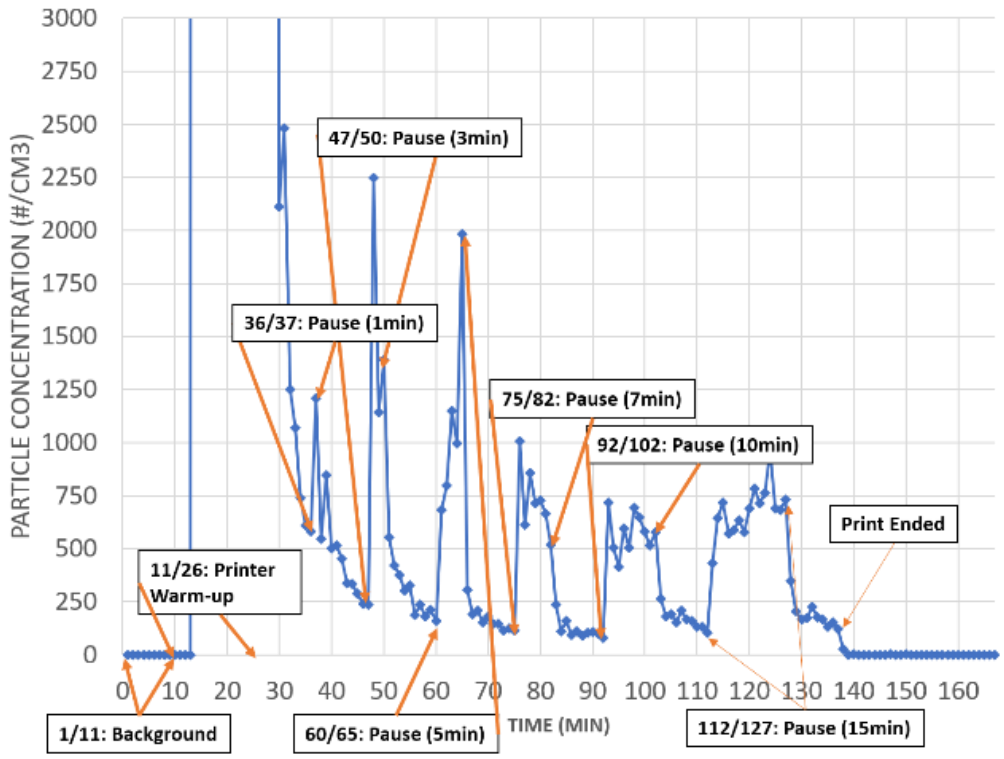

Figure 2.11 Zoomed in particle emissions with pausing periods labeled

The initial peak of particles emitted reaches around ~210,000#/cm3, however, the emission peaks during the pausing periods of the print are less than 2250#/cm3. Still, spikes in particle emission are observed with each pause in the printing process and a steep reduction in particle emission can be seen when printing resumes. While there is an increase of particles being emitted during the pauses in the print the peaks are much smaller when compared to the initial spike detected directly after the extruding nozzle reaches the desired temperature. While the duration of the pauses extends the duration of elevated particle emissions, the peak concentration of emitted particles does not increase with duration. Furthermore, it can be concluded that while residence time of filament sitting inside the nozzle contributes significantly to the particle emission it is not the leading factor causing the initial spike in particle formation.

If residence time had been the leading cause of the initial peak observed there would have been several changes in observed data. First the spike observed in Figure 2.11 would not have occurred right after the nozzle finished heating up (about 3 to 4 minutes after heating began i.e. Minute 14). The spike more likely would have occurred at the start of printing. Additionally, if these residence time tests were positive for the proposed hypothesis it would not have effected

duration of elevated emissions during the pauses in printing but rather spikes would have more likely been observed when printing began after each pause.

It should be noted that changing speed of printing as well as material flow would also result in variable residence times of filament sitting inside the extrusion nozzle before exiting onto the printing surface. This would offer no help in explaining the initial spikes observed but may explain how changes in emission occurs durng the printing of inner layers in a part.

Figure 2.12 and Figure 2.13 show results of changing speed and material flow. As the print speed increases from 25% of default speed to 150% the particle emission fluctuating between ~5,000#/cm^3 and ~19,000#/cm^3. As material flow increased particle emissions went from spiking near ~2250#/cm^3 to nearly 0. As material flow decreases the time filament is left in the nozzle increase so this is expected.

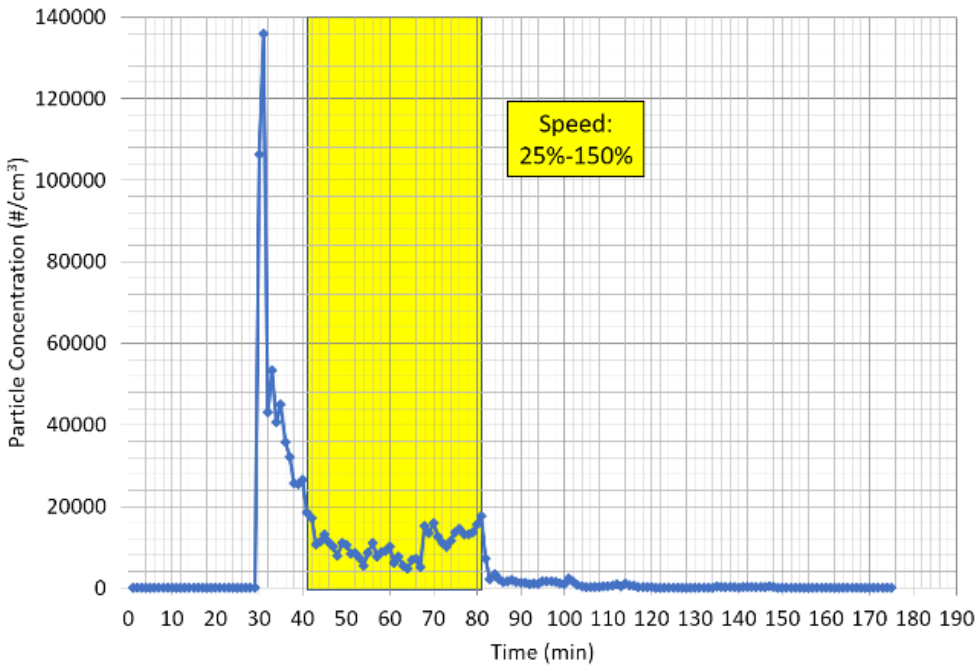

Figure 2.12 Linear change in print speed from default settings

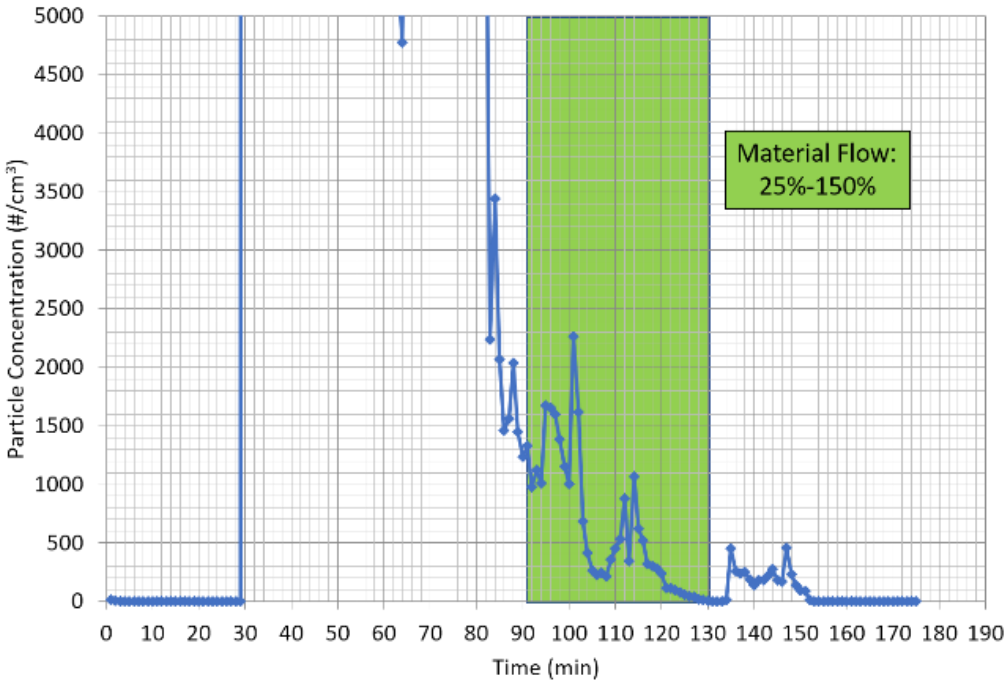

Figure 2.13 Linear change in material flow as offset from default settings

Although the hypothesis on residence time could explain changing particle emissions with printing parameters, it cannot explain the initial spike occurring before printing start. During experiments it has been observed that dipping of semi-liquid filament out of heated nozzle is correlated with particle emission spike. Filament being extruded above the glass transition temperature begins to cool immediately after it hits the surface it is being deposited onto. Before that the semi-liquid filament is exposed to air and could emit semi-volatile compounds which are in turn condensed to become particles. To avoid dripping during nozzle heat up, filament is retracted back into the nozzle 2 to 3 cm before test. Emissions have been observed in all measurements taken around minute 13 or 14 (i.e. right after the nozzle reached 230℃). The nozzle temperature could reach as high as 240℃ after heating finishes and then cools to 230℃. This is exactly when the initial spike is observed and nearly every test exhibits dripping of semi-liquid filament out of the nozzle.

Results from these tests are shown in Figure 2.14. The first 10 minutes of background measurements are nearly 0 as expected and there is a spike of particles emitted at minute 13, right after the nozzle finishes heating up. This spike nears 475,000 #/cm3.

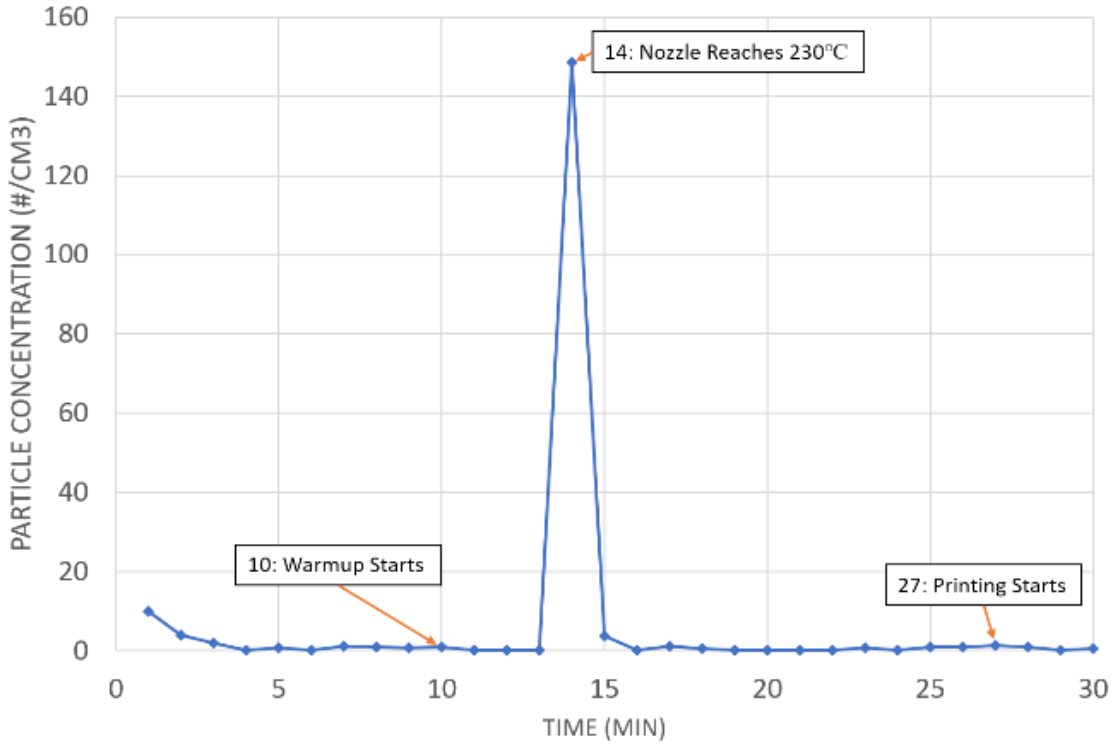

Figure 2.14 Printing results after retraction of filament

Furthermore, after a sharp decrease from the initial spike there is gradual decrease in particle emission observed from the SMPS plot after printing starts. It is important to note that during the initial warmup period there was no dripping of filament from the extruder after the nozzle reached 230℃ because the filament has been retracted back into the nozzle before heating started. Even with the retracted filament and absence of dripping filament there is still a large spike observed at the same time (minute 13). This test confirms that while dripping filament has an effect on emitted particles residual filament left in the nozzle may also be contributing a significant level of particles being emitted. This assumption can be confirmed by similar testing with a cleaned nozzle. These results are shown in Figure 2.15. As expected the cleaning the nozzle decreases the initial spike in particle emission substantially. The initial spike at minute 14 only reaches ~150#/cm3. This is about three order of magnitude lower than that seen in previous results where no cleaning of the nozzle is done. Particle emission remains near baseline after printing starts.

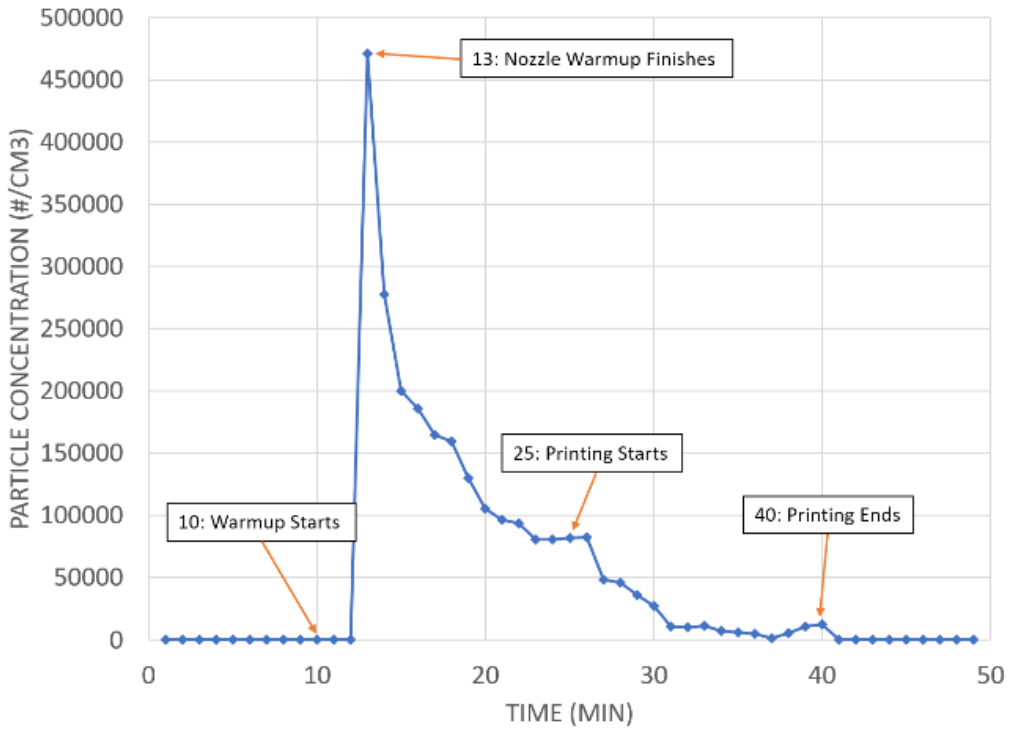

Figure 2.15 Printing results after cleaning nozzle with wire, burning out residual filament from nozzle and retraction of filament into nozzle 2-3cm.

Figure 2.16 shows results when distance between extruding nozzle and print bed are varied. Clear spikes in particle emission can be seen when filament is extruded out of the nozzle at each of the various distances. The thermal conductivity of the printer bed (although heated to 110℃) is much higher than that of air causing a faster solidification once filament reaches the bed. Consequently, the further the printing bed is from the extruding nozzle the larger surface areas of semi-liquid filament is allowed to remain in contact with surrounding air.

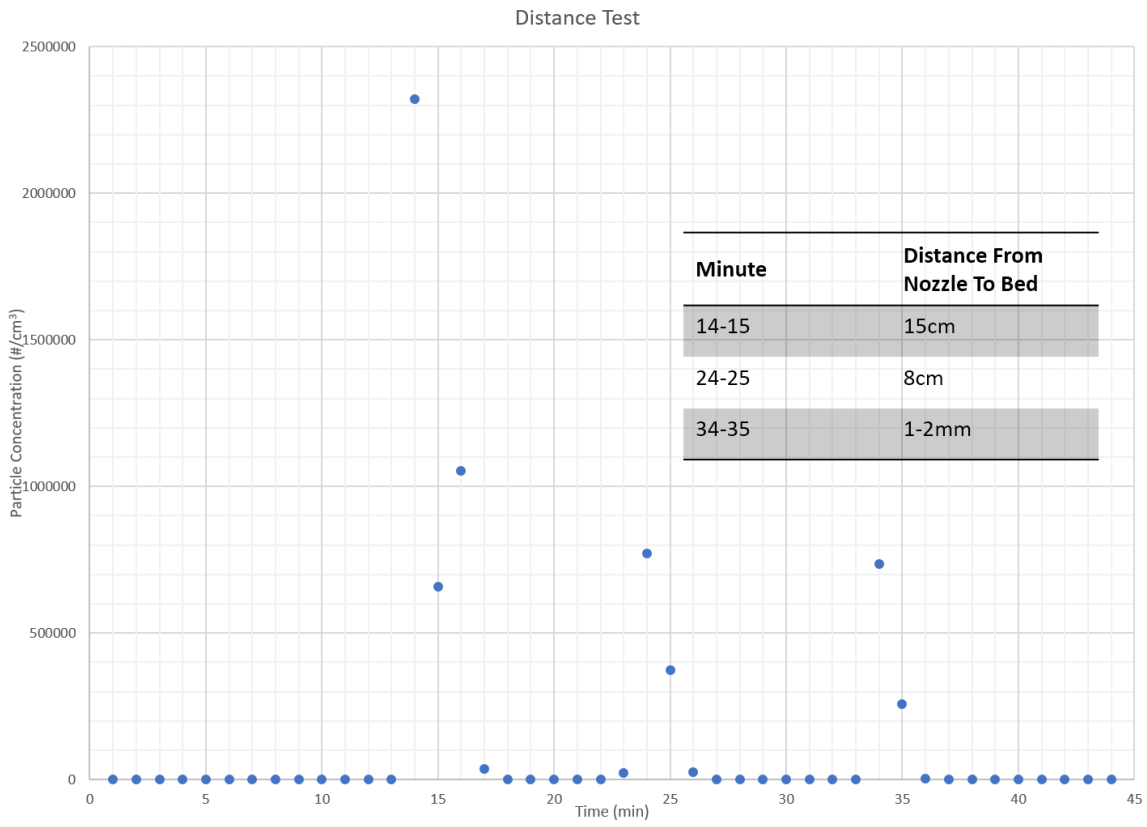

Figure 2.16 Test results from manually extruding filament at 3 distances between extrusion nozzle and printer bed (15cm, 8cm, and 1-2mm)

As pointed out earlier, particles emitted from FDM printing are largely smaller than 200nm. Figure 2.17 shows the particle size distribution during warm-up (initial spike), printing, printer pauses, and cool-down. Results confirm results of particle size distribution in other publications i.e. majority of emitted particles are less than 25nm in diameter during printing. For the initial spike, particle size tends to be bigger since larger amount of particles are formed which encourage agglomeration. During cooling down, no new particles are generated but existing particles are allowed to have more time to agglomerate. This hypothesis, although reasonable, remains to be tested in future work.

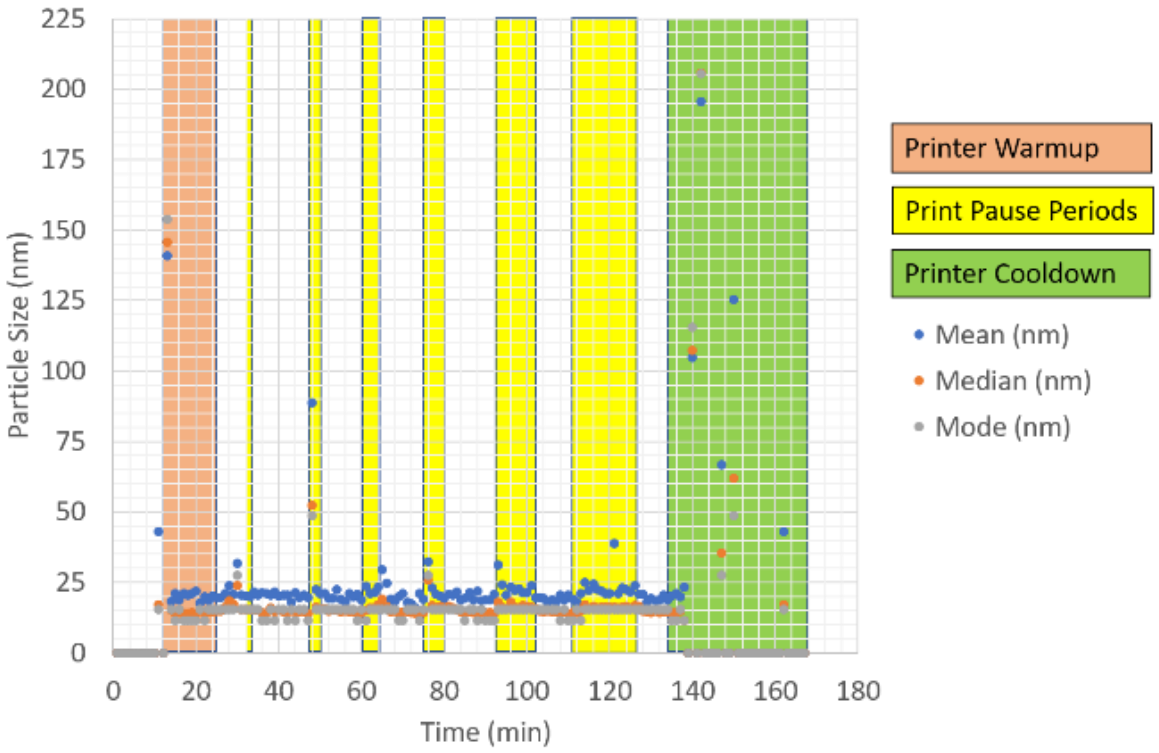

Figure 2.17 Particle size distribution during print with periodic pauses of variable durations

To study the power level of the FDM process, nine tests using 3^2 factorial design are conducted and the detail is described in Table 2.3. Several power profiles (three for different speeds and three for different material flows) are shown in Figure 2.18 and Figure 2.19 to study the power variation as process parameters change (S and MF represent speed and material flow respectively). The numbers ①, ②, ③, and ④ in the figures indicate process stages which are background, warming up, building, and cooling down, respectively.

Table 2.3 Nine tests using 3^2 factorial design

Test Number	Speed	Material Flow
1	50%	50%
2	100%	50%
3	150%	50%
4	50%	100%
5	100%	100%
6	150%	100%
7	50%	150%
8	100%	150%
9	150%	150%

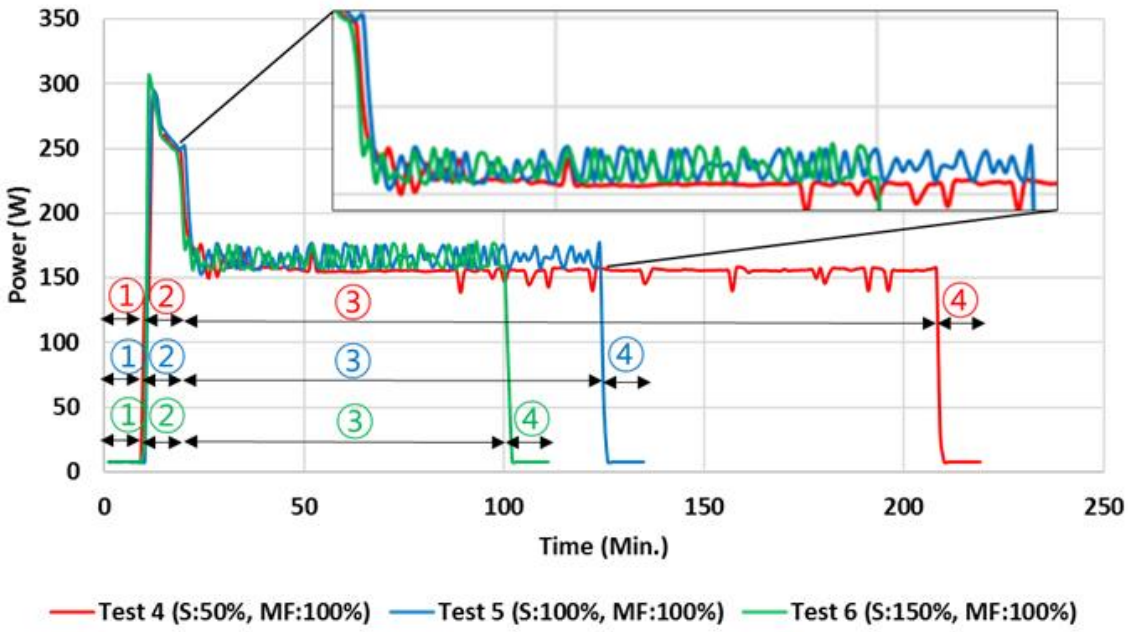

Figure 2.18 Power profile for different speed and material flows.

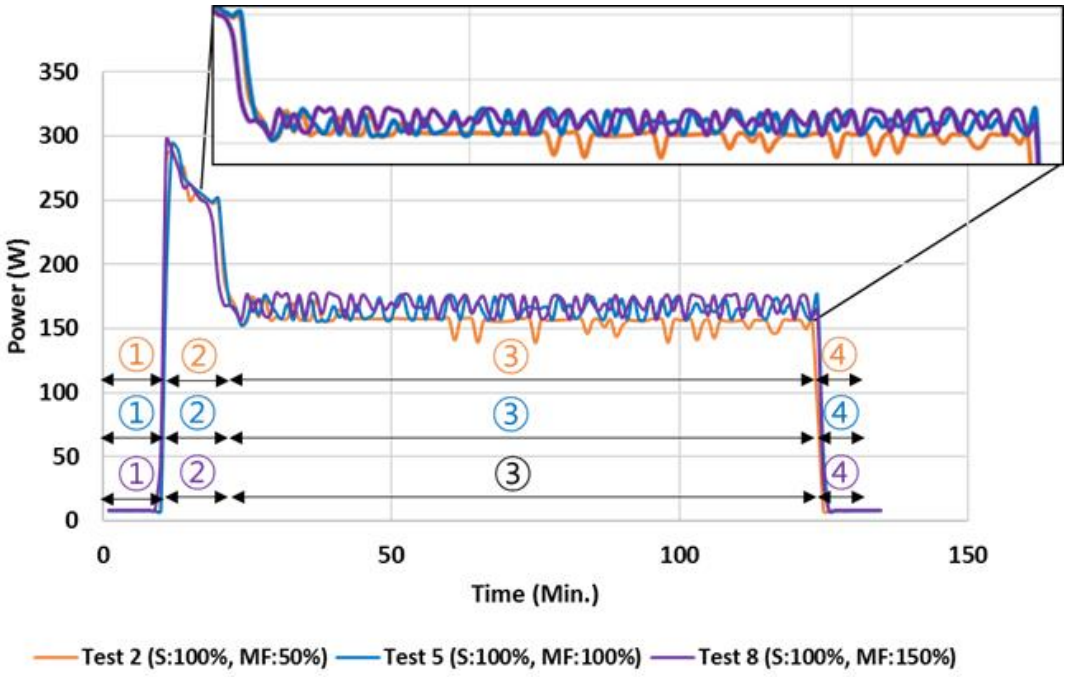

Figure 2.19 Power profile for different speeds and material flows.

As shown in both figures, the power demand of background and cooling is constant (around 8 W), which is mainly used to run the control unit. The highest power demand occurs at the beginning of the warm up stage in all tests. This is likely due to the control algorithms used to achieve desired print bed and nozzle temperature. At the beginning of the warming up, the difference between target temperature and the actual temperature is the highest, which leads to highest power demand. After that the temperature difference decreases along with the power demand. Across all tests, the time needed to arrive at the target temperature for the print bed platform and the nozzle is in the rage of 9 - 11 minutes. Although the target temperature is the same, the power demand and heating time can be affected by ambient conditions such as air temperature and humidity. In this stage, the filament extrusion nozzle is heated up first to 230℃ followed by the platform which is heated up to 110℃. Since the mass and surface area of the print bed platform is much bigger than the extrusion nozzle, much more power is needed to warm up and maintain temperature than the nozzle.

During build stage, the power demand stays at about 165W. Since build stage takes much longer time, most energy consumption happens here. As shown in the insets of Figure 2.18 and

Figure 2.19, small fluctuation on power demand exists. This is due to nozzle movement and temperature control.

Effect of the speed on power is shown in Figure 2.18. As the printing speed decreases from 150% to 100% to 50%, the build time increases from 82 minutes to 104 minutes to 189 minutes. The test with 150% speed shows the slightly higher power than the test with 50% and the averages of measured power are 166 W and 156 W respectively. Assuming the same amount of energy is used to keep the platform and nozzle temperature, the power difference is caused by travel speed of nozzle.

In addition to the speed, additional three tests are presented to study the effect of the material flow on power in Figure 2.19. Since the speed is constant, the time taken for build stage is almost same for the three tests. Also, average powers for the material flow of 50%, 100%, and 150% stage are measured as 165 W, 164 W, and 159 W, which shows that the material flow has a less significant impact on power.

From Figure 2.18 and Figure 2.19, it can be seen that the power required to maintain the platform and nozzle during build stage is much higher than moving the nozzle. Considering the surface area, likely the heat needed to maintain print bed temperature dominates the total energy consumption.

2.4 Conclusion

To begin this study, emissions from two desktop FDM printers (a Makerbot Replicator 2X and a Makeblock mElephant) are characterized by SMPS and ELPI. Two parts with distinctively different geometry i.e. a honeycomb cube with side length 1.25” and the NIST standard test part are printed using ABS filament. In all printing runs, an initial particle concentration spike is observed right after printing starts. This is likely due to the long residence time that the filament undergoes during extruder and bed heating up. TEM images of particles collected suggest that particles are formed by condensation and coagulation of vapor and droplets but this cannot confirmed.

To gain better understanding on how process conditions affect particle emissions, the Makeblock mElephant printer is enclosed in a filter box which is placed in a Class 1 cleanroom. By using ELPI, particle emissions are measured every second. Comparing particle emission profile over time between cube printing and NSIT part printing shows that particle emissions are

closely related to the filament residence time in the extruder while less related to extruding speed. Therefore, part geometry/features and build path could significantly affect particle emissions. A better understanding on how particle emissions affected by printing conditions could guide the design and operation of 3D printers for reduced environmental impacts. Additionally, more investigation into how residence time affects particle emission was needed to suggest potential solutions and predict emission behavior with more certainty.

To further these concepts, a series of experiments are conducted to investigate how operating procedure and process parameters affect particle emissions coming out of FDM printing. Experiments results suggest that most particles are formed when the semi-liquid filament travels from the nozzle to the print bed. The "wet" filament emits semi-volatile organic compounds which condense and agglomerate in the air. Print speed and material flow have some effect on particle emission but the effect is small. The initial particle emission spike observed toward the end of warming up but before printing starts is due to elevated temperature, dripping of semi-liquid filament, and filament residue in the nozzle. Particle emission can be significantly reduced if nozzle is cleaned and filament is retracted out of heating zone of the nozzle before test. The particles formed are below 200nm with majority being less than 20nm during printing. Particle size tends to be larger during initial spike and cool-down. This could be due to the higher particle concentration and extended contact time, both encourage agglomeration.

Power profiles under different print speed and material flow are also recorded. Compared with heating, especially heating of the print bed, the power needed to drive the motors is much smaller. For FDM, most of the electricity consumed is to heat up the print bed and maintain its temperature.

According to the research findings, it is possible to reduce particle emissions during FDM printing by changing operating procedures and process parameters. Before printing starts, the filament should be held out of the hot zone and after each run the nozzle should be completely cleaned. During printing it is desired to have the tip of the extruder to the printed part as close as possible. When print quality allows higher material flow rate should be used. In addition, operating at a higher speed while maintaining print quality will lead to reduction on energy consumption.

3. A STUDY OF FUSED DEPOSITION MODELING PARTICLE AND GAS EMISSION CHARACTERIZATION

Several studies have shown that while additive manufacturing (AM) offers many avenues and alternatives to traditional manufacturing techniques there are environmental implications associated with using these technologies. Previous research has shown high concentrations of ultrafine particle emissions as well as volatile and semi volatile organic compound emissions from the fused deposition modeling (FDM) 3D printing process. While the health consequences of exposure to ultrafine particles in the atmosphere is somewhat understood it is unknown what happens to such particles chemically after entering the human body. It has been shown that while printing with acrylonitrile butadiene (ABS) plastic, gaseous vapor emissions condense into particulates averaging 30nm in diameter. By collecting the exhaust and suspending in a type 1 water solution, environmental emission from FDM printers printing ABS plastic filament can be chemically characterized. Using solid phase microextraction (SPME), contaminate analytes within collected samples are adsorbed or absorbed on a fiber coating and analyzed with gas chromatography mass spectrometry (GCMS). The goal was to characterize particulate and gaseous emissions by identifying chemical makeup and molecular structure of that which would remain in the human body after exposure to FDM printing environments. Several compounds were successfully identified in printer emissions and on the filament prior to extrusion. The most predominant compound was Styrene, followed by various Benzene aromatic chains, nitrogenated aromatics, and siloxanes. Based on findings several conclusions were drawn regarding the source and make-up of emissions.

3.1 Introduction

Additive manufacturing (AM) has been suggested as a promising substitute to several conventional manufacturing (CM) techniques as a way to improve design, efficiency, and sustainability of a product. The general advantages of AM over CM are 1) more customized products (e.g., personalized health care and possibility of advanced geometries), 2) simplified supply chain (e.g., better responsiveness on the customers' demand), and 3) reduced environmental impact (e.g., less wasted material and fewer emissions). There are a number of different AM

technologies available on the market, most notably for production of metallic and plastic parts, and they can be distinguished based on feed materials (e.g., powder, wire, and ABS) and energy source (e.g., electrical beam and laser). ISO/ASTM52900-15 classified AM into seven categories which are shown in Table 1 [ref: ISO/ASTM52900-15].

Table 3.1 AM technique and relevant mechanism for production

Technique	Approach / Mechanism
1. Material Extrusion	• Fused deposition modeling (FDM)
2. Vat Photopolymerization	• Stereolithography (SLA) • Digital light processing (DLP)
3. Powder Bed Fusion	• Electron beam melting (EBM) • Selective laser sintering (SLS) • Selective heat sintering (SHS) • Direct metal laser sintering (DMLS)
4. Material Jetting	• Multi-jet modeling (MJM)
5. Binder Jetting	• Powder bed and inkjet head 3D printing (PBIH) • Plaster-based 3D printing (PP)
6. Sheet Lamination	• Laminated object manufacturing (LOM) • Ultrasonic consolidation (UC)
7. Direct Energy Deposition	• Laser metal deposition (LMD)

Each technology has its own merits and drawbacks when considering benefits from improved design features and manufacturing sustainability. These topics have been studied thoroughly from a life cycle (LC) perspective with consideration of a variety of AM technologies.

With FDM being the most widespread of AM application, there have been numerous studies conducted with a focus on input / output material and energy flows. Efforts to expand the use of FDM printers in industry to be adopted beyond prototyping has been thoroughly investigated due to potential environmental benefits and superior performance of products during the use phase. As these technologies gain in popularity, it becomes increasingly important to place emphasis on concentration, characterization, and identification of detected emissions. Several studies have identified large concentrations of ultrafine particulate (UFP) emission and volatile organic compound (VOC) gaseous emission during the FDM printing process [13], [32], [34], [35], [54].

There nevertheless exists a gap in knowledge when considering chemical makeup of identified emission.

When investigating life cycle performance of a product ISO 14040:2006 standard considers environmental impact to the natural world as well as human health factors. Identifying emission size distribution and concentration can be used to identify a number of health and environmental risks but without knowing the composition of detected emissions knowledge on the issue remains limited. Several studies have been conducted to investigate the impact on human exposure to ultrafine particle emission. A study on the effect of exposure to UFPs on heart rate showed a positive correlation between short-term UFP exposure in concentrations from $5.70 \times 10^3\ \#/cm^3 - 3.60 \times 10^4\ \#/cm^3$ in healthy adults from ages 23 to 57 and increased heart rate of up to 6 bpm [55]. Additional studies show metabolic signatures of short- and long-term exposure to $PM_{2.5}$ being linked to inflammation, oxidative stress, immunity, and nucleic acid damage and repair [56]–[60]. This is without consideration of gaseous emission and mostly focusing on air pollution. Health risks associated with VOCs emitted from plastics has also been a topic of increased interest as manufacturing and recycling of various types of plastic persists or gains in popularity. When solid waste recycling workshops were evaluated [61], it was found that according to the occupational exposure limits' (OEL) assessment, workers suffered from both acute and chronic health risks in the acrylonitrile-butadiene styrene (ABS) and polystyrene (PS) workshops. It was indicated that the highest concentration of total VOCs (TVOC) occurred in the ABS recycling workshop originating from the plastic extruding process. Lifetime cancer risk assessment suggested residents of the plastic workshop suffer a definite cancer risk [61]. ABS plastic was also found to be the most toxic material used when studying indoor air quality in the presence of FDM 3D printers [62]. This is partially due to the higher concentration of UFP and VOC emission [33], [52], [53], but also can be directly related to the chemical composition of detected emissions. In a separate study on acute health effects of desktop 3D printers, 26 healthy adults were exposed to emission from an FDM 3D printer printing both high UFP emitting ABS and low-emitting polylactic acid (PLA) for 1 hour [63]. It was found that while no acute effects were detected on nasal secretion and urine inflammatory markers, symptoms of mild illness and odor nuisance were observed after ABS exposure. Additionally, an increase in exhaled nitric oxide was observed suggesting temporary inflammation in the airways after 1 hour exposure [63]. Upon deliberation of work that has been done, it is established that adverse health effects from UFP and

VOC FDM printer exposure are most likely related to both particle size and composition presenting the need for further investigation.

There have been some conducted studies identifying substances contained in VOC emission from FDM 3D printers each testing ABS and a variety of other filament types [53], [64]–[66]. Three of these studies used similar air sampling and analysis techniques. Sorbent sampling tubes contained in a test chamber are used to collect printer emitted VOC compounds to be analyzed by thermal desorption gas chromatography mass spectrometry (TD-GC/MS) [53], [64], [66]. In the fourth study Silonite-coated canisters were used to collect VOC samples to be analyzed by GC/MS [65]. Results from referenced work were consistent in many of the detected compounds for FDM printers extruding ABS plastic filament. All studies using the sorbent sampling tubes found highest concentrations of Styrene with several other included VOCs in smaller concentrations. Table 3.2 shows a list of detected VOC emission from FDM printers in order from highest detected emission rates to lowest from referenced studies.

Table 3.2 Detected VOCs from referenced studies listed from highest concentration to lowest. Compounds in green cells were found in all four studies, compounds in yellow were found in three of the studies, and compounds in yellow were found in 2 of the studies. Azimi et al. (2016) [53], Floyd et al. (2017) [64], Gu et al. (2018) [66], Stefaniak et al. (2017) [65]

Azimi et al. (2016)	***Floyd et al. (2017)***	***Gu et al. (2018)***	***Stefaniak et al. (2017)***
Isopropyl Palmitate	Styrene	Styrene	Styrene
Acetophenone	Ethylbenzene	Ethylbenzene	Isopropyl alc
Nonane,2,2,4,4,6,8,8-Heptane	Acetophenone	Sum of C3-Benzenes	Ethanol
Styrene		Benzaldehyde	Acetaldehyde
Ethylbenzene		Acrylonitrile	Acetone
Decane		Trichloroethene	Ethylbenzene
Hexanal		m,p-Xylene	Acetonitrile
Glycerin		o-Xylene	Benzene
Propylene Glycol		Phenol	m,p-Xylene
		Acetophenone	n-Hexane
		Benzoic Acid	Chloroform
		2-Phenylpropenal	Toluene
		Dodecamethylcyclohexasiloxane	o-Xylene
		4-Phenylbutyronitril	
		2-isopropenylindolizine	
		4-phenylcyclohexene	
		Sum of iso/cycloalkanes	
		Sum of other siloxanes	

As can be seen in Table 3.2 by the color coding, items in green were found in all studies, yellow in three of the four studies, and orange in two of the four studies. While there was a great deal of consistency between results, three studies found a number of compounds that were not identified in the others. This is most likely due to the color and manufacturer of ABS filament used as well as the difference in manufacturers for the printers themselves. Indeed, this was shown within the studies as two of them tested different ABS filament colors [53], [66] showing varying results and

one of them even used a variety of FDM printers produced by different manufacturing companies which also caused variation in results [66].

The purpose of investigating the composition of material output flows from AM processes is to gain a better understanding of potential environmental and human health risks. VOCs and their adverse health risks have been studied for several years now due to the suspected risks associated with environmental exposure. In an updated styrene exposure assessment it was found that health effects include potential human cancers and ototoxicity (hearing or balance problems) [67]. It has been shown that VOC and UFP emissions can be characterized by collecting air emission in sorbent tubes and assessing composition with GC/MS. There are other collection techniques that could potentially offer more comprehensive results. By diffusing FDM printer exhaust into an aqueous solution a better understanding of what could remain suspended in the aqueous bloodstream is established. Particles released from FDM printers printing ABS plastic average about 30nm in diameter [33] which is small enough for passage into a human's blood circulation through the aveolar capillary membrane if inhaled [68]. Figure 3.1 shows a schematic of the aveolar capillary membrane where particles of size less than 100nm in diameter can find passage into the bloodstream if inhaled.

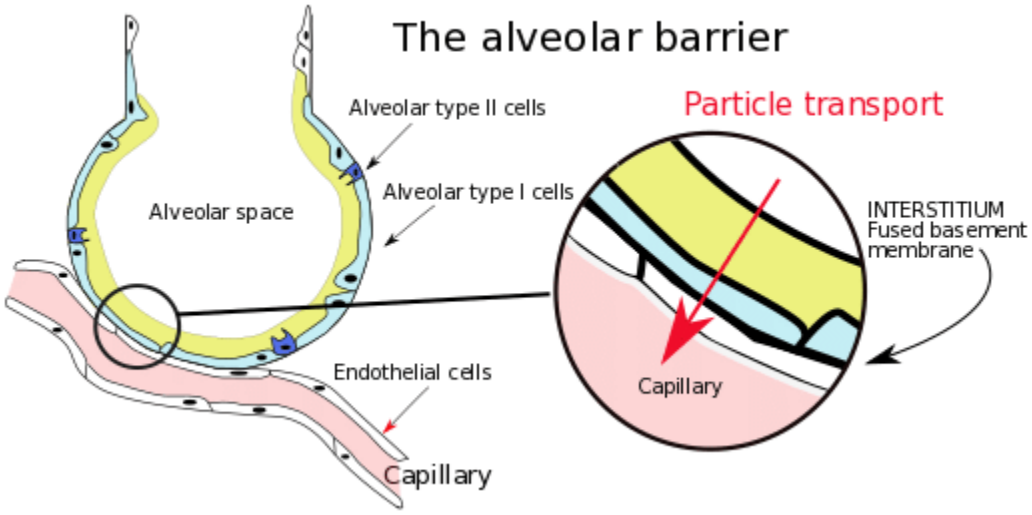

Figure 3.1 Schematic of the aveolar capillary membrane barrier [69]

By testing AM emission capable of remaining suspended in an aqueous solution, a more thorough understanding of the health implications of exposure can be addressed. Another

identified gap in the literature exists with testing what exists on AM filament before being extruded through the printing nozzle. Particle and gaseous emission off a 3D printer is assumed to be produced from the extrusion process but the same compounds may exist on the filament before being extruded. In this study we will be investigating VOCs that remain suspended in an aqueous solution during the printing process and exploring what compounds may exist as a layer on the outside of ABS filament before being extruded in the FDM process. This is done using a procedure never done before and will aid in filling in the gaps left over from similar studies.

3.2 Methodology

Methods for this project were developed based on the objective to identify chemical makeup and molecular structure of particulate and gaseous emission off FDM 3D printers dissolved in aqueous solution. This was done to develop a better understanding of health-related risks associated with exposure to FDM printer technology. To do so a procedure was developed to collect printer exhaust, suspend it in an ultrafiltered water solution, and analyze the resulting contaminated solution using a methodology applicable for gas chromatography mass spectrometry measurements. Figure 3.2 shows a schematic of the setup described here for emission collection and analysis.

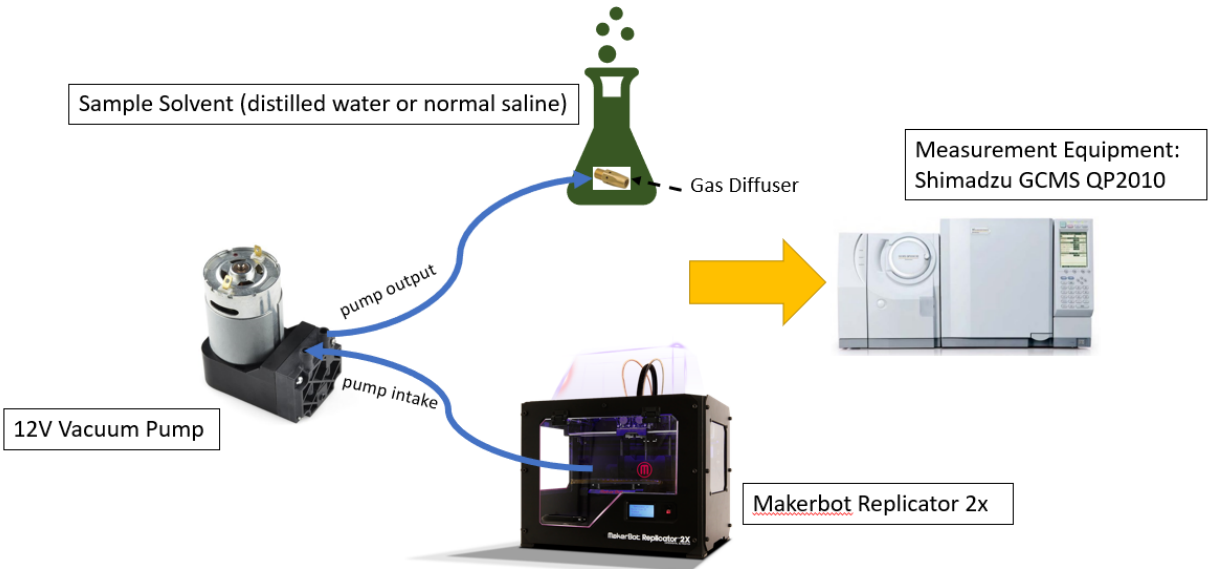

Figure 3.2 Setup for FDM printer emission collection and analysis

3.2.1 FDM Emission Collection Procedure

This study aimed to assess emissions from a popular desktop FDM printer, printing ABS plastic filament. Therefore, experiments were conducted using white ABS filament manufactured by MakerBot and printed using the MakerBot Replicator 2X FDM 3D printer. All experiments were performed in a sectioned off lab/office with a modern HVAC system built in 2011. The printing chamber was sealed off with plexiglass on the 3 exposed sides and a plastic covering on top so as to limit airflow from the printing chamber to the outside environment (see Figure 3.2). Air emissions were collected at the start of the printer warm-up period where the filament nozzle is heated from ambient temperature to 230^{o}C and the print bed is heated from ambient temperature to 110^{o}C. During measurements we printed the NIST additive manufacturing standardized test artifact. NIST designed this artifact to be used in testing performance of an AM system [70]. It is unique in it's complex geometry and is a good way of testing emission from the AM process under a variety of performance conditions. The NIST artifact that was printed can be viewed in Figure 3.3.

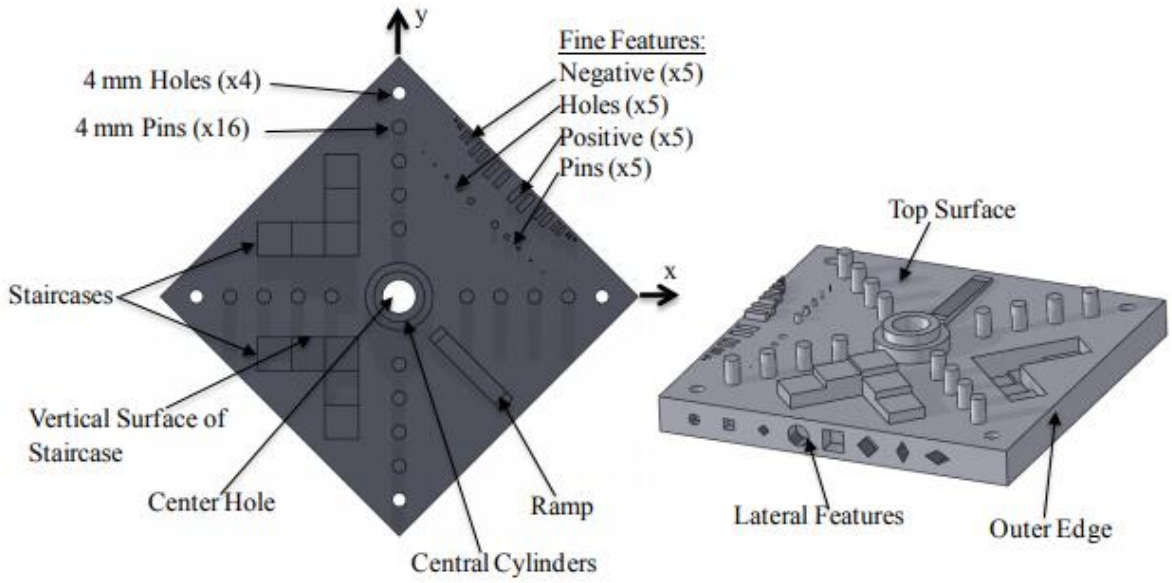

Figure 3.3 NIST additive manufacturing test artifact [71]

To circulate air from the system a 12V Karlsson Robotics vacuum pump was used and set to 8V to pull air at ~0.30cfm. From the pump intake, silicone rubber tubing was run through the same inlet the ABS filament was fed through to be connected to the printing head. The silicon

rubber tubing was equipped with embedded carbon to dissipate static buildup that could affect the flow of particulates through the system. At the pump output the same rubber tubbing was used to circulate printer exhaust from the printing chamber into a 300mL Type 1 water solution. Type 1 water is ultrapure and good for use in sensitive lab procedures like gas chromatography. A diffuser was connected at the end of the tubbing that was fed into the water solution contained in a conical flask and sealed off with aluminum foil. The diffuser bubbled air emissions into the water to increase solution uptake of contaminates.

After the printing tests were concluded the water solution was placed in sealed vials for measurements. For this study three different samples were prepared to assess and compare. The first sample was taken printing the NIST test artifact described above. To confirm detected compounds came from the printer and not the external printing environment, a second solution was prepared by pumping air from the room through the diffuser for the same amount of time it took to run a print test. This included the printer warm-up time and time to print the artifact (~4hrs). Finally, a third vial was prepared by placing cut up pieces of the white ABS filament into the type 1 water solution and allowing it to soak for two weeks.

3.2.2 Compound Analysis

To sample analytes for measurement Solid Phase Microextraction (SPME) was used. SPME is a preferred technique for environmental volatiles (VOC) testing. SPME works by using a fiber coated extraction phase where equilibrium is established between sample and fiber. The fiber coating extracts analytes from solution using absorptive coatings comprised of a pure polymer liquid or adsorptive coatings comprised of adsorptive particles embedded in a polymer. Once the SPME fiber extracts compounds from the sample it is inserted into a GC injector for thermal desorption and analysis. SPME is great for detection of trace amounts of analytes because it concentrates analytes on the fiber before desorption to the GC column providing quantitative results for a wide range of concentrations. There are a wide range of optional coatings available, each favorable for testing different analyte types. This study used three different Millipore Sigma manufactured SPME fibers that can be referenced in Table 3.3. Thermal desorption and sample analysis was performed using Agilent's 7000C Triple Quadrupole GC/MS. A 0.75mm ID Supelco SPME Injection Sleeve was used for the GC injection liner.

Table 3.3 SPME fibers used for compound extraction.

SPME Fiber Coating	Film	Polarity	Molecular Weight (MW) Range ($^{g}/_{mol}$)	Analyte Type
$75\mu m$ Carboxen-PDMS	Adsorption	Bipolar	30-225	• Gases and Low MW Compounds
$65\mu m$ PDMS-DVB	Adsorption	Bipolar	50-300	• Volatiles • Amines • Nitro-aromatic Compounds
$85\mu m$ Polyacrulate	Absorption	Polar	80-300	• Polar Semi-volatiles

Polydimethylsiloxane (PDMS): used as binder
Divinylbenzene (DVB): porous adsorbent particles

Adsorptive films typically are considered to be stronger and more efficient extraction mechanisms. For this reason, two of the three coatings used adsorption as the sampling mechanism. As shown in Table 3.3 the fibers used for this study cover a wide range of analyte types that would be expected to show up from ABS plastic extrusion. With the use of all three sampling techniques, quantitative results were expected to be achieved.

There are two extraction procedures commonly used with SPME, headspace analysis and direct immersion. Since compounds were suspended in water which is considered to be less volatile than other organic solvents, a direct immersion extraction mode was used. Direct immersion is favorable under circumstances where expected analytes are of low to medium volatility and high to medium polarity, where liquid sample matrix can be simple or complex, and if higher extraction efficiencies are desired. The disadvantages of direct immersion include fouling, shorter fiber lifetime, and sometime the need for sample pretreatment. Fortunately, none of these were issues of concern for this study. All fiber coatings used in this study had 30min recommended conditioning times at conditioning temperatures from 250°C-300°C.

Before exposing the SPME fibers to samples, fibers had to be conditioned. Fiber conditioning removes compounds adsorbed or absorbed from environmental exposure before sampling. Thermal conditioning is done by exposing the SPME fiber in the high temperature GC inlet for a set conditioning time (30min) to clear out environmental contaminants. After conditioning, the GC oven temperature was ramped to remove any contaminants that may have

entered the column. Conditioning and operating guidelines for selected fibers are shown in Table 3.4 and were selected based on manufacturer instructions.

Table 3.4 Temperature, pH, and Conditioning Guidelines for Fiber Coatings

SPME Fiber Coating	pH	Maximum Temperature (℃)	Recommended Operating Temperature (℃)	Conditioning Temperature (℃)	Conditioning Time (Hrs)
$75\mu m$ Carboxen-PDMS	2-11	320	250-310	300	0.5
$65\mu m$ PDMS-DVB	2-11	270	200-270	250	0.5
$85\mu m$ Polyacrulate	2-11	300	220-280	280	0.5

After the fiber was conditioned, sample analyte extraction could begin. Extraction time is an important parameter to consider when using SPME. Sample agitation was done to improve extraction kinetics by thoroughly mixing samples before exposing the SPME fiber. After a number of tests, it was determined that equilibrium conditions were reached after 30min of fiber exposure to the samples. Consequently, SPME fibers were directly immersed into each sample for 30min followed by immediate injecting in the GC to run analysis. Upon conclusion of each test, GC/MS chromatograms were integrated and compounds were statistically identified by a NIST/EPA/NIH mass spectral library search containing 276,248 reference spectra and 242,466 reference compounds.

3.3 Results and Discussion

3.3.1 PDMS/DVB Fiber Extraction Results

Table 3.5 shows the list of identified compounds from the PDMS/DVB SPME fiber measurements. Corresponding compounds are numbered in the chromatograph results shown in

Figure 3.4 - Figure 3.6. It is common for the same compound to show up in more than one peak at different retention times, therefore, only the highest peak of each identified compound is recognized in each chromatograph. In general, it is assumed that higher peaks with greater integrated areas have increased concentrations, comparatively. However, some compounds may have better affinity with the detector causing peaks to appear larger than their relative concentration. To solve this issue, standards with known concentration of compounds can be run to assure accurate readings. This was not done in this study, so concentrations are not shown in table results. Nevertheless, several conclusions can still be drawn from shown results. Compounds identified from background measurements that show up in printer measurements can be neglected and assumed to have already been present in the printer environment prior the starting the print. Results from PDMS/DVB fiber extractions showed negligible overlap between background and print measurements. The dominant analytes identified in the print tests were Styrene and Siloxane compounds. Results from the filament wash also showed styrene as the most predominant compound with added Benzene aromatic variants and Ethylbenzene. These results were consistent with what was shown in other studies which only tested emissions during a print.

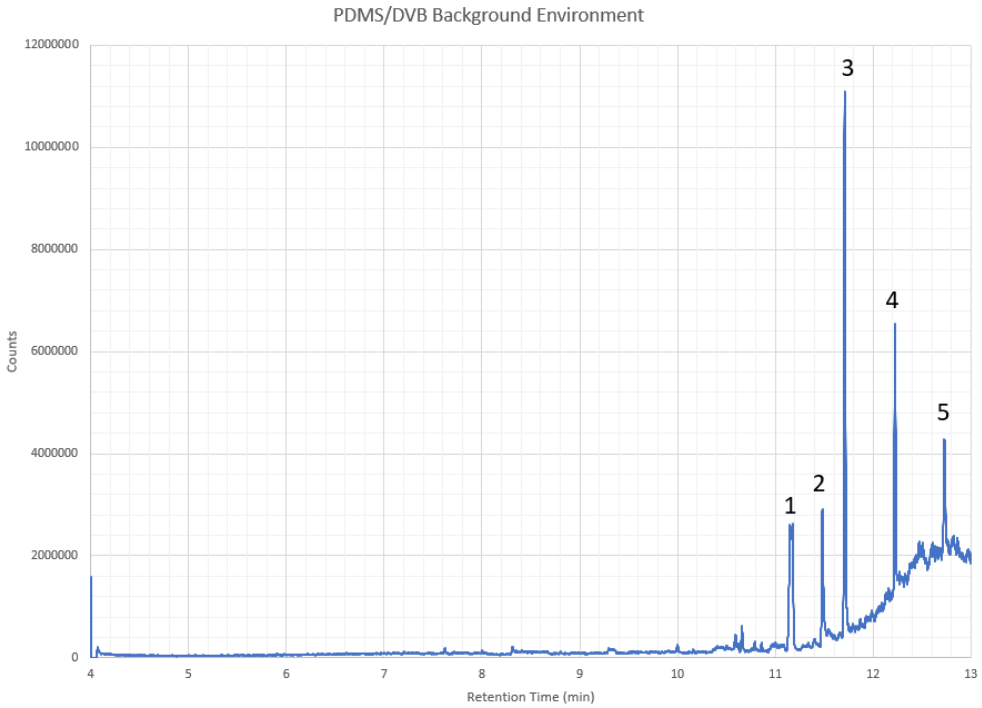

Figure 3.4 GC/MS Chromatogram results for background environment measurements using PDMS/DVB fiber coating.

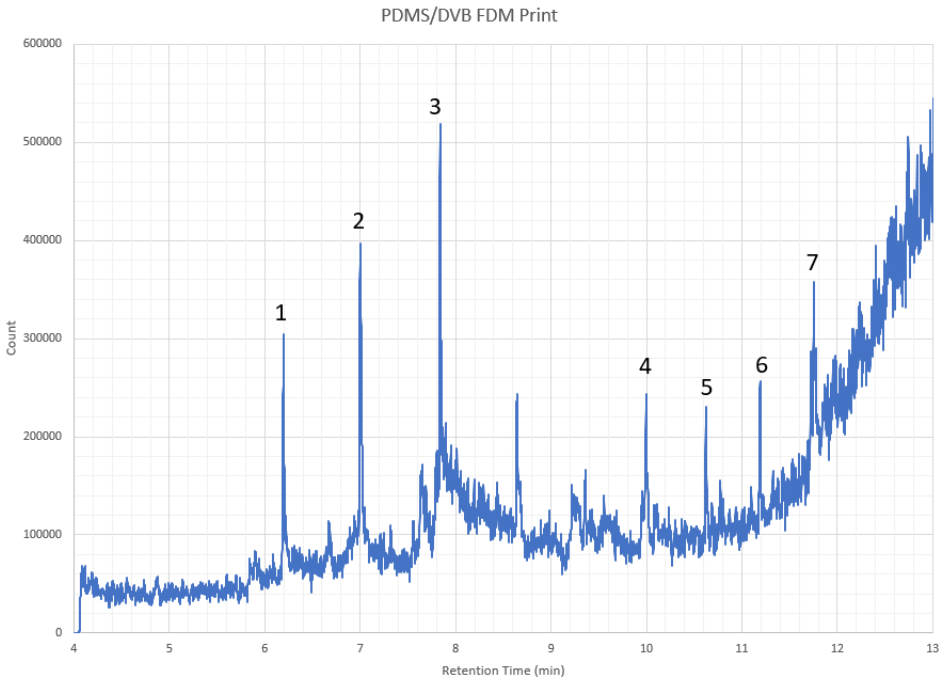

Figure 3.5 GC/MS Chromatogram results for NIST test artifact using PDMS/DVB fiber coating.

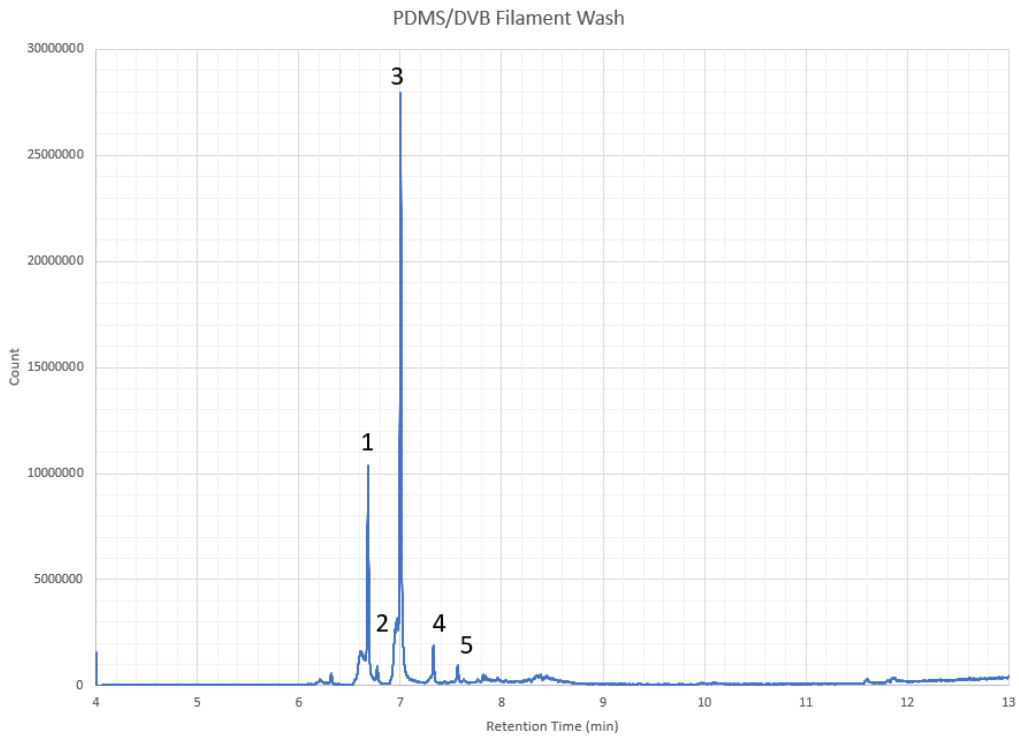

Figure 3.6 GC/MS Chromatogram results for filament wash using PDMS/DVB fiber coating.

Table 3.5 List of identified compounds from PDMS/DVB fiber measurements.

PDMS/DVB Background Environment			
Comp #	**Compound Name**	**RT**	**Area**
1	3,6-Dioxa-2,4,5,7-tetrasilaoctane, 2,2,4,4,5,5,7,7-octamethyl-	11.15	3465929
2	Ethylamine, 2-((p-bromo-.alpha.-methyl-.alpha.-phenylbenzyl)oxy)-N,N-dimethyl-	11.48	2874005
3	Trisiloxane, 1,1,1,5,5,5-hexamethyl-3,3-bis[(trimethylsilyl)oxy]-	11.71	9977318
4	11,13-Dimethyl-12-tetradecen-1-ol acetate	12.47	604517
5	2,4-Dodecadienoic acid, 11-methoxy-3,7,11-trimethyl-, methyl ester, (E,E)-	12.73	2575706
PDMS/DVB FDM Print			
1	Cyclotrisiloxane, hexamethyl-	6.20	225737
2	Styrene	7.00	400731
3	Cyclotetrasiloxane, octamethyl-	7.84	228290
4	2,6-Dihydroxyacetophenone, 2TMS derivative	9.99	68695
5	Benzoic acid, 4-methyl-2-trimethylsilyloxy-, trimethylsilyl ester	10.63	85857
6	Cyclopentene, 3,3-dimethyl-4-methylene-1,2-bis(trimethylsilyloxymethyl)-	11.19	103497
7	Ethanol, 1-(methylenecyclopropyl)-1-(methylene-1-trimethylsilylcyclopropyl)-	11.76	64679
PDMS/DVB Filament Wash			
1	Benzene, 1,3-dimethyl-	6.68	11059112
2	Ethylbenzene	6.77	736135
3	Styrene	7.00	30657345
4	Benzene, (1-methylethyl)-	7.33	1804379
5	Benzene, propyl-	7.57	852190

3.3.2 Polyacrylate Fiber Extraction Results

Results from the Polyacrylate SPME extraction are shown in Table 3.6 which references labeled compounds from Figure 3.7 - Figure 3.9 chromatographs. While the PDMS/DVB fiber coating picked up volatiles and aromatics, the Polyacrylate coating picks up polar semi-volatile

analytes yielding much different results. Several new compounds were identified from environmental background measurements but only Pyridine, 4-(1-pyrrolidinyl) also showed up in the printing emissions test. Benzene, 1,3-diisocyanato-2-methyl was found in the highest concentrations and hadn't been picked up in previous measurements using the PDMS/DVB fiber. It also was not picked up in previous studies to our knowledge. Comparing the print test results to the filament wash test, several more compounds are seen. Here Styrene was again identified but in lower concentrations than some of the other compounds that were found. A similar aromatic to that found in the print test was picked up, Benzene, 2,4-diisocyanato-1-methyl-, and is shown at peak 4 with one of the highest integrated areas. This again shows that many of the identified compounds that are being emitted during a print cycle are also found when simply washing the filament in water.

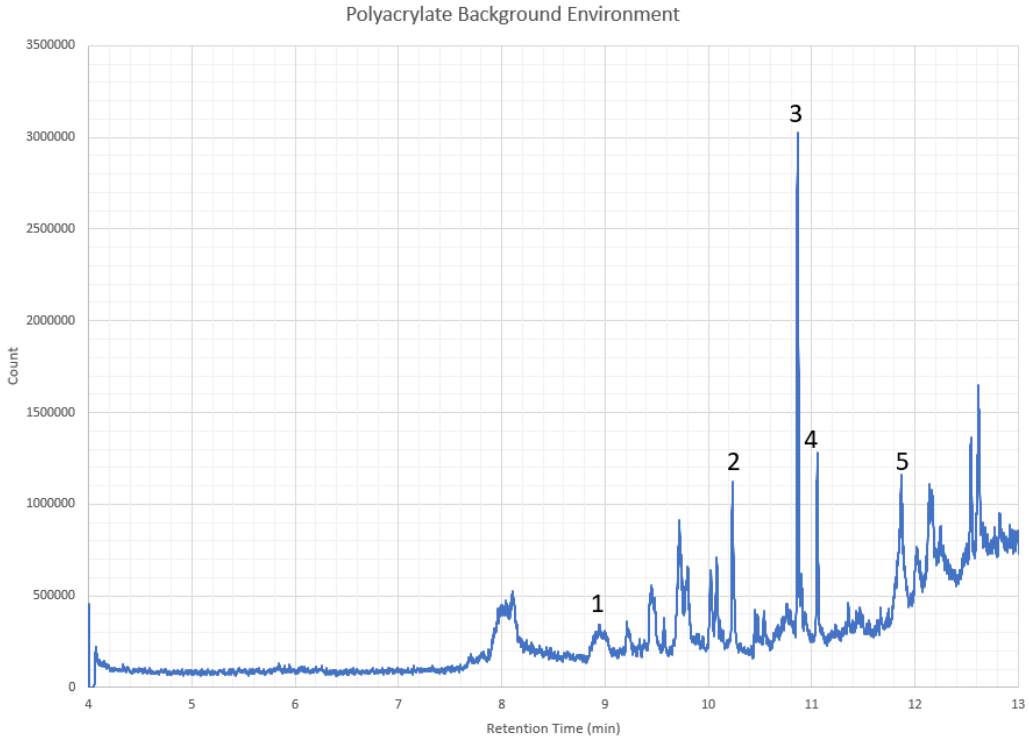

Figure 3.7 GC/MS Chromatogram results for background environment measurements using Polyacrylate fiber coating.

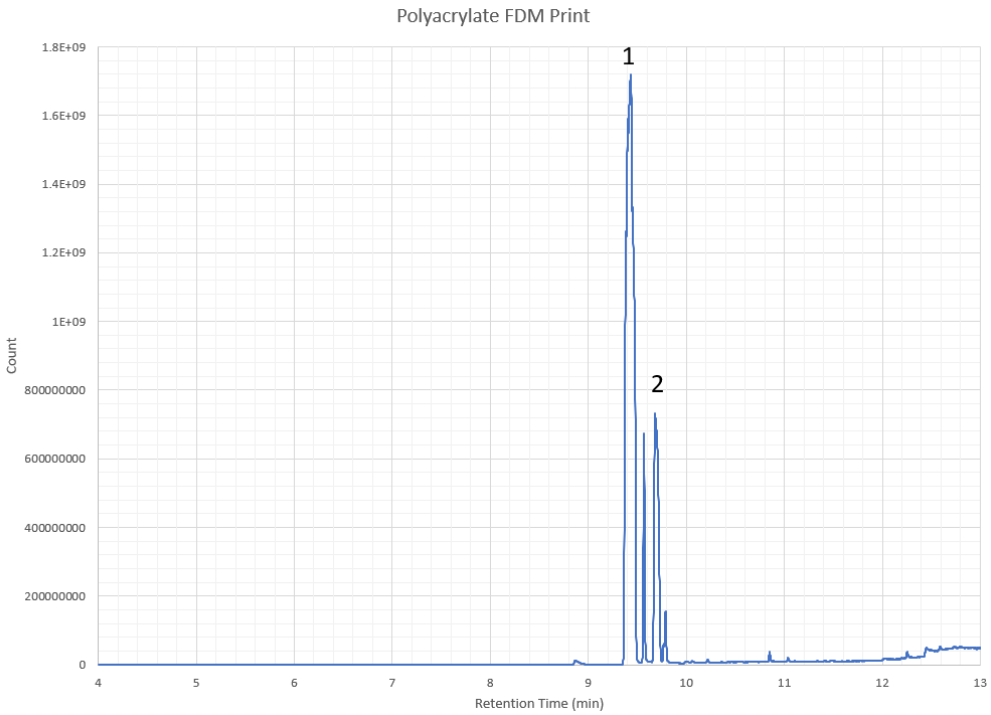

Figure 3.8 GC/MS Chromatogram results for NIST test artifact using Polyacrylate fiber coating.

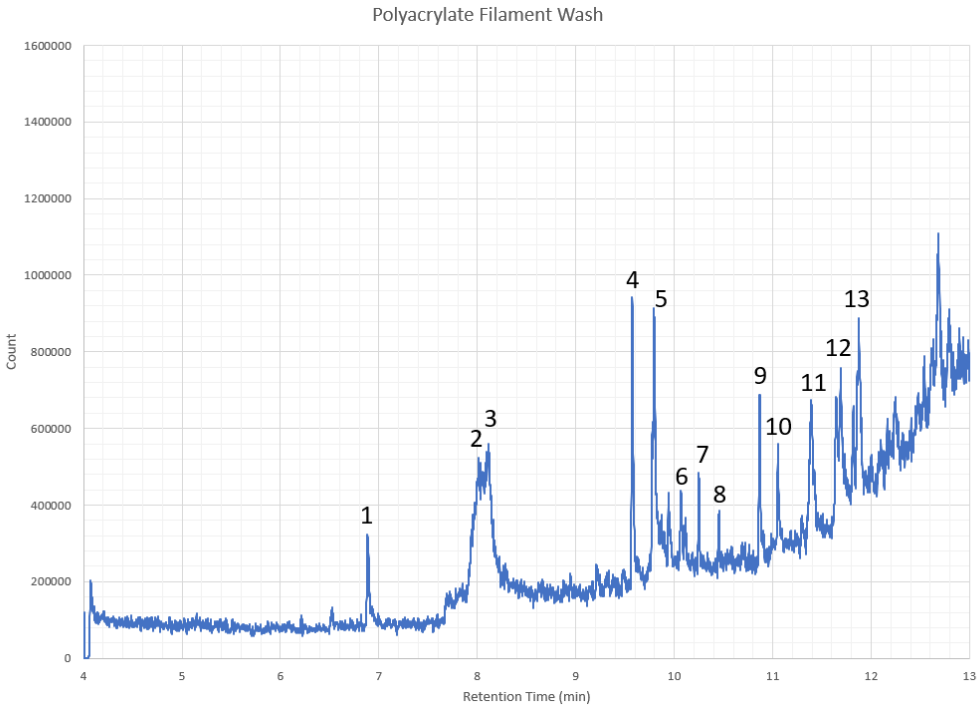

Figure 3.9 GC/MS Chromatogram results for filament wash using Polyacrylate fiber coating.

Table 3.6 List of identified compounds from Polyacrylate fiber measurements.

Polyacrylate Background Environment			
Comp #	**Compound Name**	**RT**	**Area**
1	Pyridine, 4-(1-pyrrolidinyl)-	9.72	805578
2	Aziridine, 2-methyl-2-(2,2,4,4-tetramethylpentyl)-	10.234	1058264
3	1(2H)-Naphthalenone, 3,4-dihydro-3,3,6,8-tetramethyl-	10.866	2766538
4	Giparmen	11.055	1040936
5	Phosphinous acid, diphenyl-	11.869	552863
Polyacrylate FDM Print			
1	Benzene, 1,3-diisocyanato-2-methyl-	9.434	4.09E+09
2	Pyridine, 4-(1-pyrrolidinyl)-	9.684	2.17E+09
Polyacrylate Filament Wash			
1	Styrene	6.88	318625
2	Silane, (butoxymethyl)trimethyl-	8.06	12859
3	Boric acid, trimethyl ester	8.12	128806
4	Benzene, 2,4-diisocyanato-1-methyl-	9.57	737390
5	(6-Hydroxymethyl-2,3-dimethylphenyl)methanol	9.80	370876
6	Quinazolin-4(3H)-one, 6-bromomethyl-2-methyl-	10.07	248302
7	9-Hexadecenoic acid	10.25	203152
8	Diethyl Phthalate	10.46	112808
9	Benzene, 3-[3-iodo-2-(iodomethyl)-2-methylpropyl]-1,2,4,5-tetramethyl-	10.87	435514
10	1,25-Dihydroxyvitamin D3, TMS derivative	11.05	256381
11	Pyrrolidine, 1-[4-(4-chlorophenyl)-3-phenyl-2-butenyl]-	11.39	394331
12	Phen-1,4-diol, 2,3-dimethyl-5-trifluoromethyl-	11.65	318443
13	2-Methoxy-6,10-dimethyl-dodeca-2E,6Z,10Z-trienoic acid, 12-acetoxy-, methyl ester	11.88	865210

3.3.3 Carboxen/PDMS Fiber Extraction Results

The last set of measurements were done using a Carboxen/PDMS fiber coated extraction and are shown in Table 3.7 which references compounds from chromatographs in Figure 3.10 - Figure 3.12. Several new compounds were identified with the Carboxen/PDMS SPME fiber extraction. Carboxen/PDMS adsorbs analyte gases and low molecular weight compounds. Background measurements had some overlap in detected compounds with printer measurements although several new analytes were identified. While printing the NIST test artifact greatest peak was identified as Phenol, 4,4’-(1-methylethylidene)bis- which is yet another complex aromatic.

Additionally, there were several siloxane variants identified that were supported by measurement results in the other two fibers used. N-Methyl-1-abamantaneacetamide was another nitrogenated compound that was identified in measurements with Carboxen/PDMS and not seen in background measurements. The greatest peak in the water-soaked filament test was Styrene which was supported by all three fiber extraction methods. It was puzzling, however, to find that Styrene analytes were identified in both Carboxen/PDMS and Polyacrulate filament soak tests without having showed up when printing the NIST test artifact. This may be due to the changing nature of the compound as an emission, which only allowed for identification in printer measurements with the PDMS/DVB fiber recognized as being superior when identifying volatile analytes in solution. Furthermore, the filament soak test picked up high concentrations of complex aromatic benzene chains and nitrogenated aromatic compounds.

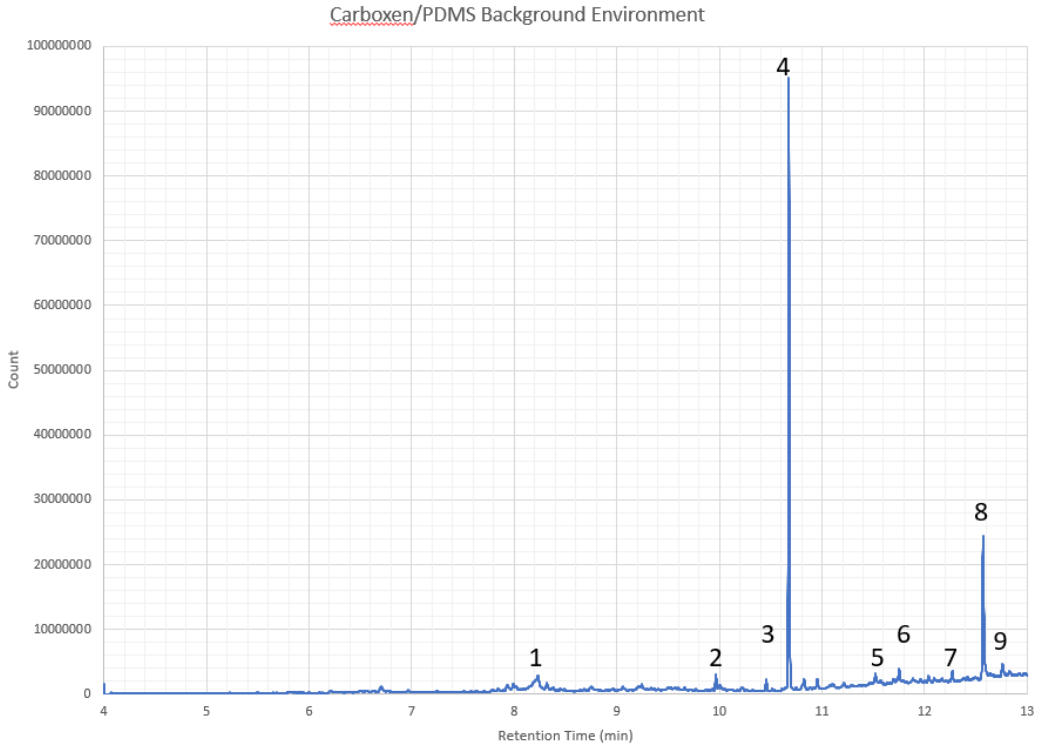

Figure 3.10 GC/MS Chromatogram results for background environment measurements using Carboxen/PDMS fiber coating.

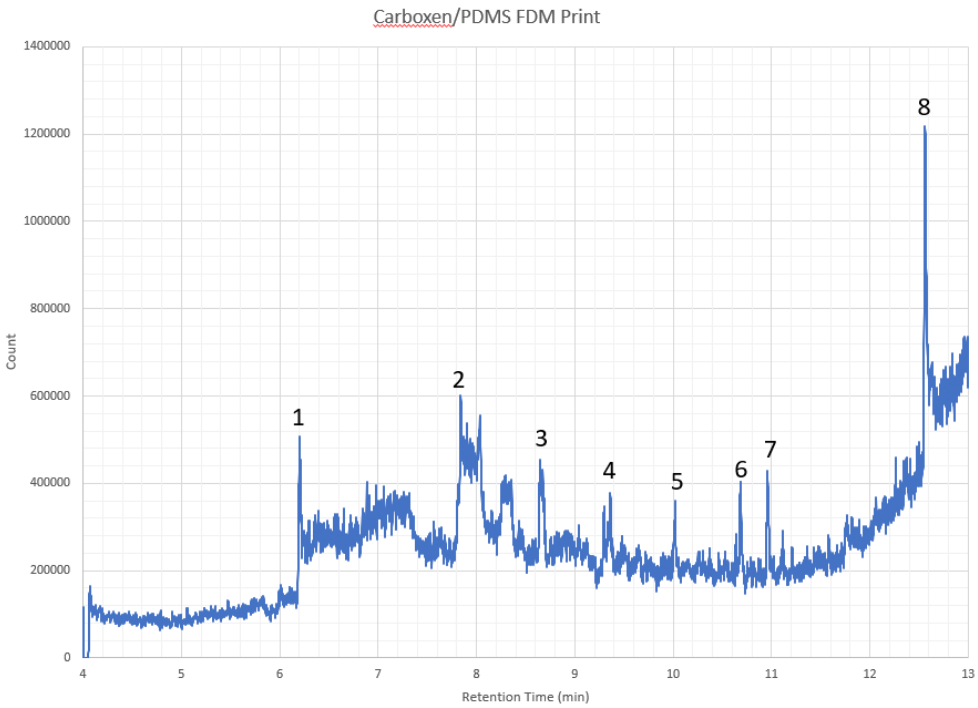

Figure 3.11 GC/MS Chromatogram results for NIST test artifact using Carboxen/PDMS fiber coating.

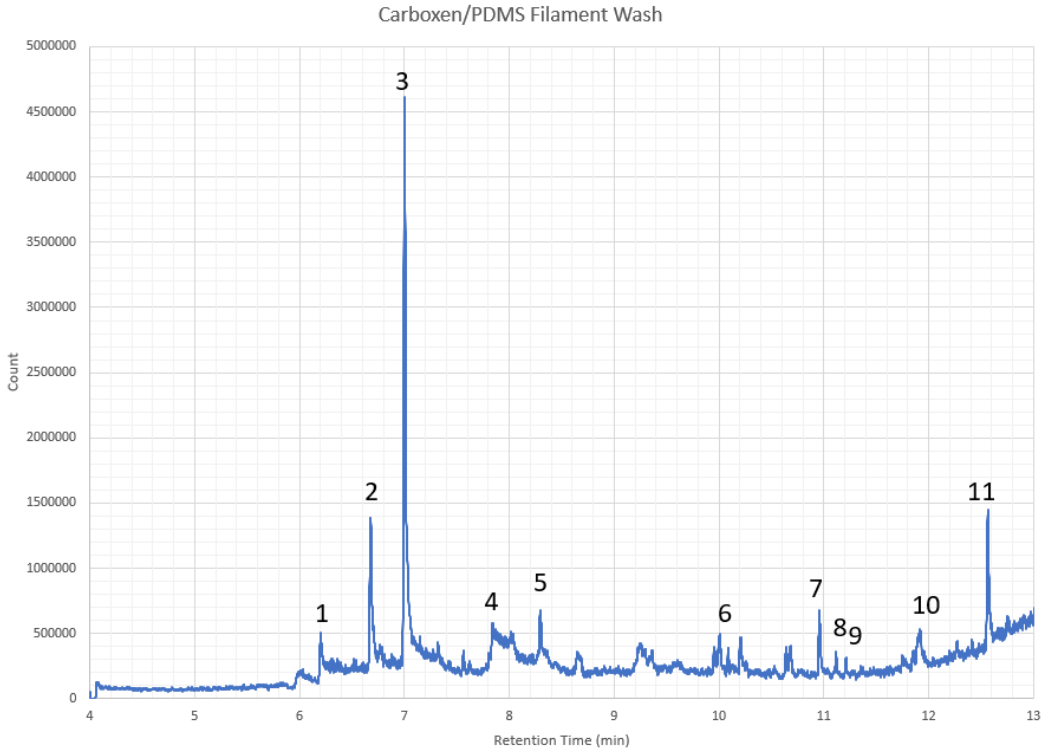

Figure 3.12 GC/MS Chromatogram results for filament wash using Carboxen/PDMS fiber coating.

Table 3.7 List of identified compounds from Carboxen/PDMS fiber measurements.

Carboxen/PDMS Background Environment			
Comp #	**Compound Name**	**RT**	**Area**
1	Benzoic acid	8.23	4173831
2	2,5-Cyclohexadiene-1,4-dione, 2,6-bis(1,1-dimethylethyl)-	9.97	2243474
3	2,2,4-Trimethyl-1,3-pentanediol diisobutyrate	10.46	1595421
4	Succinic acid, 2-(2-chlorophenoxy)ethyl ethyl ester	10.68	72655886
5	Benzenemethanol, 4-hydroxy-.alpha.-[1-(methylamino)ethyl]-, (R*,S*)-	11.52	1601088
6	2,4-Dodecadienoic acid, 11-methoxy-3,7,11-trimethyl-, methyl ester, (E,E)-	11.75	1433415
7	3-(1,5-Dimethyl-hexa-1,4-dienyl)-2,2-dimethyl-4-trimethylsilylcyclopentanol	12.27	1505365
8	Phenol, 4,4'-(1-methylethylidene)bis-	12.57	21840428
9	2,2-Dimethyl-6-methylene-1-[3,5-dihydroxy-1-pentenyl]cyclohexan-1-perhydrol	12.76	2613112
Carboxen/PDMS FDM Print			
1	Cyclotrisiloxane, hexamethyl-	6.20	323118
2	Cyclotetrasiloxane, octamethyl-	7.84	34001
3	Tetrasiloxane, 1,1,3,3,5,5,7,7-octamethyl-	8.65	324411
4	Tris(tert-butyldimethylsilyloxy)arsane	9.30	110247
5	Benzoic acid, 4-methyl-2-trimethylsilyloxy-, trimethylsilyl ester	10.02	143985
6	N-Methyl-1-adamantaneacetamide	10.67	288527
7	4-Phenyl-3,4-dihydroisoquinoline	10.96	302055
8	Phenol, 4,4'-(1-methylethylidene)bis-	12.56	1050299
Carboxen/PDMS Filament Soak			
1	Cyclotrisiloxane, hexamethyl-	6.20	427492
2	Benzonitrile, m-phenethyl-	6.68	1297121
3	Styrene	7.00	6404516
4	Cyclotetrasiloxane, octamethyl-	7.84	92642
5	3-Benzoylmethyl-3-hydroxy-5-nitro-2-indolinone	8.30	443818
6	2,6-Dihydroxyacetophenone, 2TMS derivative	10.01	291468
7	Benzene, 1,1',1'',1'''-(1,2,3,4-cyclobutanetetrayl)tetrakis-	10.96	560973
8	Salicyl alcohol, 2TMS derivative	11.12	133221
9	1,4-Cyclohexadiene, 1,3,6-tris(trimethylsilyl)-	11.21	127404
10	Thiocarbamic acid, N,N-dimethyl, S-1,3-diphenyl-2-butenyl ester	11.92	521570
11	Phenol, 4,4'-(1-methylethylidene)bis-	12.56	1221919

3.3.4 Discussion of Final Results

SPME fiber extraction followed by immediate GC/MS thermal desorption proved to be a useful measurement technique in this study. The differing fiber coatings allowed for diverse identification of analyte types of an expansive range in molecular weight. In addition to using type 1 water as a solvent, acetone was also tested as a solvent to collect emissions in this study due to the increased potential to better suspend plastics and resulting emissions in solution. This was not discussed in methodology or results because even when taking headspace measurements, solvent interference was too high in GC/MS results to obtain accurate readings of picked up analytes. Different SPME fibers than the ones in this study could perhaps yield better results when using acetone as a solvent. Nevertheless, several conclusions can be drawn from the described results.

Aside from the extraction methods used, this study was uniquely different from others found in literature due to the added filament wash test. Several compounds that were identified in the printing and filament wash tests were in agreement with those found in other comparable studies. Based on results from this study and others it was confirmed that the most predominant compound identified in measurement was Styrene. Considering the chemical structure of ABS plastic, this is of no surprise. The monomers of acrylonitrile butadiene styrene are shown in Figure 3.13.

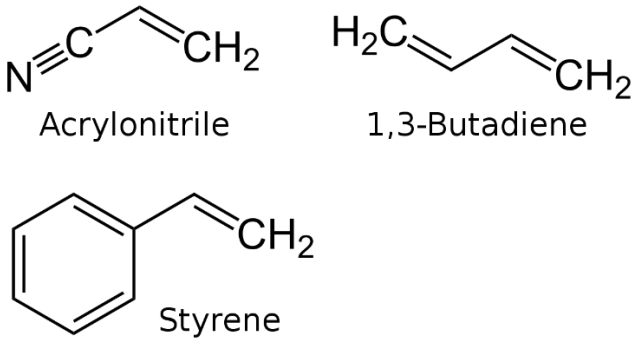

Figure 3.13 Acrylonitrile butadiene styrene (ABS) monomers

While printing ABS filament plastic using the FDM technique, the filament extrusion nozzle reaches temperatures around 230^{o}C which is far greater than the glass transition temperature ABS is to be extruded at 105 ^{o}C-110^{o}C. At temperatures high enough to melt the plastic and release subsequent particles and gases, emissions would likely be broken up pieces of the polymer chain. This was shown in results from this study by the identification of Styrene, several complex

Benzene aromatics, and nitrogenated aromatic compounds. However, several compounds identified in emission tests were also picked up in the filament wash test. This suggests that several of the emitted compounds may already exist on the filament before being put through the printing process. Additionally, with VOCs, SVOCs (semi-volatile organic compounds), and particles of ultrafine size range mixing together, it is highly likely that reactions are taking place between substances to form some of the new compounds that were identified in this study. Results suggest that by washing the filament before it is extruded, several of these emissions could conceivably be reduced in emitted concentrations or in some cases eliminated. This hypothesis will need to be investigated in future studies.

It is also common for plastic manufactures to add a number of additives for coloring and to improve on material properties. There have been studies that suggest siloxanes as effective thermoplastic additives to act as a lubricant or dispersing agent and to improve surface characteristics and scratch resistance [72]. It is specifically mentioned that siloxane additives can reduce pressure build up and improves on energy efficiency in various extrusion processes. Ultra-high-molecular-weight siloxanes have been shown to improve these plastic characteristics even more and can be fed or mixed as solids in higher concentrations with plastics during compounding, extrusion, or injection molding [73]. Variations of siloxane compounds were picked up in substantial concentrations from both printer emission tests and filament wash tests. This confirmed the presence of siloxane additives in white ABS filament plastic. The addition of the additive is likely to improve on material properties of a printed part and to better FMD extrusion efficiency. With FDM nozzle clogs being one of the major drawbacks to this manufacturing technique, it is of no surprise that filament manufacturers would do whatever possible to mitigate the issue.

Although the human effects of siloxane exposure are not fully understood, studies on environmental siloxane concentrations [74] make reference to research on observed adverse health effects due to exposure in animals [75]–[80]. Additional studies suggest that while plastics have had detrimental effects on marine inhabitance, chemical additives can also cause considerable harm to ecosystems as they are leached out of plastic pollutants and spread contamination [81].

3.4 Conclusions

In this study emission off a desktop FDM 3D printer printing white ABS plastic were collected by circulating printer exhaust through a diffuser into a solution of type 1 water.

Compounds were extracted using SPME fiber extraction than analyzed by GC/MS thermal desorption. Additionally, measurements were taken by performing a filament wash of the same white ABS plastic prior to extrusion. Results showed several identified VOCs and SVOCs contained in the solution matrix. The most predominant analyte was Styrene followed by a variety of Benzene aromatic compounds, Nitrogenated aromatic compounds, and Siloxanes. Measurements identified substantial cross over between compounds found from printer emission and filament wash tests suggesting that some emissions could possibly be reduced, or in some cases, even eliminated by washing 3D printer filament prior to use. Additional studies need to be performed to test this hypothesis. Further work is also necessary to test results using other filament types in varying color to determine which additives are contained in the plastic to improve material properties and extrusion efficiency and which are coloring agents. The work done in this study used methodology different from other studies similar in nature and tested washed filament offering an improved and more extensive understanding of FDM printer emissions.

4. REUSABLE UNIT PROCESS LIFE CYCLE INVENTORY FOR MANUFACTURING: FUSED DEPOSITION MODELING AND STEREOLITHOGRAPHY

Additive manufacturing technologies have been implemented in a variety of industries such as aerospace, automotive, health care, and military. The increasing application is owing to the unique capability of AM for fabricating parts layer by layer. Compared to traditional manufacturing processes, AM can achieve enhanced design and manufacturing complexity. In addition, it has been argued that AM could also reduce the environmental footprint of a product. However, recent studies reveal that AM processes may cause environmental consequences. With an uptake in interest within the AM industry it is important to understand the full potential and implications of using such a process. Characterization of manufacturing processes for their environmental performance can be achieved by evaluating input and output material and energy flows. The unit process life cycle inventory methodology is a promising approach to develop reusable models and tools to calculate these flows. The unit process life cycle inventory models can be connected to estimate the total material/energy consumption of and emissions from product manufacturing based on a process plan. In this chapter, we develop a unit process life cycle inventory model for two of the most widely used additive manufacturing processes i.e., Fused Deposition Modeling (FDM) and Stereolithography (SLA). FDM fabricates parts using a filament extrusion technique while SLA fabricates parts by using ultraviolet light to solidify the photosensitive liquid resin in a matter of seconds layer by layer. The models are constructed with the knowledge of physical and chemical principles and is based on production information and equipment specifications. A case study is provided to demonstrate how to use the unit process life cyle inventory model on Fused Deposition Modeling and Stereolithography.

4.1 Introduction

Additive manufacturing (AM) is a novel production technology with great potentials for innovating and advancing the manufacturing sector by addressing limitations of conventional manufacturing (CM) processes through enhanced geometric complexity and improved material utilization [44]. The general advantages of AM over CM are 1) more customized products (e.g., personalized health care and possibility of advanced geometries), 2) simplified supply chain (e.g.,

better responsiveness on the customers' demand), and 3) reduced environmental impact (e.g., less wasted material and fewer emissions). There are a number of different AM technologies available on the market, most notably for production of metallic and plastic parts, and they can be distinguished based on feed materials (e.g., powder, wire, and ABS) and energy source (e.g., electrical beam and laser). ISO/ASTM52900-15 classified AM into seven categories which are shown in Table 4.1 [ref: ISO/ASTM52900-15].

Table 4.1 AM technique and relevant mechanism for production

Technique	Approach / Mechanism
1. Material Extrusion	• Fused deposition modeling (FDM)
2. Vat Photopolymerization	• Stereolithography (SLA) • Digital light processing (DLP)
3. Powder Bed Fusion	• Electron beam melting (EBM) • Selective laser sintering (SLS) • Selective heat sintering (SHS) • Direct metal laser sintering (DMLS)
4. Material Jetting	• Multi-jet modeling (MJM)
5. Binder Jetting	• Powder bed and inkjet head 3D printing (PBIH) • Plaster-based 3D printing (PP)
6. Sheet Lamination	• Laminated object manufacturing (LOM) • Ultrasonic consolidation (UC)
7. Direct Energy Deposition	• Laser metal deposition (LMD)

Each technology has its own merits and drawbacks when considering benefits from improved design features and manufacturing sustainability. These topics have been studied thoroughly from a life cycle (LC) perspective with consideration of a variety of AM technologies.

With the increasing applications and implementations of AM technologies in different industries, the environmental sustainability of AM has been of great concerns considering its energy consumption, waste generation, water usage, and potential environmental impacts caused by fabricated products [82]. Generally, environmental sustainability has been suggested as one of the major advantages of AM due to its high material efficiency while reducing or even eliminating the need for tooling, cutting fluids, and lubricants [83]. However, more research efforts are still required to better comprehend the environmental consequences of AM processes and materials

[84]. To quantify the material and energy flows in AM processes under different operating conditions, the unit process life cycle inventory (UPLCI) methodology is often adopted.

The Unit Process Life Cycle Inventory (UPLCI) aims to develop reusable models and tools that can be used to predict the material and energy flows of a certain manufacturing process with minimal experimental efforts. In current literature, the energy and material utilization have been studied and compared for several forms of AM techniques such as fused deposition modeling, binder jetting, electron beam melting, and selective laser sintering/melting. The majority of these studies focus on the energy consumption [15]. In addition, most of the existing studies use experimental based approaches and investigate the influence of AM process parameters [85], which can significantly hinders the reusability of the results because they are obtained from certain experimental conditions. To address this issue, in this study, a UPLCI model is developed for two of the most commercialized AM technologies i.e., Fused Deposition Modeling (FDM) and Mask Image Projection (MIP) Stereolithography (SLA), aiming to provide quantitative information on the material and energy flows in these processes.

4.2 Fused Deposition Modeling Model

Development of the FMD UPLCI model mostly consisted of created a framework by identifying fundamental equations to predict input and output material and energy flows. There has been a lot of work focused on creating FMD models in other studies, but by developing unique methodology for this study, it is shown how these concepts can be extended to other AM process models like SLA.

UPLCI models for AM use physical equations to calculate predicted material and energy input and output flows. To begin it is necessary to gain a thorough understanding of how the system works. FDM printers work by extruding filament layer by layer onto a heated print bed to fabricate a part. Depending on the material that is used, the print bed may or may not need to be heated. ABS plastic for example requires a heated print bed to temperatures around 110^{o}C while PLA plastic does not. By grasping the functionality of the process, the sources of input material and energy flows can be identified. Figure 4.1 shows the considered sources of material and energy input flows.

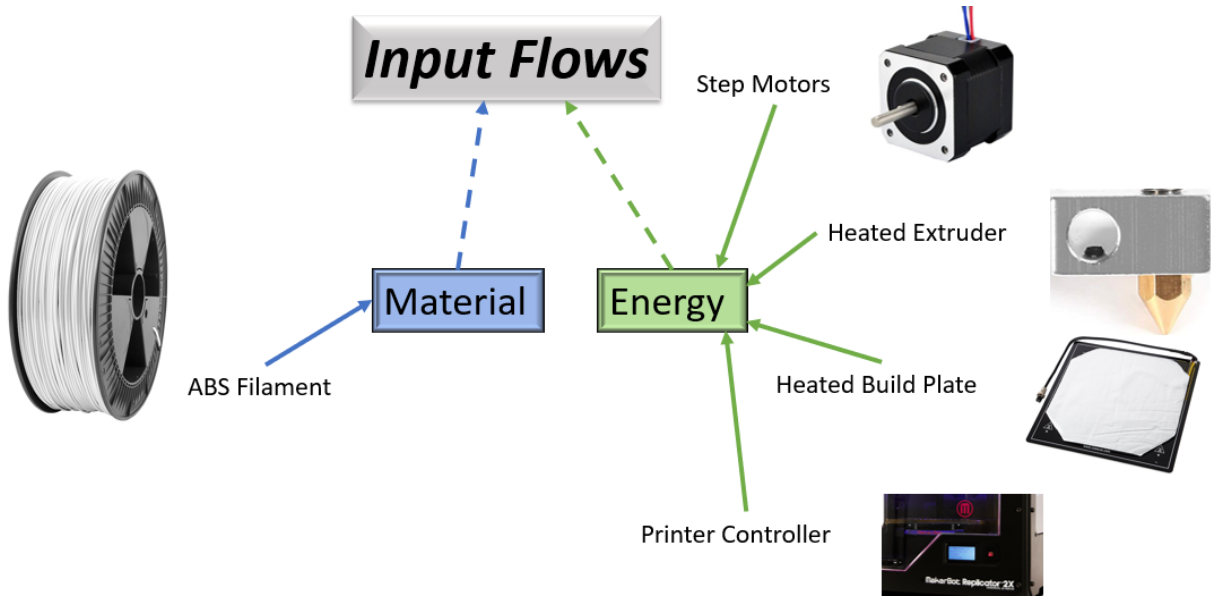

Figure 4.1 Primary sources of FDM material and energy input flows

Considering the recognized material and energy process contributors, methods were developed to calculate production output flows. Information available prior to producing includes the part STL print file, machine G-Code, machine energy specifications, and filament material characteristics. Using this information, a series of transformation functions are developed to calculate several outputs desired outputs. Transformation function outputs offer projected assumptions regarding the final part and total energy consumption both of which can be used to calculate environmental impact in 11 different environmental impact categories. The unit process flow diagram for the FDM model is shown in Figure 4.2.

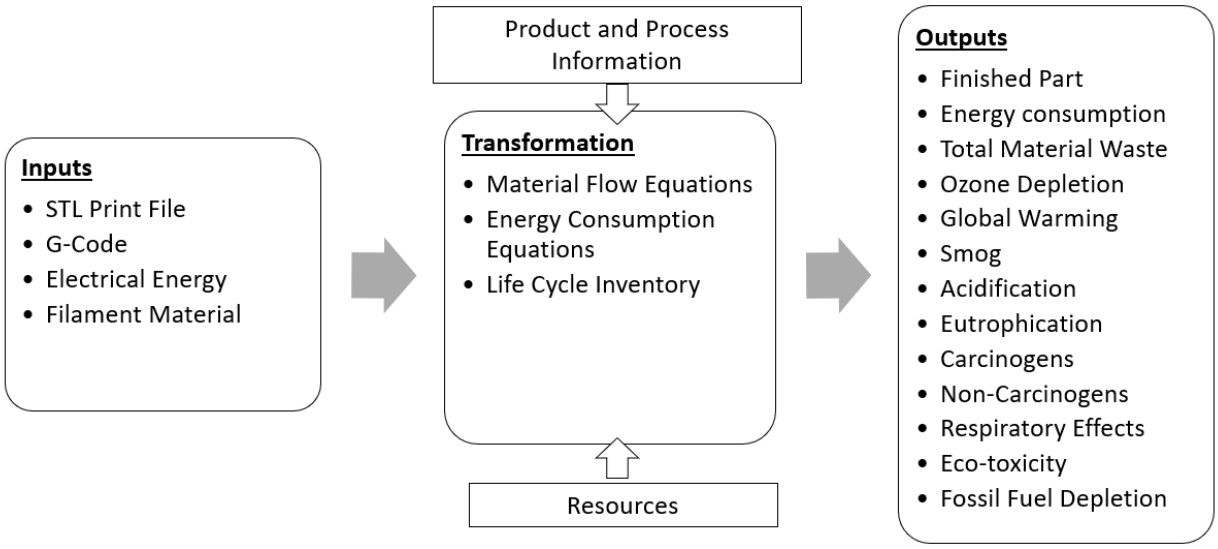

Figure 4.2 FDM unit process model material flow diagram

4.3 FDM Model Calculations

4.3.1 FDM Process Material Consumption

Material consumption for FDM 3D printers is fairly easy to assess especially when support structure is not considered. A simple mass balance can be considered to easily estimate the material input for any part. FDM printers have several set printer parameters that are considered when determining material consumption. These parameters are as follows:

- Percent Infill (%)
- Infill Design (pattern)
- Layer Height (m)
- Number of Shells (#)
- Raft (yes/no)

When a part is fabricated using FDM, most users choose to begin with the printing of a raft to facilitate a more scrupulous print with less imperfections. Additionally, a percent infill is set based on the desired strength of the part. The most structurally sound infill design is the honeycomb (hexagon) infill pattern. With junctions of 120 degrees, hexagon infill structures are the most mechanically stable. Hexagon infill patterns minimize the perimeter and total number of vertices making it optimal for FDM printing. Generally 10% is considered adequate for most parts

not undergoing significant stress or strain during use. Layer height determines the thickness of each layer, usually 0.2mm. Finally, the number of shells determines the number of layers on the outer shell of a part before infill begins, usually set to 2. With all of this considered a slicing algorithm, also used in the SLA UPLCI model, is used in the FDM model to calculate the final part volume with the input of an STL file [86]. The same slicing algorithm is used to calculate the total surface area of a given part. With the volume of the part and total surface area a simple calculation can be made to determine the overall mass of material input in order to produce a given part. This is done using equation 4.1 where m_{part} (g) is the mass of the part, SA_{part} (m^2) is the surface area of the part, V_{part} (m^3) is the part volume, and ρ is the material density (g/m^3).

$$m_{part} = [SA_{part} \times Layer\ Height \times Number\ of\ shells + (V_{part} - SA_{part} \times Layer\ Height \times Number\ of\ shells) \times Percent\ Infill] \times \rho \quad 4.1$$

4.3.2 FDM Process Energy Consumption

Energy input/output flow for FDM is calculated by determining the total amount of time required to print a part. The total print time is calculated using the printer G-Code as an input. Printer G-Code is produced simply by inputting a print file into some AM software such as Cura. The G-Code, which essentially instructs a machine in what to do, contains a lot of useful information relevant to the amount of time it takes to print an object. This includes coordinate directions the print head will move to, speeds it will be moving at between each designated coordinate, and the filament extrusion rate. A MATLAB script was created to interpret the G-Code and accurately calculate an estimated total print time for any part to print. This is done using the changing rate at which the extruder is moving between coordinate directions. Moves are performed at different speeds based on what is being printed on the part at a particular time. While no filament is being extruded, the print head will move much quicker. This method is described in equation 4.2.

$$t_{print} = \sum_{i=0}^{i=\#\ Moves} [{}^{xy_{dist,i}}/_{f_i}] \quad 4.2$$

Total energy consumption is predominantly affected by the amount of time the printer is running. With an accurate prediction of total print time, required energy input can be calculated using rated energy specification of the running FDM components. This includes 3 step motors, the

heated extrusion nozzle, and the heated bed. The equations for total energy consumption is shown in equation 4.3.

$$E_{total} = E_{controller} + E_{nozzle} + E_{plate} + E_{motors} \quad 4.3$$

Energy consumed by the motors is calculated the same way for FDM and SLA models since they both use step motors. Most FDM printers use 3 step motors each with the same power rating. A more thorough description of motor energy calculations is discussed in SLA modeling sections but the final equation for energy consumed by the step motors for FDM printers is shown in equation 4.4.

$$E_{motors} = 3 \times \sum_{i=1}^{N} P_{motor} \times t_{print} \quad 4.4$$

Consumed energy from the printer controller is calculated using the rated power of the controller and the total time it is running for. The equation used to calculated the printer controller energy consumption is shown in equation 4.5.

$$E_{controller} = P_{controller} \times t_{print} \quad 4.5$$

The final two energy consuming components in the FDM process include energy consumed by the heated nozzle and the heated build plate. These last two components contain similar calculation methods. First the total energy required to heat each component to the desired temperature is determined using the Fourier heat equation. The Fourier heat equation is shown below in equation 4.6.

$$\frac{\partial}{\partial x}\left(k\frac{\partial T}{\partial x}\right) + \frac{\partial}{\partial y}\left(k\frac{\partial T}{\partial y}\right) + \frac{\partial}{\partial z}\left(k\frac{\partial T}{\partial z}\right) + \dot{e}_{gen} = \rho c\frac{\partial T}{\partial t} \quad 4.6$$

When calculating required energy to heat the nozzle the parts of the nozzle heating element and their material composition need to be considered. The heated extrusion nozzle is composed of five parts. The heat block is composed of aluminum and is the main component all other elements screw into. The thermistor, which takes temperature readings, fits into a small slot directly in the heat block. The heat break is a threaded rod composed of stainless steel, a non-heat conducting metal, and screws into the upper portion of the heat block where filament is fed through. The extrusion nozzle is threaded into the bottom of the heat block and is composed of brass, a highly thermally conductive metal. Finally, the heater cartridge supplies the energy and heat to the system, has a power rating of 40W and is fed into the side of the heat block. The outside of the heat block

is generally insulated to maintain constant temperature during the printing process. A picture of the disassembled heated extrusion nozzle is shown in Figure 4.3.

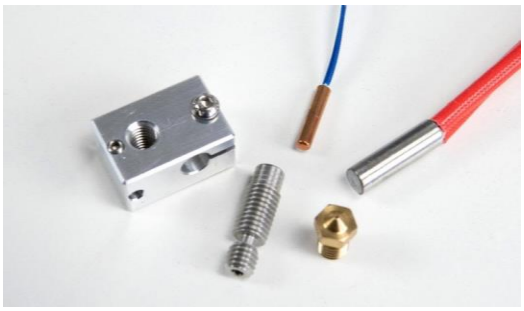

Figure 4.3 Disassembled FDM extrusion nozzle

The heated bed is generally composed of aluminum and is just a flat plate requiring 140W power input. It was shown in our previous study that the required energy to maintain nozzle and bed temperatures is somewhat constant throughout the printing process. That considered the final equations for energy consumed by the heated extrusion nozzle and print bed are shown in equations 4.7 and 4.8.

$$E_{nozzle} = dE_{nozzle,w} + P_{nozzle} \times t_{print} \quad 4.7$$

$$E_{plate} = dE_{plate,w} + P_{plate} \times t_{print} \quad 4.8$$

As shown in the final equations for nozzle and bed energy, after the initial energy to heat the components is found, only the power and total print time are considered.

Conclusively, model calculations in the FDM printing process are predominantly determined by machine specifications, material properties, designer inputs, and total time to print. A summary of this is shown in Table 4.2. Particulate and gaseous emissions were not considered in this model although there have been studies that have created equations to predict FDM printing emissions [53]. In the following section a similar procedure is followed to model the SLA process with included validation testing.

Table 4.2 Summary of model inputs and final equations for FDM printing process

Model Inputs by User	Equations

Material
• Part Printing Parameters
  ○ Defined by user
• STL File
• Material Properties
  ○ Based on filament being used
	Total Material Consumption:
	$m_{part} = [SA_{part} \times Layer\ Height \times Number\ of\ shells + (V_{part} - SA_{part} \times Layer\ Height \times Number\ of\ shells) \times Percent\ Infill] \times \rho$

Time
• G-Code
  ○ Generated using 3D printer software
  ○ Uses STL file as input
	Total Print Time:
	$t_{print} = \sum_{i=0}^{i=\#\ Moves} [{xy_{dist,i}}/{f_i}]$

Energy • Machine Energy Specifications ○ Varies by machine	***Total Energy Consumption:*** $E_{total} = E_{controller} + E_{nozzle} + E_{plate} + E_{motors}$

4.4 Stereolithography Model

Using the SLA process, the photosensitive liquid resin is solidified by certain light sources (i.e., Ultraviolet light) layer by layer. This liquid resin usually consists of monomers/oligomers, photoinitiators, and some additives. During the photopolymerization process, the chains of molecules are linked to form polymers in the presence of light sources, and the layered polymers constitute the final 3D products. The viscosity of the photosensitive resin is affected by the monomers/oligomers. In addition, the photoinitiators that are used in the resin can determine the required wavelengths of the Ultraviolet (UV) light to solidify the resin. When the curing process takes place the monomers and oligomers form long chain and cross-linked molecules via polymerization.

The SLA production has three main stages, i.e., printer warmup, production, and printer cooldown. The three stages are explained as follows, which are also illustrated in Figure 4.4.

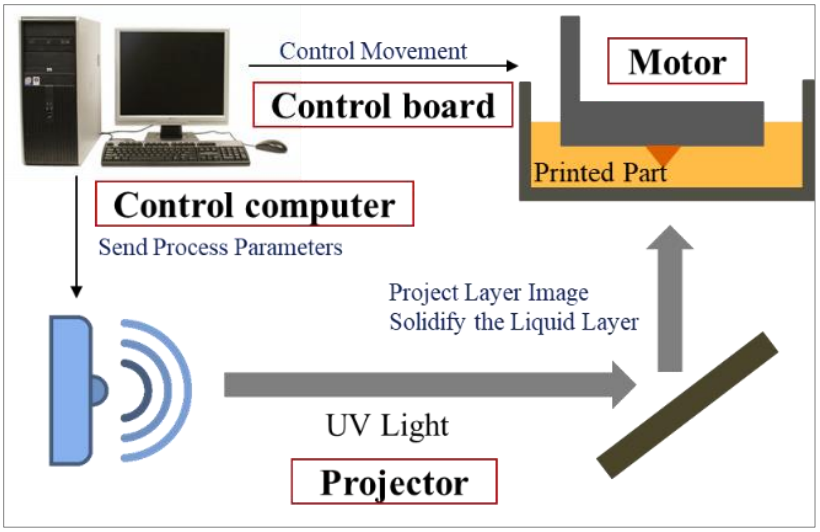

Figure 4.4 Illustration of mask image projection (stereolithography) printing setup

(1) Printer warmup stage. During this stage, the 3D CAD design is imported to the control software of the 3D printer, and sliced into a certain number of layer images based on the selection of process parameters such as layer thickness and print orientation.

(2) Printing stage. To start the production, the layer image of the first layer is projected onto the build platform, and solidified by the UV light. After the first layer is fabricated, the build platform moves up to get ready for the next layer. This entire "project-cure-move" process is repeated until the final product is fabricated.

(3) Printer cooldown stage. The fabricated product is retrieved from the build platform, and further post-processed if necessary. Possible post-processing activities include cleaning, post-curing, surface finishing, etc.

This study considers only the printer warmup, cooldown, and printing stages of SLA. The post-processing stage is highly dependent on the part being printed and its intended use thus it is difficult to develop a reusable model. The primary components of an SLA machine include a computer, control board, projector, and motor. An illustration of how this process works can be observed in Figure 4.4.

Other studies have modeled similar AM processes with a focus on material efficiency and global warming potential (GWP). Material recycling in laser beam melting powder-bed based processes has been investigated by considering powder reuse cycle as well as resource and energy

consumption [87]. Similar to the study done here separate models are made for material and energy calculations to both be considered in GWP and general efficiencies of the manufacturing process.

This paper serves as a part of a series of UPLCI papers focusing on different manufacturing processes starting with the process of grinding [88]. There is much more information regarding UPLCI for high production traditional manufacturing processes, however, with AM technologies still progressing from prototyping to production there is less information on process flows pertaining to this industry [15]. Several aspects of AM are still in development especially in the area of high production manufacturing.

4.5 Methodology for Unit Process Life Cycle Inventory Model

The UPLCI methodology adopts the concept of unit operations, which enables reusability and connectivity thus facilitating the assessment of a unit manufacturing process as well as a product for environmental performance. The model for unit process life cycle inventory consists of inputs, product and process information, outputs, and a set of transformation functions. The transformation from input to output considered in this study consists of three LCI characteristics, i.e., input materials, energy required, and material losses. With these LCI characteristics considered, the flow chart of establishing the unit process model can be interpreted as shown in Figure 4.5.

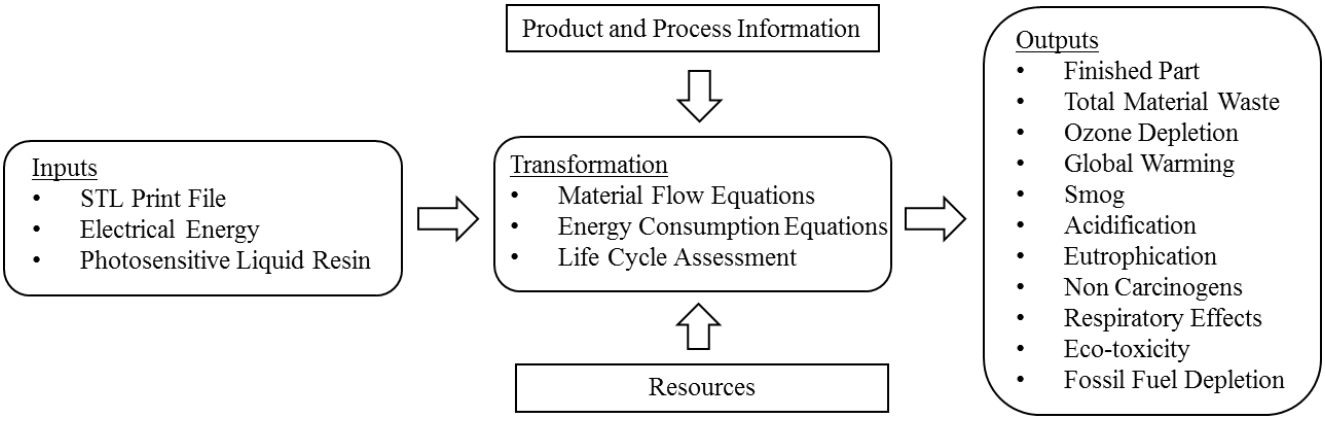

Figure 4.5 Unit process model material flow diagram for experimental setup

4.5.1 SLA Process Energy Consumption

A typical MIP SLA machine has four main electricity consumers, i.e., computer, control board, projector, and motor. Therefore, the total energy consumption of this SLA process is modeled based on the electricity usages from these four components, which can be formulated as shown in Equation (4.9).

$$E_{total} = E_{projector} + E_{motor} + E_{computer} + E_{board} \tag{4.9}$$

Determining the energy consumption of the four primary components separately entails quantifying the impact from relevant parameters involved in a print. All parameters and variables considered for the UPLCI model are categorized in the list of symbols. The influence of these parameters can be better assessed if broken down by the four primary energy-consuming components.

A large number of the printing parameters listed can be determined by inputting the STL file for the desired part into a slicing algorithm which slices 3D CAD models into a set of layers. That is, with a given layer thickness, this algorithm cuts the 3D model into multiple parallel 2D planes (with varying surface or cross section areas). As an example, a NIST artifact is imported to the algorithm and sliced with 50 intervals/layers in Figure 4.6. Then, the exposure area (surface area) of each layer can be calculated. In the file, triangular facets approximate the geometry information using an outward normal and coordinate points (x, y, and z) [89]. More details can be found in [86].

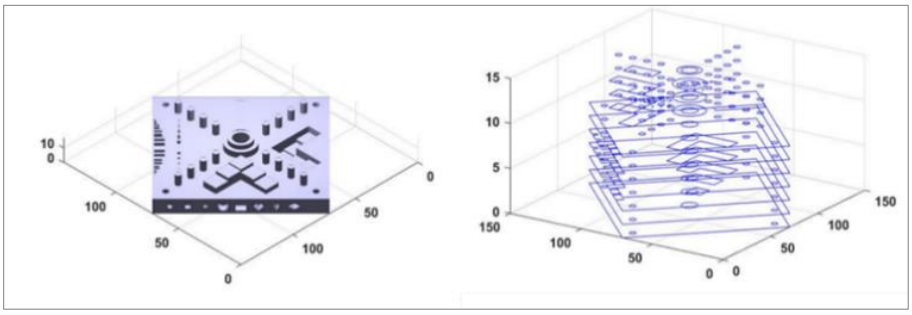

Figure 4.6 STL slicing algorithm to calculate exposure area of each layer

After obtaining multiple 2D planes from a 3D model, various parameters based on exposure area can be calculated. For the purpose of simplification, parameters calculated with the

use of the slicing algorithm are assumed as known in various equations. Depending on the software that is used, information such as part volume, surface area, layer print times, and other variables affected by user defined printing parameters may be determined differently for different types of SLA printers. These parameters are key in the following equations when solving for energy consumption as they affect the time all four components are running and the total energy input.

4.5.2 Computer & Control Board Energy Required for SLA

Both the computer and control board consume energy during the printing process. The energy consumption can be determined using the power required to run the computer and control board, and the total print time for a part. For simplification reasons, the computer and control board power requirements are assumed to be the same as shown in the specifications. Energy consumption for the computer and control board can be seen in Equations (4.10) and (4.11).

$$E_{computer} = P_{computer} \times T_{printing} \tag{4.10}$$

$$E_{board} = P_{board} \times T_{printing} \tag{4.11}$$

The total print time is a function of the total number of layers and the curing time for each layer. Number of layers and curing time are both functions of the user identified layer thickness. The total print time can be estimated using Equation (4.12) or acquired from the 3D printing software depending on the SLA machine being used. Nomenclature and units can be found in the list of symbols.

$$T_{printing} = N_{bottom} \times \left(T_{LS} + T_{curing,b}\right) + (N - N_{bottom}) \times \left(T_{LS} + T_{curing}\right) \tag{4.12}$$

4.5.3 Projector Energy Required for SLA

In the SLA process, photosensitive liquid resin is cured by exposing UV radiation, known as a photopolymerization process. In this process, photoinitiator molecules absorb energy emitting photons from a light source to initialize polymerization. Here a projector was used as the UV light source. In that sense, the power required for the curing is proportional to the exposure area (surface area of each layer), which can be described by the UV radiation intensity (W/mm2). Depending on the resin used for printing the required UV light intensity may vary. Different resins may contain variable types of photoinitiator molecules that required more or less energy from a photon.

Once required light intensity on the exposure surface area is determined from material properties, a light source with ample intensity is used as the printer power source.

To calculate the energy consumed to cure the resin, each layer exposure area is used from the described slicing algorithm and input into the UPLCI model. If the surface area of each layer, light intensity (W/m2), and exposure time are known, then the energy consumed by the projector can be estimated using Equations (4.13)-(4.15).

$$E_{curing} = P_{curing} \times T_{printing} \tag{4.13}$$

$$E_{idle,p} = P_{idle} \times T_{idle} \tag{4.14}$$

$$E_{projector} = E_{curing} + E_{idle,p} \tag{4.15}$$

While the material is used to determine how strong a light source is needed, once the light source is obtained the user must identify the power output while projecting UV and while idling in order to determine the total energy consumption of the source. Power during idle and curing can be obtained by nameplate values or measured experimentally. Here the term *P* represents the power from UV light source and is multiplied by time (*T*) in order to calculate the total energy (*E*). Values of curing power and idle power from the specified UV light source may vary substantially depending on what is used for a given SLA machine. Curing power required during projection of a layer often times does not deviate much from idling which will be further evaluated in the experiments.

The approach given in this section is universal among different resin materials used in different industries. This includes standard resins for general prototyping, engineering resins with specific mechanical and thermal properties, dental and medical resins with biocompatibility certifications, and castable resins [90]. Depending on the resin used for the SLA process, the energy requirement from an absorbed photon may vary slightly based on the photointiator in the material. All will display different and unique properties from one another offering a variety of uses.

4.5.4 Motor Energy Required for SLA

Generally, to calculate the energy consumed to move the platform using a stepper motor, each layer's exposure area and its accumulated weight should be used. As more layers accumulate on a printed part, the energy consumption of the motor will increase. This results from the increase

in overall weight and required torque to spin the threaded rod. However, with most SLA printers the downward force resulting from the part is not great enough to make a significant difference in power delivery from the motor, therefore, the nameplate power delivered from the motor can be used to calculate total energy required to run the stepper motor for a print, as formulated in Equation (4.16).

$$E_{motor} = P_{motor} \times T_{printing} \tag{4.16}$$

Similar to the energy use of the UV source (projector) the power of the motor (P_{motor}) can be determined by using nameplate values or through experimental measurements.

4.5.5 SLA Process Material Consumption

The material flows for the SLA process are then categorized by state: solid, liquid, and gaseous materials. The input material (photosensitive resin) begins as the liquid form and changes into one of the three chemical states. The solid material consumption makes up the total mass of the printed part while the liquid and gaseous material makes up the waste streams in the process. The calculation for material consumption or material input is shown by Equation (4.17). Here there are three components considered as contributors to total material input including material from the final part (m_{part}), liquid material waste from the resin containment ($m_{waste,l}$), and material waste as gaseous emission ($m_{waste,g}$).

$$m_{input} = m_{part} + m_{waste,l} + m_{waste,g} \tag{4.17}$$

The mass of the fabricated part depends on the total volume and density of printed part, as shown in Equation (4.18).

$$m_{part} = \rho_{part} \times V_{part} \tag{4.18}$$

During the SLA production process, the photosensitive liquid resin can (1) leave residues on the building platform and printed parts, and (2) cause gaseous emission due to the volatilization process. Hence, both types of material wastes are studied in this work.

4.5.6 Quantifying Liquid Waste

When considering liquid material waste there are several different pathways for which liquid resin may escape the printer without becoming part of the finished product. This includes

but is not limited to resin sticking to the solidified part, discharge of liquid outside of the batch containment, and entrapment of liquid within various portions of the printed part. Many of these sources can be difficult to characterize based on physics. The amount of liquid material waste can be influenced by several factors including depth of liquid resin in the containment vessel, the outer surface area of the printed part, and the batch size. Without certainty of quantity of contribution from all factors the amount of liquid waste can be difficult to model. It was found that much of the liquid waste was as a result of resin sticking to the finished part through surface tension at the conclusion of the print. Since the material that is used remained consistent the surface tension never changes during printing. Nevertheless, surface area does change and is the primary variable considered when calculating the liquid material waste stream. In this study the primary variable considered to impact total liquid waste is based on the surface area of the finished part.

Similar to the slicing algorithm used to calculated surface area of each layer of the part, the triangulated STL file can be used to calculate the estimated total surface area of the print to predict the amount of liquid resin escaping with the solidified part. This could be done with a variety of different programs as long as the total surface area of a printed part can be estimated. The equation for liquid material waste is shown in Equation (4.19).

$$m_{waste,l} = \alpha \times S_{part} \times \rho_{resin} \tag{4.19}$$

Liquid material waste resulting from part surface area is highly dependent on material properties such as surface tension and therefore results will vary depending on the photosensitive resin that is used in the SLA process. By determining an average thickness of liquid resin coating the final part the total surface area of a part can be used to determine an estimate of liquid material waste.

4.5.7 Quantifying Gaseous Waste

Gaseous waste for in the SLA is due to the vaporization of resin. During printing, increased surface temperature due to energy input from UV lights may speed up vaporization but this is difficult to model. For simplification, only vaporization at room temperature is considered. Equation (4.20) can be used to calculate the total emission rate [91]. Here Q denotes mass transfer rate, M is molecular weight, and S represents the surface area.

$$ER(t)_{volatilization} = Q \cdot M \cdot S \tag{4.20}$$

In Equation (4.20), the mass transfer rate (Q) is a function of the mass transfer coefficient (K), the vapor pressure of the liquid (ρ_v), the universal gas constant (R), and absolute temperature (T) as expressed in Equation (4.21). Note that Equations (4.21)-(4.25) are functions dependent on both testing environment as well as liquid resin properties [46]. The mass transfer coefficient (K) is expressed as a function of wind speed and liquid pools size which is relative to the resin tank size in this study [92]. In Equation (4.22), v_z represents the air flow speed in the printer environment, Δz stands for the length of the air to liquid interface oriented in the direction of flow, and Sc is the Schmidt number. Equations (4.23)-(4.25) are used to calculated air viscosity (μ), air density (ρ_a), and diffusivity (D), which in turn can be used to determine Sc [93]. The term T refers to the absolute temperature while P is ambient air pressure, and M is molecular weight. Using Equations (4.20)-(4.25) the solution to Equation (4.26) can be determined.

$$Q = K\frac{\rho_v}{RT} \tag{4.21}$$

$$K = 0.0220 \times v_z^{0.78} \times \Delta z^{-0.11} \times Sc^{-0.67} \tag{4.22}$$

$$\mu = -9.426 \times 10^{-5} + 1.610 \times 10^{-5} \times \sqrt{T} \tag{4.23}$$

$$\rho_a = 0.352\frac{P}{T} \tag{4.24}$$

$$D = \frac{4.09\times10^{-5}\times T^{1.9}\times\sqrt{\frac{1}{28.97}+\frac{1}{M}}}{P\times M^{0.33}} \tag{4.25}$$

$$m_{waste,g} = ER(t)_{volatilization} \times T_{Printing} \tag{4.26}$$

4.6 UPLCI Model Validation

When constructing a model for any UPLCI manufacturing process it is important to validate the model for accuracy. For the purpose of this study special attention was targeted towards changes in part geometry and printing layer thickness. These variables in turn have effects on the entire printing process and lead to considerable differences in material and energy flows. Variations of part geometry when maintaining the same layer thickness is primarily reflected in the changed print time. Larger geometries will lead to longer print times and thus can increase energy consumption during a print. Additionally, different geometry sizes will alter material consumption and waste. Layer thickness is another critical parameter to be considered as it affects the total time it takes to print a part as well as the surface quality of the finished part.

4.6.1 Experimental Setup

To validate the proposed UPLCI model, experiments are performed to investigate the energy flow and material flow in an SLA process when fabricating the NIST AM test artifact shown in Figure 4.7 (a) and (b).

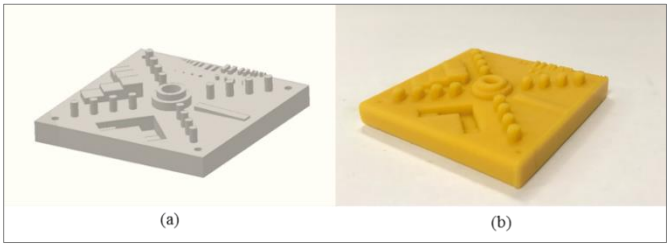

Figure 4.7 The part geometry used in model validations, adapted from [86], (a) Program file; (b) SLA printed NIST part from program file in Figure 4.7(a).

In this study, an SLA test bed is developed and used, which contains several components including a projector as the UV source, a motor that powers the building platform, a control board, control software, and a material tank. A Yokogawa CW10 power meter with 0.01 W resolution is used to measure the power consumption, a Honeywell MiniRAE 3000 VOC monitor is used to measure the real-time VOC emissions from the liquid resin, and a Taishi 200 digital scale is used to quantify the material consumption and waste generated. Three validation cases are considered with different sets of process parameters, as shown in Table 4.3. In order to consider how the model performs under different geometric condition common printer parameters were changed in each validation test. The size of the printed part was decreased for validation 3 and the layer thickness was increased by a factor of 10 for validation 2. As shown in Table 4.3 these changes result in different curing times and production times during the printing process.

Table 4.3 Illustration of different validation cases and their process parameters

	Validation I	**Validation II**	**Validation III**
Geometry Size	50%	50%	30%
$\boldsymbol{d}$	0.03mm	0.3mm	0.03mm
$\boldsymbol{T_{curing}}$	2s	12s	2s
$\boldsymbol{T_{curing,b}}$	15s	25s	15s
$\boldsymbol{T_{LS}}$	17.6s	17.6s	17.6s
$\boldsymbol{T_{pre}}$	600s	600s	600s
$\boldsymbol{T_{printing}}$	5580s	867s	3371s
$\boldsymbol{T_{post}}$	600s	600s	600s

Experimental results are split into two sections, one for the energy model validation and another for the material model validation. The same three validation cases are used for both.

4.6.2 Energy Model Validation Experimental Results

To experimentally validate the transformation functions in the energy consumption model, the power consumption is measured over time from every energy-consuming component of the SLA machine. More specifically, the power is measured every five seconds. In addition, each validation case is repeated three times to reduce the random measurement errors.

During energy modeling, simplified equations are used with the assumption of a fairly steady power profile. The average power usage from each energy consuming printer component is illustrated in Table 4.4.

Table 4.4 Average power usage from printer components

Printer Component	**Power Usage**
Computer	90 W
Control Board	12 W
Motor	20 W
Projector Idle	241 W
Projector Print	250 W

The power profiles of all four energy-consuming components are shown in Figure 4.8. It can be observed that the projector, which is used for solidifying the liquid resin by projecting UV light, plays the most significant role in terms of energy consumption. In addition, a power decrease can be observed before and after the production periods for all energy consuming components. The fluctuations of power consumption of the projector and the motor during the printing stage are shown in Figure 4.9 (a) and (b). It is important to note that although there are spikes in power profile for the different components measured the average power usage remains consistent during the printing period, as well as, before and after. The simplified equations use nameplate values to calculated energy consumption during the print time period. The decreased power consumption during idling (printer warmup and printer cooldown) only has limited effect since the duration is much shorter than printing.

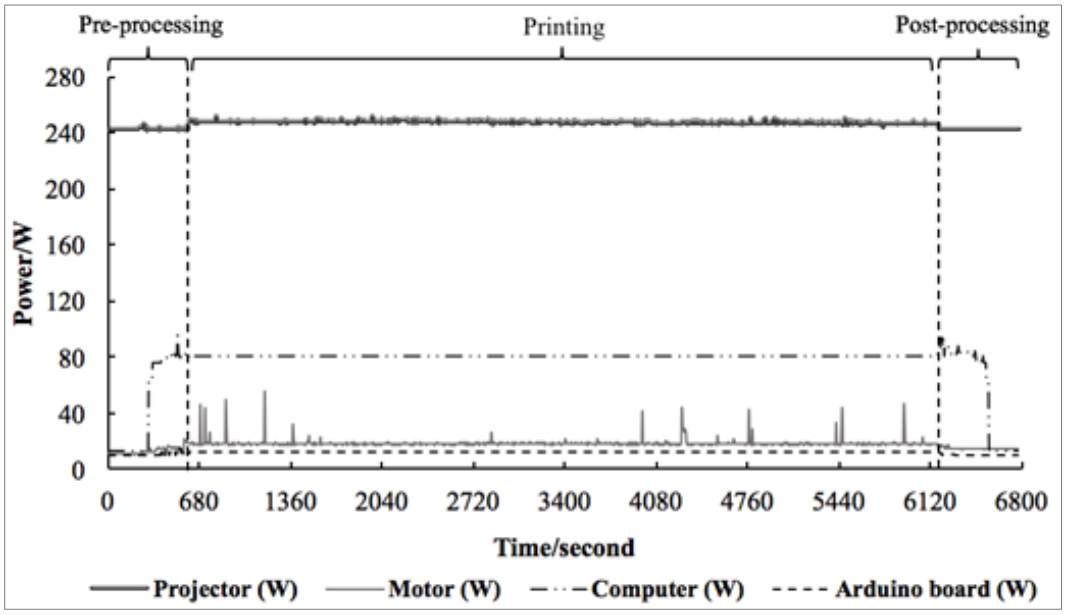

Figure 4.8 Power profile for all four energy consuming components

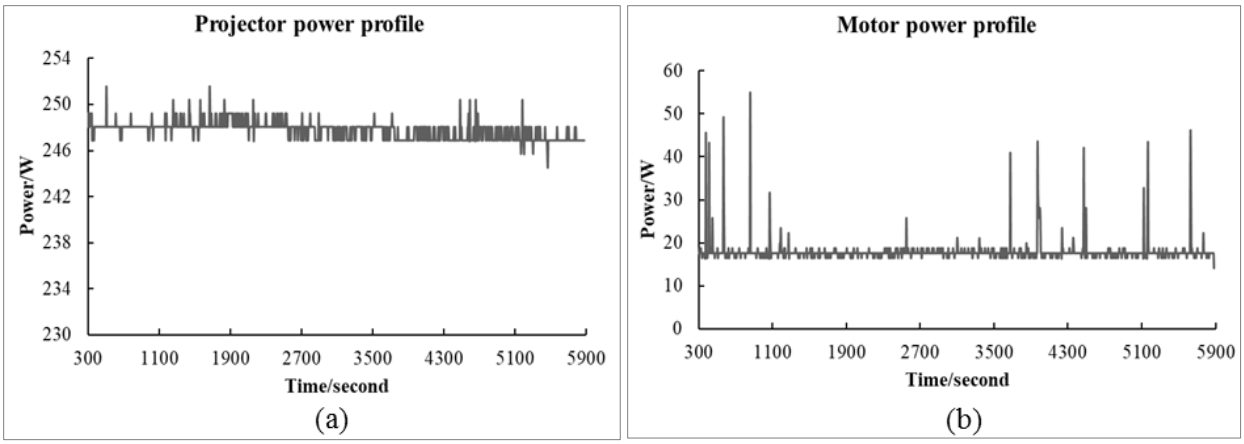

Figure 4.9 (a) The power profile of the projector (b) The power profile of the motor during printing stage

The validation results are illustrated in Table 4.5. The model calculations and experimental measurements show good agreement. The main errors of the model prediction come from the assumption of constant power profile during each stage of the printing process. Without consideration of process dynamics throughout the print the accuracy of energy consumption estimates will fall short slightly due to spikes in the given power profiles. Nevertheless, observed average power consumption for each of the four energy-consuming components is close to what is given from nameplate values.

The validation testing shown further along with the assumption of using constant power output for both the motor and projector display good accuracy despite equation simplifications.

Table 4.5 The energy consumption during the production period

		Energy consumption of different consumers (Wh)				
		Total	Projector	Motor	Computer	Control board
Validation I	Model calculation	576	387	26.1	145	18.6
	Measurement	558	386	27.5	125	20.0
Validation II	Model calculation	92.6	64.7	2.60	22.5	2.89
	Measurement	87.3	60.4	4.33	19.4	3.10
Validation III	Model calculation	345	231	15.7	87.4	11.2
	Measurement	340	236	16.8	75.6	12.1
Average model accuracy		96.4%	96.8%	82.8%	84.4%	93.3%

4.6.3 Material Model Validation Experimental Results

The experimental validation of proposed material model involves the real-time measurements of VOC emissions throughout the printing process. The parameters that are required to quantify the VOC emissions are relied on the experimental environment, and their values are shown in Table 4.6.

Table 4.6 Equation parameter constants

Parameter	**Value**
v_z	1.2 cm/sec
ρ_a	1.225 kg/m^3
ρ_{part}	1170 kg/m^3
ρ_{resin}	1090 kg/m^3
Δz	2 cm
M	100.121 g/g·mole
P	1 atm
R	8.314×10^3 cm^3·kPa/g·mole·K
T	298.65 K

The real-time measurement of total VOC is shown in Figure 4.10. The average concentration of VOC during both printer warmup and printing periods is stable with slightly increasing trends. A few seconds after the printing is finished, a peak occurs mainly due to the movement of the building platform and the opening of the machine cover. Unlike the power profiles shown, the VOC concentration is not stable throughout the printing process suggesting that gaseous emission is resulting mostly from the printing process rather than the vaporization. The trends observed in Figure 4.10 could result from a variety of different parameters including curing surface area, varying layer geometric, layer thickness, prolonged resin exposure to UV, among other printer and part properties. Without data supporting the cause of VOC emission trends in SLA, accuracy of gaseous emission estimations will be moderate at best.

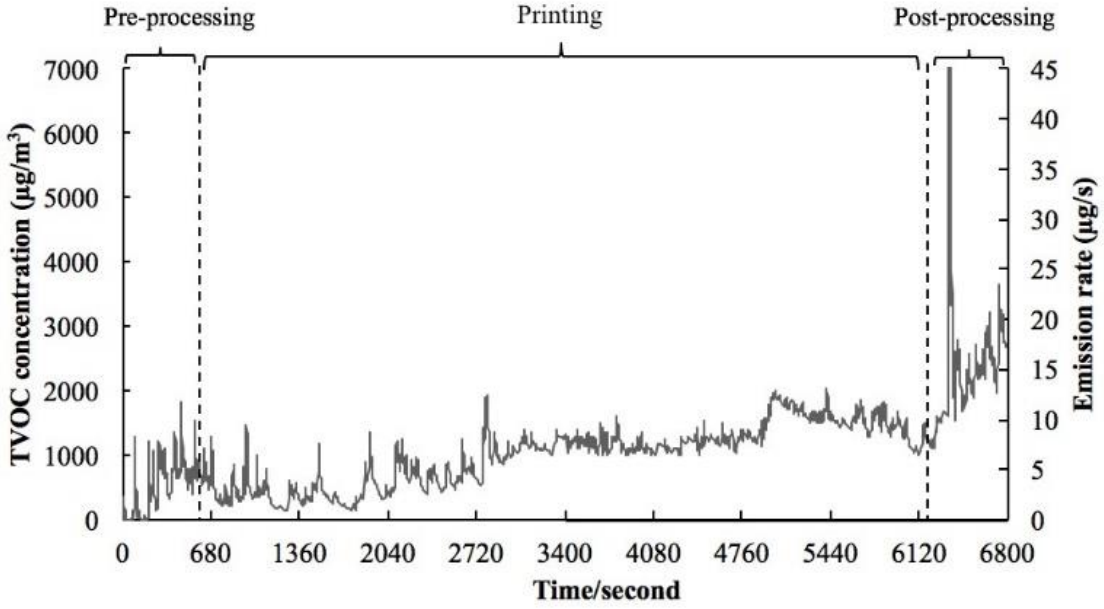

Figure 4.10 Real-time measurement of total VOC

The material waste results from two primary sources including the gaseous waste (VOC emission) and liquid waste coating the printed part and build plate of the machine. Gaseous emission is based on the calculation sourced from Equation (12) yielding an emission rate of $11.2\,\mu g/s$. Using the experimentally measured values, the material waste and total material consumption model is validated as shown in Table 4.7 and Table 4.8. The model adequately predicts the material waste and the total material consumption, with accuracies of around 91% and 95% respectively.

Table 4.7 Material waste validation

		Material waste percentage (%)		
		Total waste	Gaseous waste	Liquid waste
Validation I	Model calculation	8.04	0.422	7.62
	Measurement	7.22	0.172	7.04
Validation II	Model calculation	7.85	0.0657	7.78
	Measurement	8.31	0.0611	8.24
Validation III	Model calculation	4.87	1.18	3.69
	Measurement	4.89	0.420	4.47
Average model accuracy		94.6%	56.4%	89.6%

Table 4.8 Material consumption going into finished part

		Material consumption (g)		
		Total consumption	Total waste	Part weight
Validation I	Model calculation	15.9	1.13	14.8
	Measurement	17.3	1.14	16.2
Validation II	Model calculation	16.2	1.15	15.1
	Measurement	16.3	1.13	15.2
Validation III	Model calculation	3.34	0.120	3.22
	Measurement	3.53	0.151	3.38
Average model accuracy		95.4%	92.5%	95.4%

4.7 Conclusion and Future Work

This study is conducted aiming to enhance the understandings on the fundamental mechanisms of the SLA unit process and to develop a UPLCI information model that can represent the process reusable abstraction. To achieve this goal, mathematical, physical, and experimental based models are developed as functions of process parameters, exposure area, geometry design (obtained from STL file), resin characteristics, and production layout. The main focus of this study is to investigate energy and material flows of the SLA process to investigate the relationships among process inputs, product/process information, resources, and outputs using transformation equations. To demonstrate the effectiveness and accuracy of the proposed models, three validation tests with different settings are conducted. The experimental results show high accuracies in terms of estimations for energy and material consumption/waste.

Conclusively, the UPLCI model made to represent the SLA process material and energy flows. The model was validated using experimental data. The primary contributor to energy consumption showed to be variations in print time confirmation that simplifications in power estimates were accurate. The proposed UPLCI model demonstrates a possible application of a standard for characterizing the environmental aspect of a manufacturing process.

To further extend this work, the energy and material flows in the printer cooldown stage should be considered. As an example, during part cleaning, a certain amount of alcohol is often used, which can cause material waste and potential environmental impacts. In addition, different post-curing approaches are often used, i.e., UV chamber, oven, and microwave, and they can contribute to the energy and material consumption and therefore should be considered in the UPLCI model.

5. SUMMARY

The objective of this study was to investigate life cycle inventory (LCI) of Fused Deposition Modeling (FDM) 3D printers for the purpose of applying more accurate predictions in Additive Manufacturing (AM) life cycle assessment (LCA) studies. To accomplish the overall objective three primary studies were completed. Throughout this project it was decided to focus predominantly on acrylonitrile butadiene styrene (ABS) filament printing due to its larger impact on results when compared to other FDM filament types.

In the initial study, emission concentrations were measured from desktop FDM printers in an effort to identify the primary source of detected emissions. Ultrafine particles (UFPs) were detected in significant magnitudes at an average size of 30nm in diameter. The largest spike of emitted UFPs was detecting at the start of the printing process and part geometry proved an insignificant factor in resulting emissions. Based on information gathered from initial testing, two primary hypotheses were developed and tested. The first hypothesis was that increased residence time of filament sitting in the heated extrusion nozzle correlated with increased emissions. This hypothesis was supported by test results but proved unsubstantial relative to overall emission concentrations throughout the printing process. The subsequent hypothesis stated that filament residue left in the extruding nozzle between prints was the primary factor impacting emission spikes. Results from tests confirmed this hypothesis drawing the conclusion that particle and gaseous emissions could be reduced by cleaning the extrusion nozzle between prints.

To further this study energy consumption measurements were made during prints with varied print speeds and material flow to determine part geometry influence on overall process energy consumption. It was determined that while differing print speeds and material flow do in fact induce changes in energy demand it is insignificant compared to overall energy consumption during a print. These results concluded that power fluctuation from varying part geometries demands far less energy than that of the heated nozzle and print bed making time the dominating factor in FDM energy consumption.

The study to follow had the objective of characterizing particulate and gaseous emissions from FDM printers while printing ABS plastic to identify their chemical makeup and molecular structure. Samples were prepared by diffusing UFP and VOC/SVOC emissions through a type 1 water solution and performing a filament wash in type 1 water to compare results. Compounds

were then extracted using solid phase microextraction (SPME) to be analyzed by thermal desorption using gas chromatography mass spectrometry (GCMS). Three different SPME fiber coatings were used during extractions to allow for an expansive analysis of varying analyte types and compound molecular weights ($30 - 300\,{}^{g}/_{mol}$).

Several compounds were identified in test results that were agreeable with what can be found in literature. Styrene consistently showed up in results at high concentrations, followed by a number of benzene aromatic chains, nitrogenated aromatics, and several siloxane variants. Several of the analytes found in printer emission tests were also identified in the filament wash tests. This led to the conclusion that emissions may be reduced by washing filament before putting it through the 3D printer extrusion process, but that hypothesis must be tested in future studies. Based on the monomers of ABS plastic and their structural relations to compounds identified in this study, it was determined that through the printing process emissions are produced by the melting and breaking down of the polymer chain into UFPs and VOCs/SVOCs. The particulate and gaseous emissions were likely reacting to sometimes form new compounds. Siloxanes are commonly used as additives in different plastics to enhance material characteristics while also improving overall extrusion efficiency. Other identified compounds may have also came from plastic additives, but this should be further tested using other filament colors. The human health risk of exposure to much of what was found in this study is not fully understood. Nevertheless, several of the identified emissions are known carcinogens and can cause inflammatory responses. Conclusions from this study expanded our knowledge on risks associated with output flows in the FDM process and recognized possible solutions to reduce risk, thereby, opening a door for future studies to follow.

In the final study, methodology was introduced for producing unit process life cycle inventory (UPLCI) models for both FDM and stereolithography (SLA) 3D printers. To do so material and energy input/output flows were investigated for both processes in question. Based on results from FDM tests in our previous study it was determined that the total print time is the primary factor impacting overall FDM energy consumption due to the heated elements. With inputs available, a series of equations were made to predict FDM material and energy flows. This methodology was expanded and applied to production of the SLA UPLCI model. A series of transformation functions were developed to predict SLA input/output material and energy flow. Validation tests were run on the SLA model yielding high accuracies in estimated consumption and waste. As AM expands

use in different industries, UPLCI models serve as beneficial tools to help apply the technology in efficient ways that enable improved product life cycle scenarios.

The goal of this study was to expand our knowledge on life cycle inventory flows of the FDM printing process. Upon doing so, waste output flows were investigated to gather information on human health and environmental risks. This information is beneficial in running impact assessments on products produced using FDM AM technologies. Solutions were also developed to help improve process performance. All together this study was successful in advancing our scientific knowledge and understanding as it relates to FDM AM process life cycle inventory flows.

6. FUTURE WORK

From the start of this study there have been several other projects targeting similar objects. As research progressed, information was gathered from results of this project and many others. Future work was discussed in the conclusion of each chapter and was different based on work that was being conducted. There are four concerns that should be addressed in preceding studies:

1. Reducing emissions during the print process
2. Further characterization of emissions from differing filament types and colors to investigate AM plastic additives.
3. Environmental and human health risk and impact assessment for identified emissions.
4. Applications of UPLCI models in design development.

FDM emission rates have been thoroughly investigated in this project and many others, however, efforts to reduce emission during the print process has not been considered. Conclusions from this project offer potential solutions to mitigate FDM emissions. When identifying emitted compounds and comparing with those found in the filament wash test, it was discovered that there was a lot of overlap in results. Several compounds were found to be identical and/or similar in molecular structure. This led to the conclusion that much of what is found in emitted UFPs and VOCs/SVOCs is a pre-existing on the filament before being extruded in the printer. By washing filament before a print, emissions could potentially be reduced. This hypothesis requires further testing in future work done in this area. Additionally, it was found that the initial spike of emitted particles at the start of a print is significantly reduced by cleaning the filament nozzle between prints. If a procedure was developed to easily clean FDM extrusion nozzles between prints, the initial spike of emitted particles and particle emission rate throughout the printing process would be reduced to negligible amounts.

During characterization tests several ABS additives were identified from both FDM emissions and the filament wash. The procedure used in this project tested white ABS filament manufactured by MakerBot. Further testing should be done to investigate additives that may be present in other filament types and colors. Some studies have done this and found that emissions vary based on the manufacturer of the FDM printer, manufacturer of the filament, colors of the filament, and type of filament. The SPME extraction methodology used in this project offered more expansive results

than those found from studies similar in nature. This methodology should be adopted for use in similar studies to offer a more dynamic prospective on FDM output flows and their impact.

With known compound size and structure, future work should further investigate human health risk and environmental impact of known emissions from FDM printers. Without understanding the full impact of characterized emissions, an accurate life cycle assessment (LCA) cannot fully be completed. Studies need to further investigate the effect of FDM emissions on the different LCA impact categories to improve product assessment results.

Finally, all this information can be further adopted into UPLCI models for a variety of AM processes. The use of these models will help designers develop products designed for AM with improved sustainability during production, use, and end of life phases. Methodology from this study can be implemented in other AM processes to increase UPLCI model use in several industries benefiting from improved product manufacturing approaches.

APPENDIX A. COMPOUND STRUCTURES FROM GC/MS MEASUREMENTS

Styrene

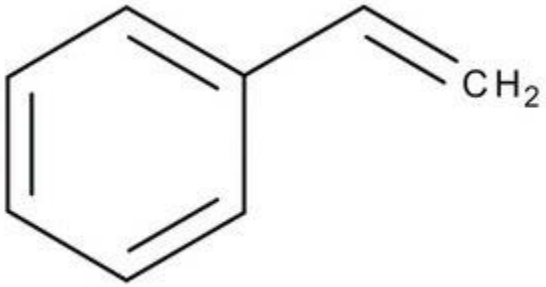

Cyclotrisiloxane, hexamethyl-

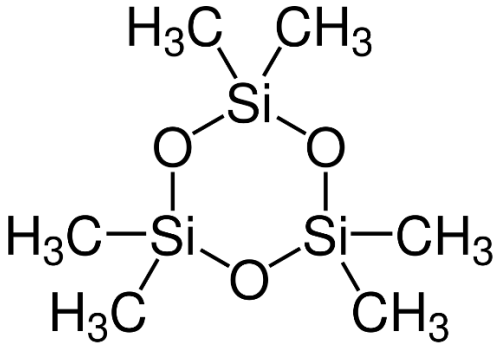

Cyclotetrasiloxane, octamethyl-

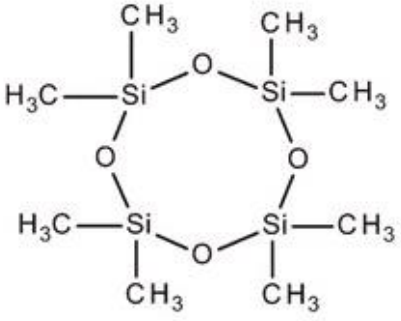

2,6-Dihydroxyacetophenone, 2TMS derivative

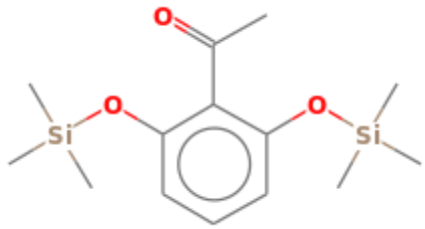

Benzoic acid, 4-methyl-2-trimethylsilyloxy-, trimethylsilyl ester

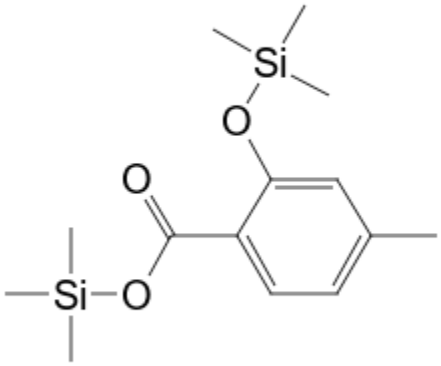

Cyclopentene, 3,3-dimethyl-4-methylene-1,2-bis(trimethylsilyloxymethyl)-

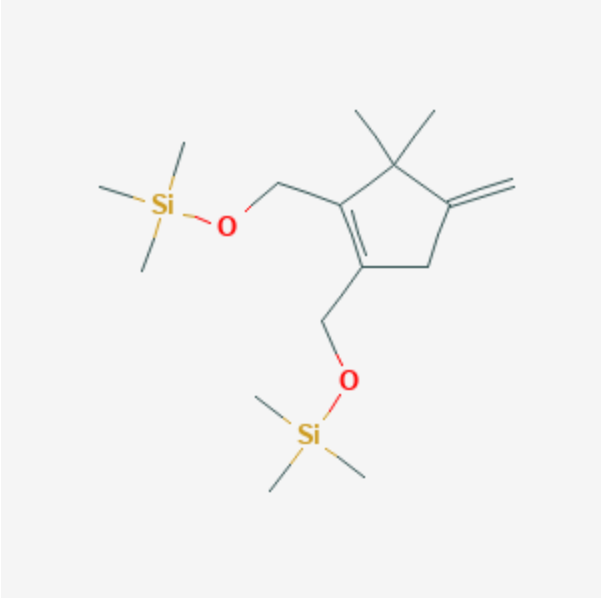

Benzene, 1,3-dimethyl-

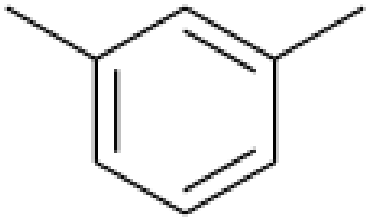

Ethylbenzene

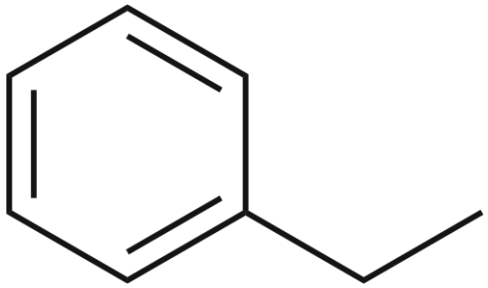

Benzene, (1-methylethyl)-

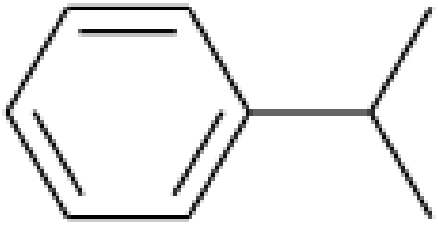

Benzene, propyl-

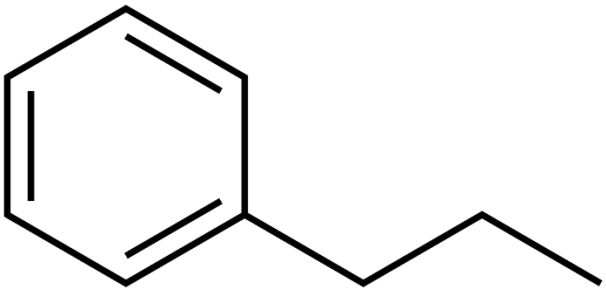

Pyridine, 4-(1-pyrrolidinyl)-

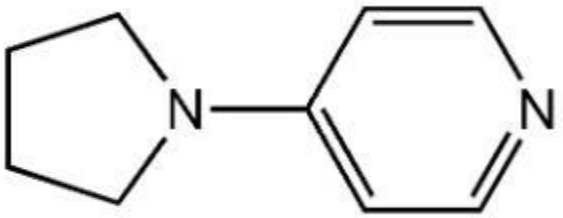

Silane, (butoxymethyl)trimethyl-

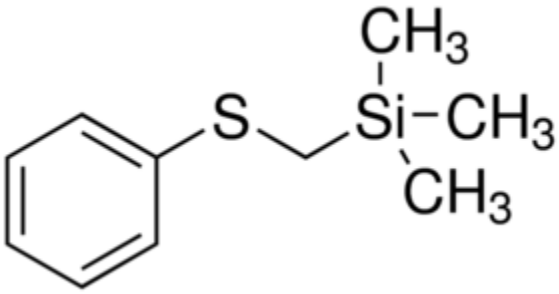

Boric acid, trimethyl ester

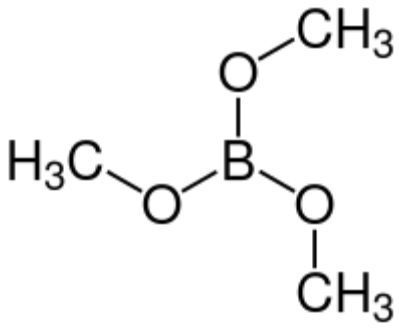

Benzene, 2,4-diisocyanato-1-methyl-

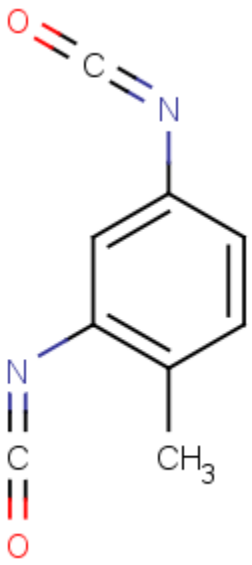

(6-Hydroxymethyl-2,3-dimethylphenyl)methanol

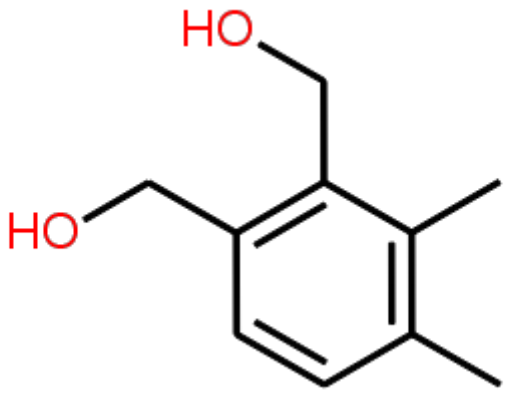

Quinazolin-4(3H)-one, 6-bromomethyl-2-methyl-

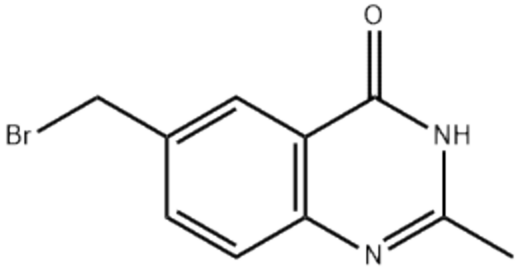

9-Hexadecenoic acid

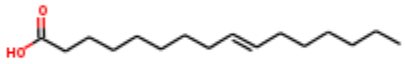

Diethyl Phthalate

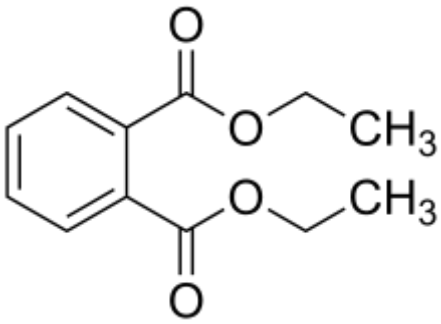

Benzene, 3-[3-iodo-2-(iodomethyl)-2-methylpropyl]-1,2,4,5-tetramethyl-

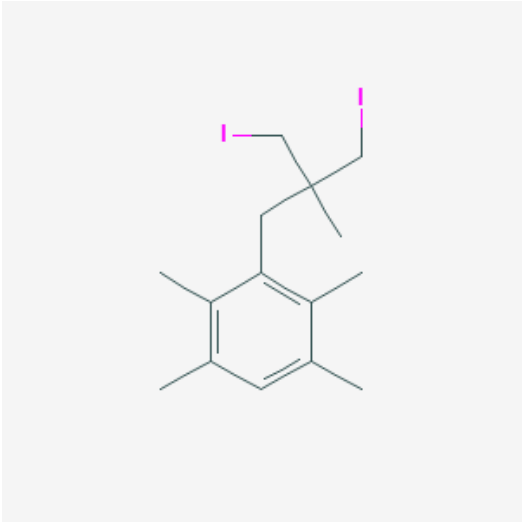

1,25-Dihydroxyvitamin D3, TMS derivative

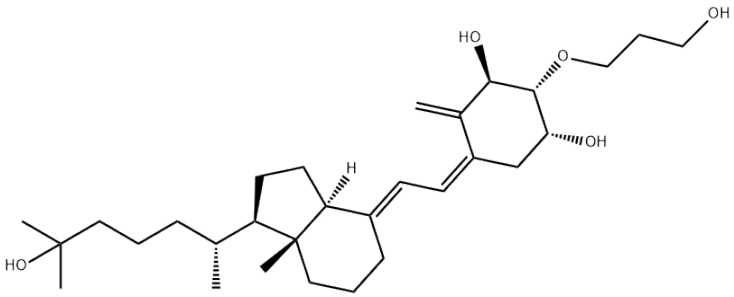

Pyrrolidine, 1-[4-(4-chlorophenyl)-3-phenyl-2-butenyl]-

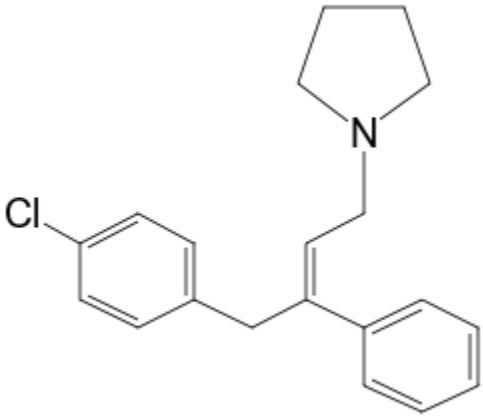

Phen-1,4-diol, 2,3-dimethyl-5-trifluoromethyl-

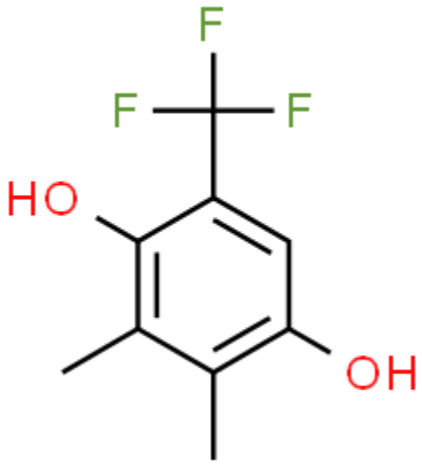

2-Methoxy-6,10-dimethyl-dodeca-2E,6Z,10Z-trienoic acid, 12-acetoxy-, methyl ester

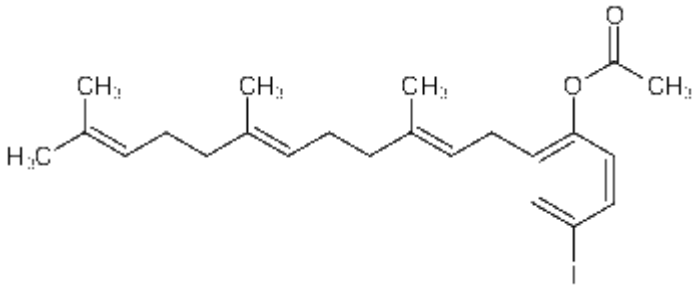

Tetrasiloxane, 1,1,3,3,5,5,7,7-octamethyl-

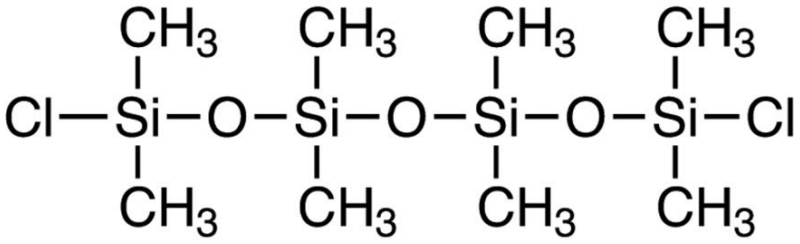

Tris(tert-butyldimethylsilyloxy)arsane

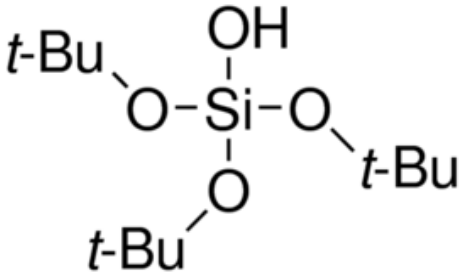

N-Methyl-1-adamantaneacetamide

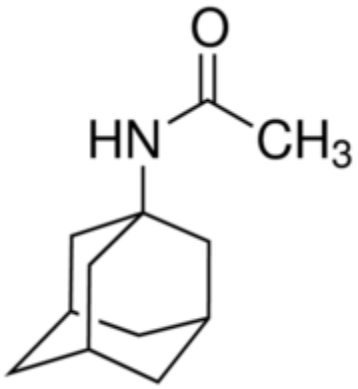

4-Phenyl-3,4-dihydroisoquinoline

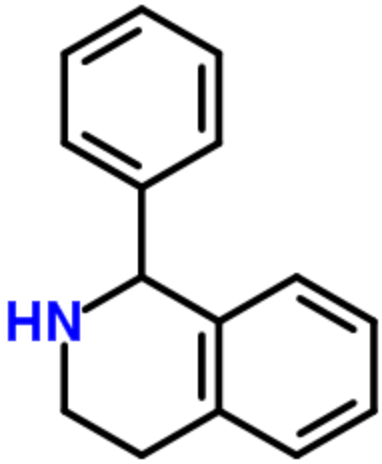

Benzonitrile, m-phenethyl-

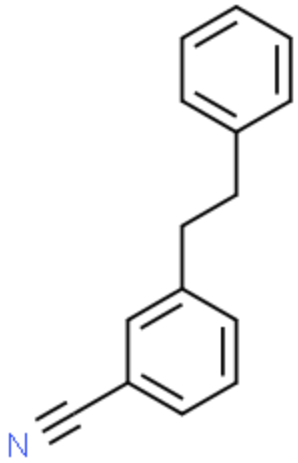

Benzene, 1,1',1'',1'''-(1,2,3,4-cyclobutanetetrayl)tetrakis-

Salicyl alcohol, 2TMS derivative

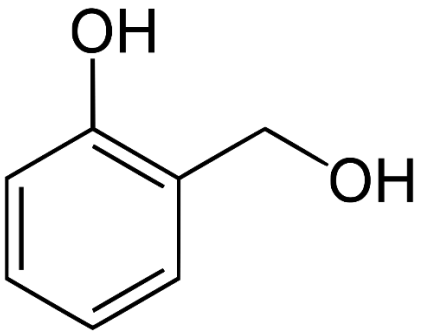

1,4-Cyclohexadiene, 1,3,6-tris(trimethylsilyl)-

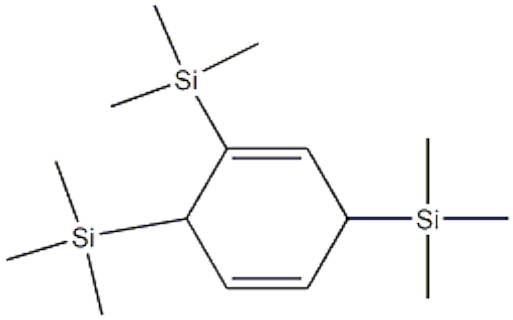

Thiocarbamic acid, N,N-dimethyl, S-1,3-diphenyl-2-butenyl ester

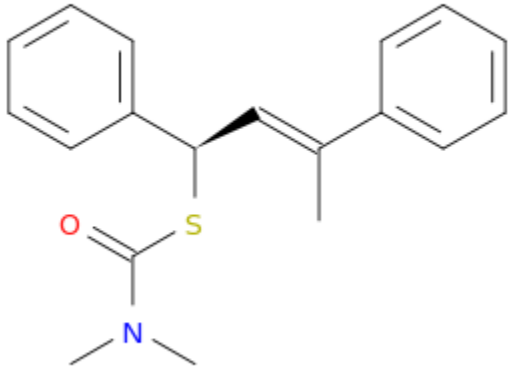

Phenol, 4,4'-(1-methylethylidene)bis-

APPENDIX B. STEREOLITHOGRAPHY UPLCI EQUATIONS

$$T_{LS} = {L_{lift}}/{V_{lift}} + {L_{retract}}/{V_{retract}} + T_{delay}$$

$$T_{printing} = N_{bottom} \times \left(T_{LS} + T_{curing,b}\right) + (N - N_{bottom}) \times \left(T_{LS} + T_{curing}\right)$$

$$L_{retract} = L_{lift} - d$$

$$N = {h}/{d}$$

$$T_{delay} = {d}/{V_{retract}} \times 60 + 1.6$$

$$T_{idle} = T_{printing} - T_{curing,b} \times N_{bottom} - T_{curing} \times (N - N_{bottom})$$

$$P_{curing,b} = [P_{idle} + (I \times A_i)]$$

$$P_{curing} = [P_{idle} + (I \times A_i)]$$

$$E_{curing} = \sum_{i=1}^{N_{bottom}} [P_{idle} + (I \times A_i)] \times T_{curing,b} + \sum_{i=N_{bottom}+1}^{N} [P_{basic} + (I \times A_i)] \times T_{curing}$$

$$E_{idle,p} = P_{idle} \times T_{idle}$$

$$E_{projector} = E_{curing} + E_{idle,p}$$

$$F_{platform} = g \times m_{platform}$$

$$F_{part,i} = g \times \varphi_{part} \times 10^{-9} \times \sum_{i=1}^{N_{bottom}} d \times A_i$$

$$F_{down,i} = F_{platform} + F_{part,i}$$

$$V_{part,i} = \sum_{i=1}^{N} A_i \times d$$

$$F_{up,i} = \rho_{resin} \times g \times 10^{-9} \times (\sum_{i=1}^{N} d \times A_i)$$

$$F_{total,i} = F_{down,i} - F_{up,i}$$

$$F_{total,i} = F_{down,i} - F_{up,i}$$

$$\tau_i = \begin{cases} c \times D_{rod} \times 10^{-3} \times F_{total,i}, & \tau_i > \tau_{min} \\ \tau_{min}, & \tau_i < \tau_{min} \end{cases} \rightarrow \tau_{min} = 0.1765\ N \times m$$

$$P_{motor,i} = \omega \times 60 \times \tau_i \times c_{factor}$$

$$E_{motor} = \sum_{i=1}^{N} P_{motor} \times T_{LS}$$

$$E_{board}=P_{board} \times T_{printing}$$

$$E_{computer}=P_{computer} \times T_{printing}$$

$$m_{input} = m_{part} + m_{waste,l} + m_{waste,g}$$

$$m_{part} = \rho_{part} \times V_{part}$$

$$m_{waste,l} = -0.2433 + 0.03723 \times D_{liquid} + 0.005253 \times S_p + 0.1138 \times b - 0.000513 \times D_{liquid} \times S_p - 0.01280 \times D_{liquid} \times b - 0.002042 \times S_p \times b + 0.000229 \times D_{liquid} \times S_p \times b$$

with R-squared value of 98.70%.

$$m_{waste,g} = E_{volatilization} + E_{AM}$$

$$Q = K \frac{\rho_v}{RT}$$

$$K = 0.0220 \cdot v_z^{0.78} \cdot \Delta z^{-0.11} \cdot Sc^{-0.67}$$

$$Sc = \frac{\mu}{\rho_a \cdot D}$$

$$\mu = -9.246 \times 10^{-5} + 1.610 \times 10^{-5} \times \sqrt{T}$$

$$\rho_a = 0.352 \cdot \frac{P}{T}$$

$$D = \frac{4.09 \times 10^{-5} \times T^{1.9} \times \sqrt{\frac{1}{28.97} + \frac{1}{M}}}{P \times M^{0.33}}$$

$$ER(t)_{volatilization} = Q \cdot M \cdot S$$

$$E_{AM} = -16{,}553 + 752 \times S_p + 140.2 \times V_m + 3.72 \times S_p \times S_p - 2.813 \times S_p \times V_m \times 10^{-6}$$ with 97.94% R-squared

$$E_{volatilization} = \int_{t=T_s}^{t=T_e} ER(t)_{volatilization}$$

$$m_{waste} = m_{waste,l} + m_{waste,g}$$

$$m_{consuption} = m_{waste} + m_{part}$$

$$T_{total} = T_{pre} + T_{printing} + T_{post}$$

$$E_{total} = E_{projector} + E_{motor} + E_{computer} + E_{board}$$

$$Cost = E_{total} \times C_{Wh} + m_{consumption} \times C_g$$

$$OD = E_{total} \times OD_{Wh} + m_{consumption} \times OD_g$$

$$GW = E_{total} \times GW_{Wh} + m_{consumption} \times GW_g$$

$$Sm = E_{total} \times Sm_{Wh} + m_{consumption} \times Sm_g$$

$$Acid = E_{total} \times Acid_{Wh} + m_{consumption} \times Acid_g$$

$$Eutro = E_{total} \times Eutro_{Wh} + m_{consumption} \times Eutro_g$$

$$Car = E_{total} \times Car_{Wh} + m_{consumption} \times Car_g$$

$$NC = E_{total} \times NC_{Wh} + m_{consumption} \times NC_g$$

$$RE = E_{total} \times RE_{Wh} + m_{consumption} \times RE_g$$

$$eco = E_{total} \times Eco_{Wh} + m_{consumption} \times Eco_g$$

$$FD = E_{total} \times FFD_{Wh} + m_{consumption} \times FFD_g$$

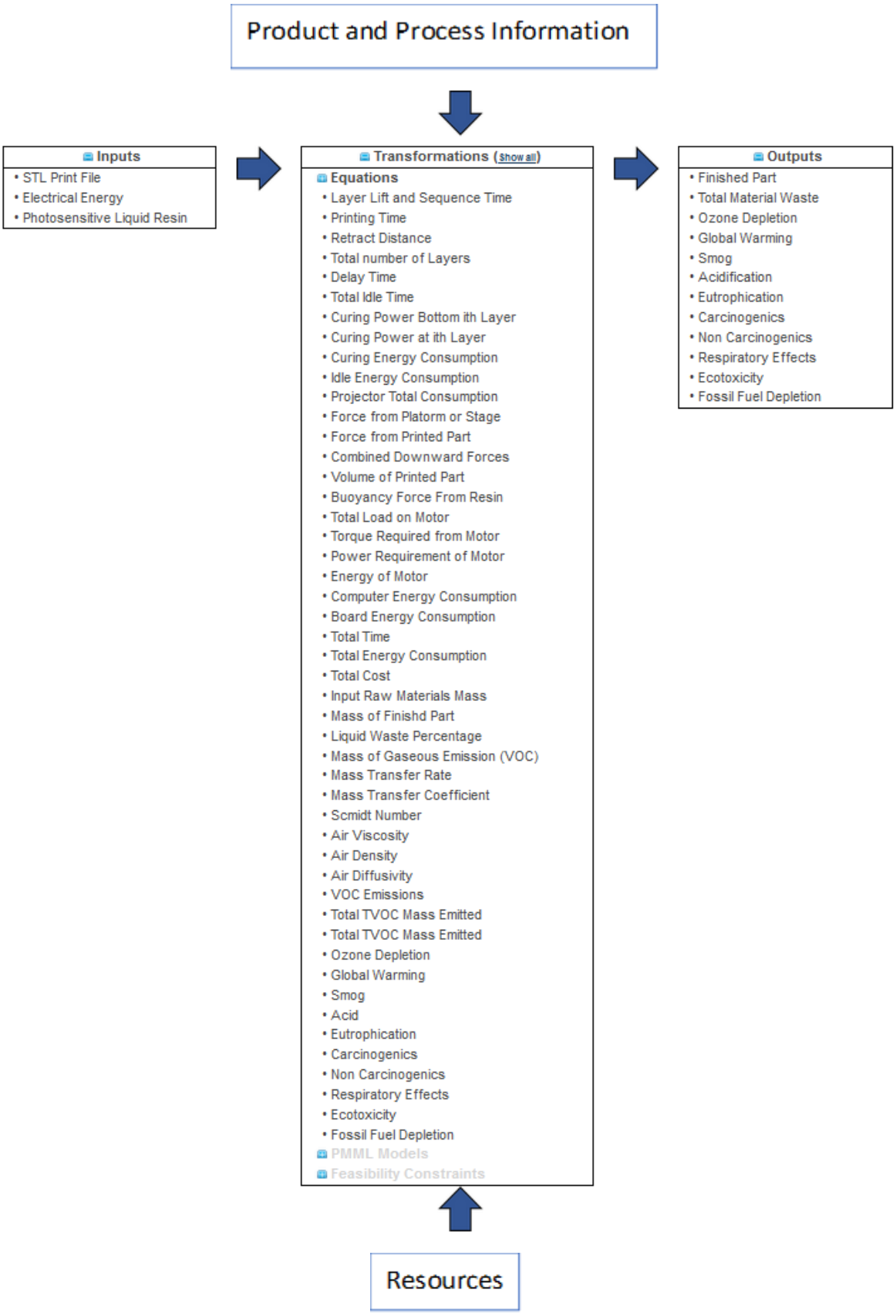
Product and Process Information
Inputs
• STL Print File
• Electrical Energy
• Photosensitive Liquid Resin
Transformations (show all)
Equations
• Layer Lift and Sequence Time
• Printing Time
• Retract Distance
• Total number of Layers
• Delay Time
• Total Idle Time
• Curing Power Bottom ith Layer
• Curing Power at ith Layer
• Curing Energy Consumption
• Idle Energy Consumption
• Projector Total Consumption
• Force from Platorm or Stage
• Force from Printed Part
• Combined Downward Forces
• Volume of Printed Part
• Buoyancy Force From Resin
• Total Load on Motor
• Torque Required from Motor
• Power Requirement of Motor
• Energy of Motor
• Computer Energy Consumption
• Board Energy Consumption
• Total Time
• Total Energy Consumption
• Total Cost
• Input Raw Materials Mass
• Mass of Finishd Part
• Liquid Waste Percentage
• Mass of Gaseous Emission (VOC)
• Mass Transfer Rate
• Mass Transfer Coefficient
• Scmidt Number
• Air Viscosity
• Air Density
• Air Diffusivity
• VOC Emissions
• Total TVOC Mass Emitted
• Total TVOC Mass Emitted
• Ozone Depletion
• Global Warming
• Smog
• Acid
• Eutrophication
• Carcinogenics
• Non Carcinogenics
• Respiratory Effects
• Ecotoxicity
• Fossil Fuel Depletion
PMML Models
Feasibility Constraints
Outputs
• Finished Part
• Total Material Waste
• Ozone Depletion
• Global Warming
• Smog
• Acidification
• Eutrophication
• Carcinogenics
• Non Carcinogenics
• Respiratory Effects
• Ecotoxicity
• Fossil Fuel Depletion
Resources

Product And Process Information

Control Parameters
- Part Height in Build Direction
- Layer Thickness
- Curing Time for Each Bottom Layer
- Curing Time for Each Layer
- ith Layer Exposure Area
- Liquid Resin Depth
- Batch Size
- Printing Surface Area

Fixed Parameters
- Total Number of Bottom Layers
- Lift Distance
- Lift Speed
- Retract Speed
- Projector Idle Stage Power
- Light Source Intensity
- Diameter of Rod
- Resin Density
- Part Density
- Acceleration of Gravity
- Coefficient of Sliding Friction
- Conversion Factor
- Revolutions per Second
- Computer Rated Power
- Control Board Rated Power
- Pre-processing Time
- Post-processing Time
- Energy Cost Per Wh
- Material Cost per kg
- Mass of Platform
- Molecular Weight
- Surface Area
- Vapor Pressure of Liquid
- Universal Gas Constant
- Absolute Temperature
- Air Flow Speed
- Length of Air-liquid Interface in the Direction of Flow
- Ambient Air Pressure
- Liquid Material Viscosity
- Ozone Depletion per Wh
- Global Warming per Wh
- Smog per Wh
- Acidification per Wh
- Eutrophication per Wh
- Carcinogenics per Wh
- Non Carcinogenics per Wh
- Respiratory Effects per Wh
- Ecotoxicity per Wh
- Fossil Fuel Depletion per Wh
- Ozone Depletion per g
- Global Warming per g
- Smog per g
- Acidification per g
- Eutrophication per g
- Carcinogenics per g
- Non Carcinogenics per g
- Respiratory Effects per g
- Ecotoxicity per g
- Fossil Fuel Depletion per g

Intermediate Variables
- Total Number of Layers
- Layer Lift and Sequence Time
- Total Printing Time
- Retract Distance
- Delay Time
- Total Idle Time
- Projector Curing Stage Power for Bottom ith Layer
- Projector Curing Stage Power for ith layer
- Projector Curing Stage Energy Consumption
- Projector Idle Stage energy Consumption
- Projector Total Energy Consumption
- Downward Force from Platform or Stage
- Downward Force from Printed Part
- Combined Downward Forced
- Volume of Printed Part
- Buoyancy Force Upward from Part in Resin
- Total Load on Motor
- Torque Required from Motor
- Power Requirement from Motor
- Energy From Motor
- Total Energy Consumption of Computer
- Total Energy Consumption of Board
- Mass of Input raw Materials (liquid)
- Mass of Finished Part (solid)
- Liquid Waste Percentage
- Mass of Gaseous Emission (VOC)
- Mass Transfer Rate
- Mass Transfer Coefficient
- Schmidt Number
- Air Viscosity
- Air Density
- Air Diffusivity
- VOC Emission Due to the Volatilization Process
- Total TVOC Mass Emitted from the AM Process
- Total TVOC Mass Emitted from the Volatilization Process

Metric of Interest
- Total Cost
- Total Energy Consumption
- Total Time
- Total Material Waste
- Total Material Consumption
- Ozone Depletion
- Global Warming
- Smog
- Acidification
- Eutrophication
- Carcinogenics
- Non Carcinogenics
- Respiratory Effects
- Ecotoxicity
- Fossil Fuel Depletion

Supporting Information

Resources
• Material List • Creation Workshop • Minitab • Matlab • Simapro

REFERENCES

[1] "What is Additive Manufacturing? Definition and Processes - TWI." https://www.twi-global.com/technical-knowledge/faqs/what-is-additive-manufacturing (accessed Nov. 17, 2020).

[2] M. Attaran, "The rise of 3-D printing: The advantages of additive manufacturing over traditional manufacturing," *Business Horizons*, vol. 60, no. 5, 2017, doi: 10.1016/j.bushor.2017.05.011.

[3] R. Bogue, "3D printing: The dawn of a new era in manufacturing?," *Assembly Automation*, vol. 33, no. 4, 2013, doi: 10.1108/AA-06-2013-055.

[4] Liang Hao, D. Raymond, G. Strano, and S. Dadbakhsh, "Enhancing the sustainability of additive manufacturing," in *5th International Conference on Responsive Manufacturing - Green Manufacturing (ICRM 2010)*, 2010, pp. 390–395. doi: 10.1049/cp.2010.0462.

[5] J. Faludi, C. Bayley, S. Bhogal, and M. Iribarne, "Comparing environmental impacts of additive manufacturing vs traditional machining via life-cycle assessment," *Rapid Prototyping Journal*, vol. 21, no. 1, pp. 14–33, 2015, doi: 10.1108/RPJ-07-2013-0067.

[6] M. Despeisse, M. Yang, S. Evans, S. Ford, and T. Minshall, "Sustainable Value Roadmapping Framework for Additive Manufacturing," in *Procedia CIRP*, Jan. 2017, vol. 61, pp. 594–599. doi: 10.1016/j.procir.2016.11.186.

[7] B. Rylands, T. Böhme, R. Gorkin, J. Fan, and T. Birtchnell, "The adoption process and impact of additive manufacturing on manufacturing systems," *Journal of manufacturing technology management*, vol. 27, no. 7, pp. 969–989, doi: 10.1108/JMTM-12-2015-0117.

[8] M. Burkhart and J. C. Aurich, "Framework to predict the environmental impact of additive manufacturing in the life cycle of a commercial vehicle," in *Procedia CIRP*, 2015, vol. 29. doi: 10.1016/j.procir.2015.02.194.

[9] R. Huang *et al.*, "Energy and emissions saving potential of additive manufacturing: the case of lightweight aircraft components," *Journal of Cleaner Production*, vol. 135, 2016, doi: 10.1016/j.jclepro.2015.04.109.

[10] K. Kellens, E. Yasa, R. Renaldi, W. Dewulf, J.-P. Kruth, and J. Duflou, "Energy and Resource Efficiency of SLS/SLM Processes (Keynote Paper)."

[11] M. Baumers, C. Tuck, R. Wildman, I. Ashcroft, and R. Hague, “Shape Complexity and Process Energy Consumption in Electron Beam Melting: A Case of Something for Nothing in Additive Manufacturing?,” *Journal of industrial ecology*, vol. 21, no. S1, pp. S157–S167, doi: 10.1111/jiec.12397.

[12] T. Simon, Y. Yang, W. J. Lee, J. Zhao, L. Li, and F. Zhao, “Reusable unit process life cycle inventory for manufacturing: stereolithography,” *Production Engineering*, vol. 13, no. 6, 2019, doi: 10.1007/s11740-019-00916-0.

[13] T. R. Simon, W. Jae, B. E. Spurgeon, B. E. Boor, and F. Zhao, “An Experimental Study on the Energy Consumption and Emission Profile of Fused Deposition Modeling Process,” *ScienceDirect*, vol. 00, 2018.

[14] K. Ramani *et al.*, “Integrated sustainable life cycle design: A Review,” *Journal of Mechanical Design, Transactions of the ASME*, vol. 132, no. 9, 2010, doi: 10.1115/1.4002308.

[15] K. Kellens, R. Mertens, D. Paraskevas, W. Dewulf, and J. R. Duflou, “Environmental Impact of Additive Manufacturing Processes: Does AM Contribute to a More Sustainable Way of Part Manufacturing?,” *Procedia CIRP*, vol. 61, no. Section 3, pp. 582–587, 2017, doi: 10.1016/j.procir.2016.11.153.

[16] H. Paris, H. Mokhtarian, E. Coatané, M. Museau, and I. Flores Ituarte, “Comparative environmental impacts of additive and subtractive manufacturing technologies”, doi: 10.1016/j.cirp.2016.04.036.

[17] Y. Tang, K. Mak, and Y. F. Zhao, “A framework to reduce product environmental impact through design optimization for additive manufacturing,” *Journal of cleaner production*, vol. 137, pp. 1560–1572, doi: 10.1016/j.jclepro.2016.06.037.

[18] M. K. Thompson *et al.*, “Design for Additive Manufacturing: Trends, opportunities, considerations, and constraints,” *CIRP Annals - Manufacturing Technology*, vol. 65, no. 2, pp. 737–760, Jan. 2016, doi: 10.1016/j.cirp.2016.05.004.

[19] F. le Bourhis, O. Kerbrat, L. Dembinski, J. Y. Hascoet, and P. Mognol, “Predictive model for environmental assessment in additive manufacturing process,” in *Procedia CIRP*, 2014, vol. 15. doi: 10.1016/j.procir.2014.06.031.

[20] P. C. Priarone and G. Ingarao, “Towards criteria for sustainable process selection: On the modelling of pure subtractive versus additive/subtractive integrated manufacturing approaches,” *Journal of cleaner production*, vol. 144, pp. 57–68, doi: 10.1016/j.jclepro.2016.12.165.

[21] F. le Bourhis, O. Kerbrat, J.-Y. Hascoet, and P. Mognol, “Sustainable manufacturing: evaluation and modeling of environmental impacts in additive manufacturing,” *The International Journal of Advanced Manufacturing Technology*, vol. 69, no. 9–12, pp. 1927–1939, 2013, doi: 10.1007/s00170-013-5151-2.

[22] C. Schulze, M. Juraschek, C. Herrmann, and S. Thiede, “Energy Analysis of Bioplastics Processing,” in *Procedia CIRP*, Jan. 2017, vol. 61, pp. 600–605. doi: 10.1016/j.procir.2016.11.181.

[23] “Characterizing the Mechanical Properties of Fused Deposition Modelling Natural Fiber Recycled Polypropylene Composites,” *Journal of Composites Science*, vol. 1, no. 1, p. 7, Jul. 2017, doi: 10.3390/jcs1010007.

[24] P. Bedi, R. Singh, and I. P. S. Ahuja, “Effect of SiC/Al2O3 particle size reinforcement in recycled LDPE matrix on mechanical properties of FDM feed stock filament,” *Virtual and Physical Prototyping*, vol. 13, no. 4, 2018, doi: 10.1080/17452759.2018.1496605.

[25] L. Feng, Y. Wang, and Q. Wei, “PA12 powder recycled from SLS for FDM,” *Polymers*, vol. 11, no. 4, 2019, doi: 10.3390/polym11040727.

[26] J. A. Slotwinski, E. J. Garboczi, P. E. Stutzman, C. F. Ferraris, S. S. Watson, and M. A. Peltz, “Characterization of Metal Powders Used for Additive Manufacturing,” *Journal of research of the National Institute of Standards and Technology*, vol. 119, no. 1, pp. 460–493, 2014, doi: 10.6028/jres.119.018.

[27] V. T. Le, H. Paris, G. Mandil, and D. Brissaud, “A Direct Material Reuse Approach Based on Additive and Subtractive Manufacturing Technologies for Manufacture of Parts from Existing Components,” in *Procedia CIRP*, Jan. 2017, vol. 61, pp. 229–234. doi: 10.1016/j.procir.2016.11.190.

[28] J. M. Wilson, C. Piya, Y. C. Shin, F. Zhao, and K. Ramani, “Remanufacturing of turbine blades by laser direct deposition with its energy and environmental impact analysis,” *Journal of Cleaner Production*, vol. 80, pp. 170–178, Oct. 2014, doi: 10.1016/j.jclepro.2014.05.084.

[29] E. Uhlmann, C. Fleck, G. Gerlitzky, and F. Faltin, “Dynamical Fatigue Behavior of Additive Manufactured Products for a Fundamental Life cycle Approach,” in *Procedia CIRP*, 2017, vol. 61. doi: 10.1016/j.procir.2016.11.138.

[30] H. Chen and Y. F. Zhao, “Process parameters optimization for improving surface quality and manufacturing accuracy of binder jetting additive manufacturing process,” *Rapid prototyping journal*, vol. 22, no. 3, pp. 527–538, doi: 10.1108/RPJ-11-2014-0149.

[31] G. C. Onwubolu and F. Rayegani, “Characterization and Optimization of Mechanical Properties of ABS Parts Manufactured by the Fused Deposition Modelling Process,” *International Journal of Manufacturing Engineering*, vol. 2014, 2014, doi: 10.1155/2014/598531.

[32] Q. Zhang, J. P. S. Wong, A. Y. Davis, M. S. Black, and R. J. Weber, “Characterization of particle emissions from consumer fused deposition modeling 3D printers,” *Aerosol Science and Technology*, vol. 0, no. 0, pp. 1–12, 2017, doi: 10.1080/02786826.2017.1342029.

[33] T. R. Simon, G. A. Aguilera, and F. Zhao, “Characterization of particle emission from fuse deposition modeling printers,” *ASME 2017 12th International Manufacturing Science and Engineering Conference, MSEC 2017 collocated with the JSME/ASME 2017 6th International Conference on Materials and Processing*, vol. 2, no. 3007, pp. 1–11, 2017, doi: 10.1115/MSEC2017-3007.

[34] P. Byrley, B. J. George, W. K. Boyes, and K. Rogers, “Particle emissions from fused deposition modeling 3D printers: Evaluation and meta-analysis,” *Science of the Total Environment*, vol. 655, 2019, doi: 10.1016/j.scitotenv.2018.11.070.

[35] Q. Zhang *et al.*, “Investigating particle emissions and aerosol dynamics from a consumer fused deposition modeling 3D printer with a lognormal moment aerosol model,” *Aerosol Science and Technology*, vol. 52, no. 10, 2018, doi: 10.1080/02786826.2018.1464115.

[36] H. Jeon, J. Park, S. Kim, K. Park, and C. Yoon, “Effect of nozzle temperature on the emission rate of ultrafine particles during 3D printing,” *Indoor Air*, 2019, doi: 10.1111/ina.12624.

[37] “FDM Fused Deposition Modeling - Engman Taylor.” https://www.3dpartsunlimited.com/blog-post/fdm-fused-deposition-modeling/ (accessed Nov. 17, 2020).

[38] V. Lunetto, P. C. Priarone, M. Galati, and P. Minetola, “On the correlation between process parameters and specific energy consumption in fused deposition modelling,” *Journal of Manufacturing Processes*, vol. 56, pp. 1039–1049, Aug. 2020, doi: 10.1016/j.jmapro.2020.06.002.

[39] Y. Saleh *et al.*, “Exposure to atmospheric ultrafine particles induces severe lung inflammatory response and tissue remodeling in mice,” *International Journal of Environmental Research and Public Health*, vol. 16, no. 7, 2019, doi: 10.3390/ijerph16071210.

[40] J. Israelachvili, *Intermolecular and Surface Forces*. Elsevier Inc., 2011. doi: 10.1016/C2009-0-21560-1.

[41] M. Feng, Z. Hua, and K. K. B. Hon, “A qualitative model for predicting energy consumption of rapid prototyping processes-a case of fused deposition modeling processe,” *IEEE Access*, vol. 7, 2019, doi: 10.1109/ACCESS.2019.2959214.

[42] M. Gebler, A. J. M. Schoot Uiterkamp, and C. Visser, “A global sustainability perspective on 3D printing technologies,” *Energy Policy*, vol. 74, no. C, 2014, doi: 10.1016/j.enpol.2014.08.033.

[43] R. Huang *et al.*, “Energy and emissions saving potential of additive manufacturing: the case of lightweight aircraft components,” *Journal of Cleaner Production*, vol. 135, 2016, doi: 10.1016/j.jclepro.2015.04.109.

[44] S. H. Huang, P. Liu, A. Mokasdar, and L. Hou, “Additive manufacturing and its societal impact: A literature review,” *International Journal of Advanced Manufacturing Technology*, vol. 67, no. 5–8, pp. 1191–1203, 2013, doi: 10.1007/s00170-012-4558-5.

[45] T. Reinhardt and G. Witt, “Experimental analysis of the laser-sintering process from an energetic point of view,” in *23rd DAAAM International Symposium on Intelligent Manufacturing and Automation 2012*, 2012, vol. 1.

[46] Y. Yang, L. Li, Y. Pan, and Z. Sun, “Energy Consumption Modeling of Stereolithography-Based Additive Manufacturing Toward Environmental Sustainability,” *Journal of Industrial Ecology*, vol. 21, 2017, doi: 10.1111/jiec.12589.

[47] M. Baumers, C. Tuck, R. Hague, I. Ashcroft, and R. Wildman, “A comparative study of metallic additive manufacturing power consumption,” 2010.

[48] V. A. Balogun, N. Kirkwood, and P. T. Mativenga, “Energy consumption and carbon footprint analysis of Fused Deposition Modelling: A case study of RP Stratasys Dimension SST FDM,” *International Journal of Scientific & Engineering Research*, vol. 6, no. 8, 2015.

[49] T. Peng, “Analysis of Energy Utilization in 3D Printing Processes,” *Procedia CIRP*, vol. 40, pp. 62–67, 2016, doi: 10.1016/j.procir.2016.01.055.

[50] N. Afshar-mohajer, C. Wu, T. Ladun, and D. A. Rajon, “Characterization of particulate matters and total VOC emissions from a binder jetting 3D printer,” *Building and Environment*, vol. 93, pp. 293–301, 2015, doi: 10.1016/j.buildenv.2015.07.013.

[51] Y. Kim *et al.*, “Emissions of Nanoparticles and Gaseous Material from 3D Printer Operation,” *Environmental Science and Technology*, vol. 49, no. 20, pp. 12044–12053, 2015, doi: 10.1021/acs.est.5b02805.

[52] B. Stephens, P. Azimi, Z. el Orch, and T. Ramos, “Ultrafine particle emissions from desktop 3D printers,” *Atmospheric Environment*, vol. 79, pp. 334–339, 2013, doi: 10.1016/j.atmosenv.2013.06.050.

[53] P. Azimi, D. Zhao, C. Pouzet, N. E. Crain, and B. Stephens, “Emissions of Ultrafine Particles and Volatile Organic Compounds from Commercially Available Desktop Three-Dimensional Printers with Multiple Filaments,” *Environmental Science and Technology*, vol. 50, no. 3, pp. 1260–1268, 2016, doi: 10.1021/acs.est.5b04983.

[54] R. Chýlek, L. Kudela, J. Pospíšil, and L. Šnajdárek, “Fine particle emission during fused deposition modelling and thermogravimetric analysis for various filaments,” *Journal of Cleaner Production*, vol. 237, 2019, doi: 10.1016/j.jclepro.2019.117790.

[55] V. Rizza, L. Stabile, D. Vistocco, A. Russi, S. Pardi, and G. Buonanno, “Effects of the exposure to ultrafine particles on heart rate in a healthy population,” *Science of the Total Environment*, vol. 650, 2019, doi: 10.1016/j.scitotenv.2018.09.385.

[56] F. L. Nassan *et al.*, “Ambient PM2.5 species and ultrafine particle exposure and their differential metabolomic signatures,” *Environment International*, vol. 151, 2021, doi: 10.1016/j.envint.2021.106447.

[57] W. Li *et al.*, “Short-Term Exposure to Air Pollution and Biomarkers of Oxidative Stress: The Framingham Heart Study,” *Journal of the American Heart Association*, vol. 5, no. 5, 2016, doi: 10.1161/JAHA.115.002742.

[58] J. C. Chen and J. Schwartz, “Metabolic syndrome and inflammatory responses to long-term particulate air pollutants,” *Environmental Health Perspectives*, vol. 116, no. 5, 2008, doi: 10.1289/ehp.10565.

[59] J. C. Nwanaji-Enwerem *et al.*, “Association of Long-term Ambient Black Carbon Exposure and Oxidative Stress Allelic Variants with Intraocular Pressure in Older Men,” *JAMA Ophthalmology*, vol. 137, no. 2, 2019, doi: 10.1001/jamaophthalmol.2018.5313.

[60] S. Panasevich *et al.*, “Associations of long- and short-term air pollution exposure with markers of inflammation and coagulation in a population sample,” *Occupational and Environmental Medicine*, vol. 66, no. 11, 2009, doi: 10.1136/oem.2008.043471.

[61] Z. He, G. Li, J. Chen, Y. Huang, T. An, and C. Zhang, “Pollution characteristics and health risk assessment of volatile organic compounds emitted from different plastic solid waste recycling workshops,” *Environment International*, vol. 77, 2015, doi: 10.1016/j.envint.2015.01.004.

[62] L. Bravi, F. Murmura, and G. Santos, “Additive manufacturing: Possible problems with indoor air quality,” in *Procedia Manufacturing*, 2019, vol. 41. doi: 10.1016/j.promfg.2019.10.020.

[63] I. Gümperlein *et al.*, “Acute health effects of desktop 3D printing (fused deposition modeling) using acrylonitrile butadiene styrene and polylactic acid materials: An experimental exposure study in human volunteers,” *Indoor Air*, vol. 28, no. 4, 2018, doi: 10.1111/ina.12458.

[64] E. L. Floyd, J. Wang, and J. L. Regens, “Fume emissions from a low-cost 3-D printer with various filaments,” *Journal of occupational and environmental hygiene*, vol. 14, no. 7, 2017, doi: 10.1080/15459624.2017.1302587.

[65] A. B. Stefaniak *et al.*, “Characterization of chemical contaminants generated by a desktop fused deposition modeling 3-dimensional printer,” *Journal of Occupational and Environmental Hygiene*, vol. 14, no. 7, 2017, doi: 10.1080/15459624.2017.1302589.

[66] J. Gu, M. Wensing, E. Uhde, and T. Salthammer, “Characterization of particulate and gaseous pollutants emitted during operation of a desktop 3D printer,” *Environment International*, vol. 123, 2019, doi: 10.1016/j.envint.2018.12.014.

[67] M. I. Banton *et al.*, “Evaluation of potential health effects associated with occupational and environmental exposure to styrene–an update,” *Journal of Toxicology and Environmental Health - Part B: Critical Reviews*, vol. 22, no. 1–4. 2019. doi: 10.1080/10937404.2019.1633718.

[68] A. Nemmar *et al.*, “Passage of inhaled particles into the blood circulation in humans,” *Circulation*, vol. 105, no. 4, 2002, doi: 10.1161/hc0402.104118.

[69] A. Laniece, “Alveoli-on-a-chip: A close-contact dynamic model of the alveolar capillary barrier: micro-engineering, microfluidics and induced pluripotent stem cells.,” *Biomechanics [physics.med-ph]*, no. Ed 564, 2019.

[70] “NIST Additive Manufacturing Test Artifact | NIST.” https://www.nist.gov/topics/additive-manufacturing/resources/additive-manufacturing-test-artifact (accessed Jun. 27, 2021).

[71] S. Moylan, J. Slotwinski, A. Cooke, K. Jurrens, and M. Alkan Donmez, “PROPOSAL FOR A STANDARDIZED TEST ARTIFACT FOR ADDITIVE MANUFACTURING MACHINES AND PROCESSES.” Accessed: Jun. 27, 2021. [Online]. Available: http://www.nist.gov/el/isd/sbm/matstandaddmanu.cfm;

[72] S. Stadtmüller, “Siloxanes as additives for plastics,” *Polymers and Polymer Composites*, vol. 10, no. 1, 2002, doi: 10.1177/096739110201000104.

[73] K. J. Ryan, K. E. Lupton, P. G. Pape, and V. B. John, “Ultra-high-molecular-weight functional siloxane additives in polymers. Effects on processing and properties,” *Journal of Vinyl and Additive Technology*, vol. 6, no. 1, 2000, doi: 10.1002/vnl.10217.

[74] T. M. Tran, A. Q. Hoang, S. T. Le, T. B. Minh, and K. Kannan, “A review of contamination status, emission sources, and human exposure to volatile methyl siloxanes (VMSs) in indoor environments,” *Science of the Total Environment*, vol. 691. 2019. doi: 10.1016/j.scitotenv.2019.07.168.

[75] J. M. McKim, P. C. Wilga, W. J. Breslin, K. P. Plotzke, R. H. Gallavan, and R. G. Meeks, “Potential estrogenic and antiestrogenic activity of the cyclic siloxane octamethylcyclotetrasiloxane (D4) and the linear siloxane hexamethyldisiloxane (HMDS) in immature rats using the uterotrophic assay,” *Toxicological Sciences*, vol. 63, no. 1, 2001, doi: 10.1093/toxsci/63.1.37.

[76] L. A. Burns-Naas *et al.*, “Inhalation toxicology of octamethylcyclotetrasiloxane (D4) following a 3-month nose-only exposure in Fischer 344 rats,” *International Journal of Toxicology*, vol. 21, no. 1, 2002, doi: 10.1080/10915810252826000.

[77] B. He *et al.*, “Octamethylcyclotetrasiloxane exhibits estrogenic activity in mice via ERα,” *Toxicology and Applied Pharmacology*, vol. 192, no. 3, 2003, doi: 10.1016/S0041-008X(03)00282-5.

[78] R. G. Meeks, D. G. Stump, W. H. Siddiqui, J. F. Holson, K. P. Plotzke, and V. L. Reynolds, “An inhalation reproductive toxicity study of octamethylcyclotetrasiloxane (D4) in female rats using multiple and single day exposure regimens,” *Reproductive Toxicology*, vol. 23, no. 2, 2007, doi: 10.1016/j.reprotox.2006.12.005.

[79] W. H. Siddiqui, D. G. Stump, K. P. Plotzke, J. F. Holson, and R. G. Meeks, “A two-generation reproductive toxicity study of octamethylcyclotetrasiloxane (D4) in rats exposed by whole-body vapor inhalation,” *Reproductive Toxicology*, vol. 23, no. 2, 2007, doi: 10.1016/j.reprotox.2006.11.011.

[80] A. L. Quinn *et al.*, “In vitro and in vivo evaluation of the estrogenic, androgenic, and progestagenic potential of two cyclic siloxanes,” *Toxicological Sciences*, vol. 96, no. 1, 2007, doi: 10.1093/toxsci/kfl185.

[81] C. G. Avio, S. Gorbi, and F. Regoli, “Plastics and microplastics in the oceans: From emerging pollutants to emerged threat,” *Marine Environmental Research*, vol. 128, 2017, doi: 10.1016/j.marenvres.2016.05.012.

[82] R. Sreenivasan, A. Goel, and D. L. Bourell, “Sustainability issues in laser-based additive manufacturing,” *Physics Procedia*, vol. 5, no. PART 1, pp. 81–90, 2010, doi: 10.1016/j.phpro.2010.08.124.

[83] S. Ford and M. Despeisse, “Additive manufacturing and sustainability: an exploratory study of the advantages and challenges,” *Journal of Cleaner Production*, vol. 137, pp. 1573–1587, 2016, doi: 10.1016/j.jclepro.2016.04.150.

[84] D. Rejeski, F. Zhao, and Y. Huang, “Research needs and recommendations on environmental implications of additive manufacturing,” *Additive Manufacturing*, vol. 19, pp. 21–28, 2018, doi: 10.1016/j.addma.2017.10.019.

[85] H. P. N. Nagarajan, H. A. Malshe, K. R. Haapala, and Y. Pan, "Environmental Performance Evaluation of a Fast Mask Image Projection Stereolithography Process Through Time and Energy Modeling," *Journal of Manufacturing Science and Engineering*, vol. 138, no. 10, p. 101004, 2016, doi: 10.1115/1.4033756.

[86] H. Xu, J. Weihua, M. Li, and W. Li, "A slicing model algorithm based on STL model for additive manufacturing processes," *Proceedings of 2016 IEEE Advanced Information Management, Communicates, Electronic and Automation Control Conference, IMCEC 2016*, pp. 1607–1610, 2017, doi: 10.1109/IMCEC.2016.7867489.

[87] M. Lutter-Günther, C. Gebbe, T. Kamps, C. Seidel, and G. Reinhart, "Powder recycling in laser beam melting: strategies, consumption modeling and influence on resource efficiency," *Production Engineering*, vol. 12, no. 3–4, pp. 377–389, 2018, doi: 10.1007/s11740-018-0790-7.

[88] B. Linke and M. Overcash, "Reusable unit process life cycle inventory for manufacturing: grinding," *Production Engineering*, vol. 11, no. 6, pp. 643–653, 2017, doi: 10.1007/s11740-017-0768-x.

[89] X. Ren, H. Shao, T. Lin, and H. Zheng, "3D gel-printing-An additive manufacturing method for producing complex shape parts," *Materials and Design*, vol. 101, pp. 80–87, 2016, doi: 10.1016/j.matdes.2016.03.152.

[90] "SLA 3D Printing materials compared | 3D Hubs." https://www.3dhubs.com/knowledge-base/sla-3d-printing-materials-compared (accessed Jan. 20, 2019).

[91] Y. Yang and L. Li, "Total volatile organic compound emission evaluation and control for stereolithography additive manufacturing process," *Journal of Cleaner Production*, vol. 170, pp. 1268–1278, 2018, doi: 10.1016/j.jclepro.2017.09.193.

[92] D. Mackay and R. S. Matsugu, "Evaporation rates of liquid hydrocarbon spills on land and water," *The Canadian Journal of Chemical Engineering*, vol. 51, no. 4, pp. 434–439, 1973, doi: 10.1002/cjce.5450510407.

[93] F. C. Arnold and A. J. Engel, "Evaporation of Pure Liquids from Open Surfaces," in *Modelling of Environmental Chemical Exposure and Risk*, Dordrecht: Springer Netherlands, 2001, pp. 61–71. doi: 10.1007/978-94-010-0884-6_6.

PUBLICATIONS

1. Simon, T.R., Aguilera, G.A., Zhao, F., (2017) “Characterization of particle emission from fused deposition modeling printers.” MSEC2017-3007
2. Simon, T.R., Cong, L., Zhai, Y., Zhu, Y., Zhao, F., (2018) “A Semi-automatic System for Efficient Recovery of Rare Earth Permanent Magnets from Hard Disk Drives.” Procedia CIRP: 916-920
3. Simon, T.R., Lee, W.J., Spurgeon, B.E., Boor, B.E., Zhoa, F., (2018) “An Experimental Study on the Energy Consumption and Emission Profile of Fused Deposition Modeling Process.” NAMRC 46
4. Simon, T.R., Yang Y., Lee, W.J, Zhao, J., Li, L., Zhao, F., (2019) “Reusable unit process life cycle inventory for manufacturing: stereolithography.” Production Engineering Research & Development